BEACON SATELLITE STUDIES OF THE IONOSPHERE OVER AHMEDABAD AND NEIGHBOURING LOW LATITUDES

presented

by

S.RAMAKRISHNAN

for

the degree of

DOCTOR OF PHILOSOPHY

of

THE UNIVERSITY OF KERALA

1967

PHYSICAL RESEARCH LABORATORY

AHMEDABAD

PREFACE

Since the discovery of the layers reflecting electromagnetic waves in the earth's high atmosphere, their physical characteristics such as virtual heights and critical frequencies have been extensively investigated by means of ground based equipments. Artificial earth satellites made it possible to study the topside of the ionosphere and the radiations reaching the earth's atmosphere from outside sources.

Space Research started in India in 1962 under the auspices of the INCOSPAR, whose Chairman is Professor Vikram Sarabhai, with the establishment of a Microlock satellite tracking station at Ahmedabad and the organisation of an equatorial Rocket launching station at Thumba. When NASA and NRL decided to orbit satellites with real time transmissions and telemetry, the Physical Research Laboratory, Ahmedabad made immediate arrangements for the reception of satellite signals so as to obtain as much information about the upper atmosphere as possible.

The thesis embodies the results of the author's work on the tracking and recording of polarised radio waves transmitted by NASA beacon satellites and on the Faraday rotation analysis of the satellite signals received at the Physical Research Laboratory. The receiving system was set up by the author in the

Microlock station. The data collected have been analysed and studied so as to determine the total electron content variations. The bottomside ionograms taken at the times of satellite transits have been subjected to true height analysis and the variations of topside and bottomside electron contents have been compared. The present study has thrown some light on the diurnal and seasonal variations of total electron content, topside electron content, bottomside electron content and maximum electron density over Ahmedabad, which is situated at a ~~the~~ latitude, where maximum F_2 peak ionisation occurs.

The role of sporadic E ionisation in producing satellite signal scintillations has not been very clear. In the present investigation, an empirical relationship between scintillation depth and f_xE_s has been found. The relationship between the ratio of 20 MHz depth to 40 MHz depth and f_xE_s has also been determined. Good correlation has been found between scintillation rate and f_xE_s.

The variations of total electron content and the equivalent slab thickness of the ionosphere upto 1000 km with 10.7 cm solar flux and with magnetic activity have also been studied. It has been found that the total electron content and the equivalent slab thickness increase linearly with solar flux.

Besides maintaining the beacon satellite tracking system, the scaling, computation and analysis of the Faraday rotation and satellite signal scintillation data were done by the author throughout the period of investigation.

S. Ramakrishnan

Author

K R Ramanathan

Countersigned
(Professor-in-charge)

ACKNOWLEDGEMENTS

Dr.Robert E.Bourdeau and Dr.Leo J.Blumle of NASA kindly provided some of the equipment~~s~~ needed for starting the beacon satellite tracking at Ahmedabad and the computed tables for the magnetic field factors for this station. The orbital ephemerides of the satellites were provided by the Goddard Space Flight Centre, U.S.A.

I am grateful to Professor Vikram Sarabhai, who took a keen interest in this project. The satellite tracking facility at Ahmedabad has been functioning under the leadership of Shri E.V.Chitnis. Dr.J.S.Shirke took interest in giving this project a smooth beginning and I express my thanks to him. Thanks are also due to Dr.R.G.Rastogi for help and advice. I have been benefitted by some valuable suggestions, given by Dr.R.V.Bhonsle. The use of computer programme, provided by Dr.S.Sanatani for the true height analysis is acknowledged. Thanks are also due to the computing section consisting of Mr.Shah, Mr.Vayeda and Mr.Rathod for providing prompt help in running the computer programmes. This section has been functioning under the leadership of Mr.S.R.Thakore. It is a pleasure to acknowledge with thanks the help given by the satellite tracking group consisting of Mr.Shakil, Miss Desai, Mr.Bhadra, Mr.Panchal, Mr.Patel and Mr.Pandya. I express my thanks to Mr.Gargesh, who assisted me in scaling the satellite records and drawing the diagrams and to Mrs.S.P.Jani, who helped me in scaling the ionograms.

Finally, I express my respects and gratitude to Professor K.R.Ramanathan for introducing me to the subject and giving valuable guidance throughout the period of investigation.

References to other workers and authors have been made in the appropriate places.

C O N T E N T S

CHAPTER I

INTRODUCTION

1.1 Role of artificial earth satellites in ionospheric studies

1.2 Basic principles involved in using artificial satellites for ionospheric studies

1.3 Various methods of studying the ionosphere using beacon transmissions from satellites

1.4 Scope of the thesis.

CHAPTER I

INTRODUCTION

1.1 Role of artificial earth satellites in ionospheric studies

The ionosphere plays a very important part in radio wave communication and it is essential to study the behaviour of the ionised layers of the upper atmosphere. A study of the physical processes taking place in the ionosphere is complicated by the fact that the physical conditions prevailing there cannot be readily duplicated and studied in the laboratory. For example, the pressure at 300 km is of the order of 10^{-6} mm of Hg and the molecular mean free path is in the vicinity of 10 km. It is impossible to provide a test chamber large compared with the mean free path and it is also difficult to duplicate in the laboratory the complex fluxes of radiant energy which are constantly present in the ionosphere. The advantages of rocket and satellite - borne instruments for ionospheric measurements stand out very clearly. The rocket is capable of exploring within a few minutes a cross section of the atmosphere through a large height range. Satellites are particularly useful to study conditions over a large part of the atmosphere within a short interval of time and continue this for a long period. Below about 200 km the life-time of satellites becomes too short to be of value for long term studies. For experiments requiring long duration, geographical coverage, and a wide range of altitudes, the satellite cannot be matched.

The domain of science now deriving most benefit from artificial satellites is atmospheric Physics and Solar Terrestrial Relationships. The sun which emits radiation over a whole spectrum of wavelengths from X-rays to radio waves and clouds of ionised matter (Plasma), largely controls the processes taking place in the atmosphere. Some of these radiations from the sun are absorbed at different levels in the atmosphere and do not reach the ground. Satellites can sample the radiation directly and analyse the changing properties of the upper atmosphere as they respond to the changing fluxes of radiation. In addition to these, an artificial satellite can also be used as a source emitting radio waves at desired frequencies. This type of satellite is very useful for the study of radio wave propagation at different levels in the atmosphere. The present study summarises the results of an integrated study of the electron content of the ionosphere over Ahmedabad ($72^{o}36'$ E, $23^{o}01'$ N) during 1964-67, the ionosphere below the F_2 peak being studied from vertical ionosonde data and the topside from the observations of the Faraday rotation of polarised radio waves transmitted by the American satellites, Explorer 22 and Explorer 27.

The study of the bottomside of the ionosphere started in 1902, when Kennelly and Heaviside independently suggested that the propagation of radio waves from England to America, round the spherical earth could ~~be~~ explained by reflection from an ionised layer in the upper atmosphere. Ionospheric reflection of radio waves was first shown to occur by using continuous wave transmissions. The introduction of group retardation method, using short pulses of waves, revealed very graphically the way in which ionisation is distributed in height. This method is now employed on a world wide scale. This method however does not enable us to study the topside of the ionosphere. In the year 1957, the first artificial satellite (Sputnik I) was launched by the U.S.S.R. and radio signals which were transmitted by it were received at ground stations. This event opened up the new field of upper atmospheric studies.

1.2 Basic principles involved in using artificial satellites for ionospheric studies

Artificial satellites used for ionospheric studies can be classified into three categories : (i) Direct measurement satellites, (ii) Topside sounder satellites and (iii) Beacon satellites. Direct measurement satellites take measurements in the vicinity of the space-craft and relay the information (either continuously or on command from the earth) in a coded form with the help of a suitable telemetry system. The carrier waves containing the information are received at ground-based tracking stations and the information is decoded to find the changes in solar radiation or in ionospheric parameters in the vicinity of the satellite. By means of topside sounding satellites it is possible to study the ionospheric region between the satellite and the level of maximum electron density. In this case, the satellite carries an ionospheric sounder, which can probe the ionosphere from above by means of a swept frequency or spot frequency pulse transmitter. By having an ionosonde in the satellite it is possible to probe the ionosphere over a large range of latitude with the same equipment. Beacon satellites are used for the study of some of the properties of the intervening space between the satellite and the earth from the propagation effects on the satellite signals as they traverse the ionosphere. The information obtained from this type of satellites is used for the investigation presented in this thesis.

The early satellite experimenters made use of the telemetry transmitters which were on board the Sputnik and Cosmos series of satellites launched by the U.S.S.R. The Russian satellites have telemetry transmissions in the region of 20 MHz. Such transmissions from Sputnik I, Sputnik III and other such earliest satellites were used by many ionospheric workers for propagation studies. Using 20 MHz and 40 MHz frequencies transmitted by Sputnik II satellite, the Royal Aircraft Establishment in U.K. (1957) obtained valuable data. Since then, many reports have been published on the determination of total electron content in the ionosphere by means of Faraday rotation of the plane of polarisation of radio waves. A general survey of work done in this field will be taken up in a later Chapter.

1.3 Methods of studying the ionosphere using beacon transmissions from satellites

The characteristics of radio waves that can be used for studying the ionosphere are (a) Amplitude and frequency, (b) direction of arrival and (c) polarisation. We shall take these up one by one and see how they can be used for ionospheric studies.

(a) Amplitude and frequency of the radio waves

The measured amplitude of signal depends on many factors which cannot be separated easily and hence the absolute measurement of the amplitude of satellite signals cannot be put to good use. Vassy (1960, 1961) made some interesting proposals for measuring the absorption of satellite signals. This was based on comparing the signal amplitude for vertical and oblique transmissions through the absorbing medium. One assumes the ionosphere to be constant for a few hundred kilo meters around the observing point. If the absorption per unit length is 'K', the received signal strength (neglecting antenna effects) would be $E = (\frac{A}{d}) \exp(-\int K ds)$. Where A is a constant, 'd' is the distance to the satellite and 'ds' is an element of path length. One can write $ds = dh \operatorname{Sec} i$ where dh is the element of height and 'i' is the local angle of incidence. For $i < 45^{\circ}$ the equation can be approximated by

$$E = \left(\frac{A}{d}\right) \exp\left(-\operatorname{Sec} i_a \int K\, dh\right)$$

where i_a is the average angle of incidence inside the absorbing part of the ionosphere. $\operatorname{Log} Ed = \operatorname{Log} A - \operatorname{Sec} i_a \int Kdh$. A plot of Log Ed against Sec i_a should give a straight line from which one could determine the total vertical absorption of the ionosphere by measuring its slope. Unfortunately, it is found to be difficult to eliminate altogether the antenna effects.

Kazantzev (1959) used another interesting approach to measure the absorption of 20 Mc/s satellite signals. He determines the mean value of received field strength as a function of sub-satellite distance for a number of transits. When comparing the mean variations of field strength for high transits with those in which the satellite passed below the F layer, he finds a systematic difference, which is due to absorption in the F layer itself. This statistical procedure does average the F layer absorption over different times of day.

Changes in the frequency of radio wave transmitted by satellites can also be used for studying the ionosphere. When a radio wave of frequency f_1, emitted from a moving transmitter, propagates through the ionosphere it will have its Doppler shift slightly altered from the free-space value as a result of dispersion in the medium. This alteration in Doppler shift is very small and can best be detected by comparative measurements on two transmitter frequencies f_1 and f_h which are harmonically related i.e. f_1 and $f_2 = mf_1$. The frequency beat between f_1 and fh/m, called differential Doppler, is proportional to the total electron content ($\int n\,dh$) if the motion of the vehicle is parallel to the stratification. When the vehicle moves along the ray path, the beat frequency will give information about the local electron density.

(b) The directions of arrival of satellite signals have been measured in elevation and bearing to an accuracy of about 1^{o}. Titheridge (1961) made use of the angle of arrival of radio waves emitted by satellites to measure the electron density between the satellite and the level of maximum ionisation. For this, he used those satellites whose heights were below the height of maximum electron density. By measuring the elevation angles of signals from satellites well above the altitude of maximum ionisation, Titheridge (1964) also calculated the total electron content and the scale height of the upper part of the F layer.

Alpert (1958) measured accurately the times of appearance and disappearance of a radio signal from a satellite. For various assumed shapes of the upper ionosphere he calculated the radio-rise and radio-set times of the satellite, as caused by refraction effects. The comparison with measured effects enabled him to choose the shape that would fit the observations best. Knowing the shape of the ionosphere which gave the most satisfactory agreement with the observed results, the total electron content was calculated.

(c) The principle of Faraday rotation of radio waves has been extensively used for studying the ionosphere. The present thesis embodies the results of measurements made at Ahmedabad using the technique of Faraday rotation of the plane of polarisation of radio waves, transmitted by the beacon satellites launched by NASA (National Aeronautics and Space Agency), U.S.A.

All the four characteristics of the satellite signal (amplitude, frequency, polarisation and direction) undergo smooth slow variation, which is due to the geometry of the satellite pass. Sometimes, however, one can notice an additional fast variation of the recorded amplitude. These are due to irregularities in the structure of the ionosphere. Such scintillations in the amplitude of satellite signals have also been investigated and the results are embodied in the thesis.

1.4 Scope of the thesis

During the International Quiet Sun Year (IQSY, 1964-65), the U.S.A. planned to launch an Ionosphere beacon satellite with real time transmissions specially meant for ionospheric studies. On 10th October 1964 the first ionosphere beacon satellite (Explorer 22 or S-66) was put into orbit. Later, on 29 April, 1965 one more similar satellite (Explorer 27) was launched by the U.S.A. More than 20 countries have been taking part in this research programme.

As part of the Indian space research programme, satellite study of the ionosphere by the Faraday rotation technique was started at the Physical Research Laboratory, Ahmedabad. Tracking of Explorer 22 and 27 satellites was started on 20th October, 1964 and 1st May, 1965 respectively.

In the last few years a large amount of data has been published concerning the variation of electron content in middle latitudes e.g. Garriott (1960), Little and Lawrence (1960), Yeh and Swenson (1961) and others. These studies have been based on measurements of radio waves from beacon satellites as they pass through the ionosphere. Relatively, there are only a few reports (Somayajulu et al 1964; Ramakrishnan, 1966; and Somayajulu and Tuhi Ram Tyagi, 1966) on the electron content variations over low latitude stations. It is the purpose of this study to present the results of a series of Faraday rotation measurements made at Ahmedabad which is a low latitude station within the geomagnetic anomaly zone. It is a well known fact that the maximum electron density in the F_2 layer increases as we go from the magnetic equator towards middle latitudes. Ahmedabad is situated at the latitude where the maximum F_2 peak ionisation occurs. This is an unique position in this region for ionospheric studies. Satellite tracking facilities have been provided here for studying the total electron content variations. The Faraday fadings are recorded at 20 MHz, 40 MHz and 41 MHz frequencies, transmitted by the two satellites. The method of calculating the difference in the angles of Faraday rotation of 40 MHz and 41 MHz ($d\Omega$) has been described by Shirke and Ramakrishnan (1966). Using these differences, the total electron content upto the satellite height has been calculated. Earlier investigators made use of a single frequency for determining the total Faraday rotation angle (Ω), or the change in the angle of Faraday rotation as the satellite moved from one point to another. In the former method, it is necessary to find the point where the Faraday rotation becomes zero. In the latter method, it is necessary to assume that there is no horizontal gradient in the total electron content. The method used in the present analysis does not have these draw-backs. For low latitude stations $d\Omega$ can be evaluated even if the point of zero Faraday rotation is not seen on the record. In the case of middle and high latitude stations, the method advocated by Little (unpublished) may be used for evaluating $d\Omega$

In Chapter II, the theory of Faraday rotation and the different methods of determining the total electron content have been described. The method of calculation adopted at Ahmedabad has also been explained. In Chapter III, the details of experimental set-up for recording the satellite signals have been described. In Chapter IV, the results of diurnal and seasonal variations of electron content, the maximum electron density and height of maximum electron density have been given in detail. In Chapter V, the electron content and equivalent slab thickness variations associated with solar activity and magnetic activity have been studied.

Since the early vertical sounding observations of Booker and Wells in 1938, the irregular variations of the ionosphere have been a subject of continued interest. In 1946 renewed interest was generated when the intensity of the radiation from radio stars was observed to fluctuate (Hey et al 1946). Later, back-scatter soundings (Peterson, 1955), Whistler mode propagation (Helli Well et al, 1956), satellite radio signals (Slee, 1958), and rocket soundings (Calvert et al, 1963) indicated the existence of irregularities. But it has not been possible to study the effect of E region irregularities in producing satellite signal scintillations in the absence of F scatter till now. Ramakrishnan (1966) reported the observation that there were occasions when there was sporadic E but no F scatter and that on such occasions there was good correlation between scintillation depths measured at 20 MHz and 40 MHz and the maximum frequency of sporadic E layer as measured at Ahmedabad. Results of further analysis are included in the thesis. While there have been a few reports connecting radio star scintillations with the occurrence of sporadic E ionisation (Bolton, 1958; and Dueno, 1955) the relationship between scintillation depths and critical frequency of sporadic E had not been investigated. In the present investigation an empirical relationship between scintillation depths and the maximum frequency of sporadic E (f_xE_s) has been found. An empirical relationship between the ratio of 20 MHz scintillation depth to 40 MHz scintillation depth and f_xE_s has also been determined.

At Illinois, a middle latitude station, Yeh and Swenson (1964) have reported that the boundary of scintillation moves southward as magnetic activity increases. In the present study, it has been found that the scintillation boundary moves northward with increase in magnetic activity. In Chapter VI, all the results of satellite signal scintillations are given in some detail.

CHAPTER II

FARADAY ROTATION

CHAPTER II

FARADAY ROTATION

2.1 Theory of Faraday rotation

When a linearly polarised electromagnetic wave passes through an ionised medium its phase velocity is increased above the velocity of light. This is due to the induced movement of free electrons in the medium. If there is a magnetic field also present, the more complicated induced movement of the free electrons has an effect of rotating the plane of polarisation around the direction of propagation.

Appleton, Hartree and Lassen have calculated the effects on a wave traversing a magneto-ionic medium. In the present work, the simplified form of the refractive index μ , which neglects collisions, and which assumes quasi-longitudinal propagation will be used for deriving an expression for the Faraday rotation angle.

$$\mu_o^2 = 1 - \frac{f_o^2}{f(f + f_H \operatorname{Cos}\theta)} \qquad (1)$$

$$\mu_x^2 = 1 - \frac{f_o^2}{f(f - f_H \operatorname{Cos}\theta)} \qquad (2)$$

Where f_o is the critical frequency of the medium f the frequency of the wave, f_H the gyromagnetic frequency, θ is the angle between the wave normal and the direction of the magnetic field. The frequencies (f) used for this experiment are 40.010 Mc/s and 41.010 Mc/s, which are very high compared to f_H. They are high compared to the critical frequency (f_o) also. Under these conditions, equations (1) and (2) can be written as

$$\mu_0 = 1 - \frac{f_0^2}{2(f^2 + f f_H \cos\theta)} \qquad (3)$$

$$\mu_x = 1 - \frac{f_0^2}{2(f^2 - f f_H \cos\theta)} \qquad (4)$$

and $$\mu_0 - \mu_x = f_0^2 f_H \cos\theta / f^3 \qquad (5)$$

Since the plasma frequency is proportional to the square root of electron density, equation (5) can be written in terms of electron density. Gyro frequency also can be written in terms of the magnetic field. If $f_o^2 = K_1 n$ (where n is the electron density), equation (5) can be written as

$$\mu_0 - \mu_x = K_1 n H \cos\theta / f^3 \qquad (6)$$

Phase velocity is defined as c/μ where c is the velocity of light in vacuo. The time taken by a wave crest to traverse a length d s in the magneto-ionic medium is, therefore;

$$dT = (\mu/c)\, ds \qquad (7)$$

The difference in the times of passage of the two components is, therefore:

$$T_0 - T_X = \frac{1}{c} \int (\mu_0 - \mu_X)\, ds \tag{8}$$

The phase difference between the two oppositely rotating circular components is :

$$\phi = 2\pi f\,(T_0 - T_X) \tag{9}$$

The spatial rotation of the plane of polarisation (Ω) is equal to half the phase difference.

Therefore $$\Omega = \frac{1}{2}\phi = (T_0 - T_X)\,\pi f \tag{10}$$

Combining (8) and (10)

$$\Omega = \frac{\pi f}{c} \int_S (\mu_0 - \mu_X)\, ds \tag{11}$$

Substituting the value of ($\mu_0 - \mu_X$) from equation (6) in equation (11),

$$\Omega = \frac{K}{f^2} \int_S n\, B \cos\theta\, ds \tag{12}$$

This is the basic simplified equation for the rotation of the plane of polarisation of a linearly polarised electro-magnetic wave as it passes through the ionosphere. It can be seen that the rotation angle is inversely proportional to the square of the frequency.

If ds = dh sec χ (dh is an element of the vertical height and χ is the angle between the vertical and ray) equation (12) becomes

$$\Omega = \frac{K}{f^2} \int_0^h B \cos\theta \sec\chi \; n \; dh \qquad (13)$$

Strictly speaking, an average value of B cos θ sec χ in the ray path has to be taken for the calculation of Ω. But Garriott (1963) has found that it is sufficient to take the value of B cos θ sec χ at a height, which is above the height of maximum electron density by about 50 km. Equation (13) can then be written as

$$\Omega = \frac{K}{f^2} (B \cos\theta \sec\chi) \int_0^h n \; dh \qquad (14)$$

The second factor within the brackets depends on the direction of the geomagnetic field, the integral is the total electron content in the ionosphere in a vertical column of unit cross section.

As the satellite moves across the sky the geometrical term changes considerably and the integrated electron content also varies slightly. The effect of this is that the polarisation angle, as measured at a receiver on the earth, will vary with time as the satellite moves. When receiving on a linear antenna, for instance a horizontal dipole, a periodic fading will be recorded with minima corresponding to the times when the polarisation plane of the incoming wave is at right angles to the plane formed by the receiving antenna and the direction of the ray. An actual example of an amplitude record of a beacon satellite signal is shown in Fig.2.1.

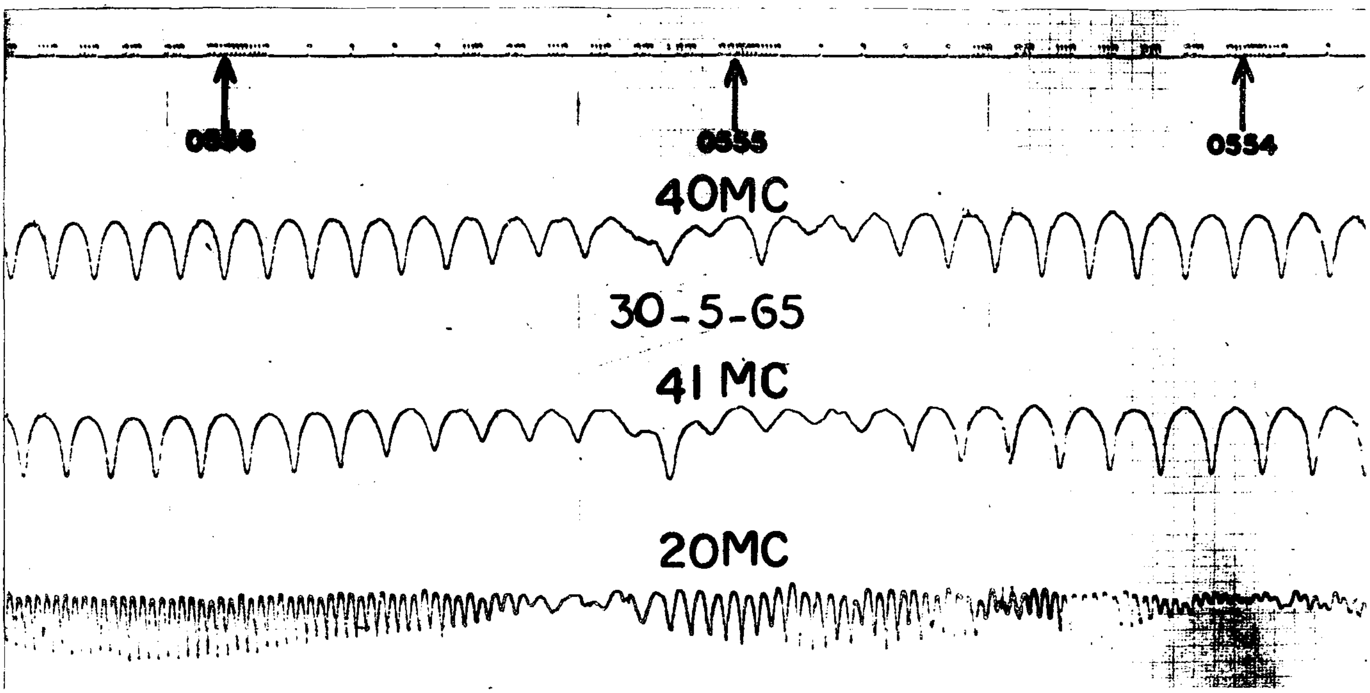

Fig.2.1 An example of a record showing Faraday fading of satellite signals. Quasi transverse (QT) region can also be seen on the record.

From equation (14) it can be seen that by finding the total rotation angle (Ω) experimentally and by calculating the magnetic field factor ($B \cos\theta \sec\chi$), the total electron content (N_T) can be determined. In practice it is generally not possible to measure the total angle of rotation. Instead, the rate of rotation and the number of complete rotations between two points on the orbit can be determined. In the following pages, the different methods of determining the total electron content will be described.

2.2 Methods of determination of N_T by measurements of Faraday rotation angle

The methods can be grouped into 3 categories :-

(a) Single frequency method,

(b) Multiple frequency methods and

(c) Closely spaced frequency method.

2.1.1 Single frequency method

If there is only one frequency available in the satellite, it is necessary to make use of the total angle of rotation (Ω) to calculate the total electron content. Unfortunately, under typical conditions Ω amounts to many complete revolutions so that the integral in equation (14) cannot be determined unambiguously. However, if the ionosphere is assumed to have no horizontal gradients and if the satellite is above most of the electrons in the ionosphere, then $\int n\, dh$ will be the same for any path. Consider the satellite to move from point 1 to point 2. The difference $\Omega_1 - \Omega_2$ is the differential rotation of the electric vector seen by the observer during this interval. The electron content can then be determined unambiguously as

$$\int n \; dh = \frac{\Omega_1 - \Omega_2}{M_1 - M_2} \; \frac{f^2}{K} \tag{15}$$

The method is called the differential rotation method. In this method, it is necessary to neglect the horizontal gradients in the ionosphere. The method was used at the time when satellites were transmitting at one frequency only.

2.1.2 Multiple frequency method

By having another frequency which is a higher multiple of the lower frequency, it is possible to make corrections for the high frequency approximations and for refraction. Yeh (1960) has derived the second order formulae for multiple frequencies. For this purpose it is convenient to use two harmonically related frequencies. The difference of the refractive indices ($\mu_0 - \mu_x$) can be derived from the Appleton - Hartree formula (Appleton, 1932). By using the higher order terms in the binomial expansion of Appleton Hartree formula, Yeh (1960) derived the equation giving integrated electron density correct to the second order. The formula is given by

$$\int n \; dh = \frac{f^2}{K(m^2-1)} \; \frac{m^4 \Delta\Omega_{(mf)} - \Delta\Omega_{(f)}}{M_1 - M_2} \tag{16}$$

in which $\Delta\Omega$(mf) and $\Delta\Omega$(f) are the rotations (in radians) of the frequencies mf and f observed as the satellite moves from point 1 to point 2, and M_1 and M_2 are the magnetic field factors for the two points.

2.1.3 "Closely spaced frequencies" method

The use of two closely spaced frequencies permits an unambiguous determination of the total angle through which the electric vector is rotated in traversing the ionosphere. The methods 2.1.1 and 2.1.2 require the calculation of ($\Omega_1 - \Omega_2$) which is the difference in the Faraday rotation angle as the satellite moves from point (1) to (2). It is necessary to assume that the total electron content is the same at points (1) and (2). In other words, it is necessary to assume that there are no horizontal gradients in the ionosphere. In the case of "Closely spaced frequencies" method, this assumption need not be made. In this method the difference in Faraday rotation angles of two closely spaced frequencies ($\Delta\Omega$) is determined. This angle can be used to calculate the total electron content. It is also possible to calculate the total rotation angle Ω from $\Delta\Omega$ The method of determination of $\Delta\Omega$ will be discussed later in this chapter. From equation (13)

$$\int n \, dh = \frac{f^2}{K} \frac{\Omega}{M} \tag{17}$$

$$\frac{d\Omega}{df} = -\frac{2\Omega}{f} \doteq \frac{\Delta\Omega}{\Delta f} \tag{18}$$

$$\Omega = -\frac{f}{2} \frac{\Delta\Omega}{\Delta f} \tag{19}$$

Knowing $\Delta\Omega$, Ω can be determined from equation (19). $\int N\, dh$ can be determined by substituting this value of Ω in equation (17).

2.3 Determination of N_T by Faraday rotation rate

The total electron content can be calculated by measuring the Faraday rotation rate also. Theoretically, a determination can be made for a given instant of time for a given ray path. In practice it is necessary to measure the number of revolutions of the plane of polarisation in a finite time in order to determine the rate accurately enough. The rate of rotation method constitutes the simplest means of obtaining an approximation of $\int N\, dh$.

The basic equation as derived by Bowhill (1958), is

$$\int n \, dh = \frac{z f^2}{K_1 H_x V_x} \dot{\Omega} \tag{20}$$

where $K_1 = \dfrac{e^3 \mu_0}{8\pi^2 m^2 c \epsilon_0}$ = 0.0297 (M.K.S. rationalised units).

z = altitude of the satellite in meters.

f = radio frequency in C.P.S.

H_x = component of earth's magnetic field in the direction of V_x.

V_x = horizontal component of the velocity of satellite with respect to the observer (meters/sec).

$\dot{\Omega}$ = rate of change of Faraday rotation angle in radians/sec.

This formula was derived under the assumptions of a horizontally moving satellite, a plane earth and a horizontally stratified ionosphere. Yeh (1960) has derived the second order formula for Faraday rotation rates also. The measurement of Faraday frequency is severely affected by the horizontal gradients of the total electron content, as can be seen by carrying out the differentiation of equation (14).

$$\frac{d\Omega}{dt} = \frac{K}{f^2}\left\{\frac{d(B\cos\theta\sec\chi)}{dt}\cdot\int n\,dh + \frac{d(\int n\,dh)}{dt}\cdot B\cos\theta\sec\chi\right\} \quad (21)$$

If $\int n\,dh$ is constant underneath the satellite path, $\frac{d\int n\,dh}{dt}$ becomes zero and it is straight forward to calculate $\int n\,dh$, knowing $\frac{d\Omega}{dt}$ and $B\cos\theta\sec\chi$

2.4 Errors in the calculation of N_T by Faraday rotation

2.4.1 High frequency approximation

In developing equation (14) it has been assumed that the operating frequency (f) > f_o (Critical frequency). When this is not the case an appreciable error is introduced. This error can be corrected to a first approximation by a correction factor to equation (14) which is a function of the maximum ionisation. When $f = 20$ Mc/s and $f_o = 10$ Mc/s one gets a correction of about 10 % for high satellite passes.

2.4.2 Path splitting

In the calculation of Ω it has been assumed that the ordinary and extra ordinary rays travel along the same path. When the angle of incidence gets larger than 45° this is no longer the case. As the refractive index for both rays is different it is clear that they will be bent differently and will follow separate paths. Hibberd (1959) shows qualitatively how this path splitting affects the Faraday rotation frequency.

2.4.3 Satellite spin

The plane of polarisation of the wave transmitted from a satellite depends on the momentary orientation of the satellite's antenna. A tumbling satellite will create an oscillating plane of polarisation. More precisely, let us assume that the satellite antenna is a dipole rotating around an axis at a certain angle to this dipole. The dipole will describe a cone. As Thomson (1958) has pointed out, the satellite spinning rate will add to the Faraday frequency if the observer is inside the cone described by the antenna. Only a phase wobble of the Faraday frequency will be generated when the observer is outside the cone. A Faraday record may, therefore, show a sudden jump in frequency when the observer's position relative to the satellite passes through the surface of the cone. This has been measured, for instance, by Blackband et al (1959) on Sputnik I. When a satellite has circularly polarised antennas, such as Explorer 7, the Faraday rotation is not affected by satellite spin except for a possible phase wobble. On the other hand, the depth of fading is influenced by the satellite orientation, as has been pointed out by Mass (1962).

2.4.4 Horizontal gradient in total electron content

If the electron density ($\mathcal{N}$) is a function of altitude only $\int \mathcal{N}\, dh$ is the same wherever measured, geographically. In reality $\mathcal{N}$ changes horizontally as well, so that it is not possible to neglect the horizontal gradient in $\int \mathcal{N}\, dh$. The differential Faraday rotation method on single frequency and multiple frequencies neglect this gradient. "Closely spaced frequencies" method is more suitable to determine the horizontal gradient in $\int \mathcal{N}\, dh$.

2.5 Desirable characteristics of a beacon satellite

Swenson (1963) described the desirable characteristics of a beacon satellite. In the previous section of this chapter the errors in the calculation of N_T have been described. Some of the errors can be minimised by having transmissions at various frequencies and by spin stabilising the space craft. The desirable characteristics of a beacon satellite are described below.

To give the widest geographical coverage and to permit studies of the polar ionosphere, the satellite orbit should be inclined approximately 90° from the earth's equatorial plane. In order to keep the satellite well above the regions producing scintillation and above most of the electrons in the ionosphere, the satellite altitude should be at least 1000 km. A circular orbit can simplify the analysis. An orbit meeting these criteria is relatively free from atmospheric drag, permitting accurate production of observation times and simplifying the computation of accurate post factum ephemerides.

In the past, considerable difficulty has been experienced as a result of spinning or tumbling of satellites. It is desirable either that antennas have electro-magnetic symmetry about the spin axis or that the satellite be spin-stabilised in such a way that the antenna aspect presented to a ground observer changes only very slowly.

It is very useful to have several transmitting frequencies and it is important that they be locked together in phase. Sufficient power must be radiated by the transmitters to permit reception with good signal-to-noise ratio even by simple equipment on the ground.

2.6 Early history of Faraday rotation experiments

The study of total ionospheric electron content through the Faraday effect on satellite signals began after the launching of the first satellite in 1957. Blackband et al (1959) published the first results of total electron content measurement by this technique. They were calculating the total Faraday rotation by counting the fading cycles from a point on the trajectory for which it was known that $\theta = 90^{\circ}$, which would give zero rotation. This method was also advocated by Garriott (1960). Unfortunately it is not always possible to record the satellite signal under these conditions. Also this procedure is somewhat doubtful due to nonvalidity of equation (14) in the neighbourhood of $\theta = 90^{\circ}$.

A more accurate approach is the one used by Little and Lawrence (1960) and by Rawer and Argence (1962). Here the procedure is inverted. One assumes a model ionosphere, the lower part of which is deduced from vertical soundings. The upper part is assumed to follow a certain form with one free parameter. A computer program uses the Appleton Hartree equation and calculates the polarisation rotation for several positions of the satellite. A comparison with the actual Faraday fading record will decide the best fitting parameters for the higher ionosphere. Little and Lawrence have good results in the cases where there are low horizontal gradients of total electron content. In the other cases they find no consistent results.

Garriott (1960a) used a slightly different approach to determine the actual number of rotations, in the cases where no QT conditions are recorded. In many cases he observes a reversal in direction of polarisation rotation. This occurs near the point where the satellite trajectory is perpendicular to the plane of the magnetic meridian. At the point of reversal the total rotation is at a minimum. Garriott calculates on a computer the ratio of rotations at the minimum and at closest approach. Knowing the absolute number of rotations between these two points, from the recordings, one can calculate the absolute number of rotations at the minimum and all along the path. Garriott (1960b) gives results of total electron content for one year using the Russian satellite, Sputnik 3.

Yeh and Swenson (1961) have used an approach based on equation (15) with high frequency corrections. These authors have given results of the total electron content for a period of more than one year.

Determination of Ω by means of "Closely spaced frequencies" has been tried by Evans et al (1961). They made use of the rotation of the plane of polarisation of moon reflected signals. The earlier artificial satellites were not provided with closely spaced frequencies. ~~In 1964~~ The Beacon Explorer - B satellite which was launched by the U.S.A. transmits radio signals on 40.01 MHz and 41.01 MHz. The method used in the thesis has been reported by Shirke and Ramakrishnan (1966).

2.7 Method of analysis at Ahmedabad

At Ahmedabad the method of "Closely spaced frequencies" has been used for calculating the total electron content. The method of scaling the Faraday fading records of 40 MC and 41 MC will be described in this section.

From equation (14), we know that

$$\Omega = \frac{K}{f^2} M \int_0^{h_s} n \, dh$$

Therefore,

$$\Omega_1 = \frac{K}{f_1^2} M \int n \, dh$$

$$\Omega_2 = \frac{K}{f_2^2} M \int n \, dh$$

where Ω_1 and Ω_2 are the Faraday rotation angles for the frequencies f_1 and f_2 respectively.

$$\Delta\Omega = \Omega_1 - \Omega_2$$
$$= K \left[\frac{1}{f_1^2} - \frac{1}{f_2^2} \right] M \int_0^{h_s} n \, dh \qquad (22)$$

$\Delta\Omega$ is determined experimentally by measuring the relative phases of the Faraday nulls received at 40 MC and 41 MC. Strictly speaking, $\Delta\Omega$ will be indeterminate by 'n' where 'n' is a small integer number if Δf is small. Little (unpublished) has suggested an arithmetical method of determining the value of 'n' for high latitude stations. In the present analysis, 'n' has been determined with reference to the QT region, where Ω and $\Delta\Omega$ reduce to zero. At Ahmedabad, which is a low latitude station in the northern hemisphere, QT region is located to the north of the station. As this region is approached, the satellite signal becomes elliptically polarised and the resulting amplitude record is characterised by shallow Faraday rules. The QT region can be seen on the record, which is shown in Fig.2.1. At Ahmedabad, it has been observed that the QT region can always be seen on the amplitude records of the polar satellite (BE-B, Explorer 22). In the case of low inclination satellite (BE-C Explorer 27) often the QT region is not seen. In such cases it is difficult to determine the total Faraday rotation angle (Ω) with respect to the QT region. But it is possible to judge the value of $\Delta\Omega$ without difficulty. Since both the satellites have been used for calculating the total electron content, the method of closely spaced frequencies has been used at Ahmedabad. Equation (22) has been used for calculating the total electron content. The calculation of $\Delta\Omega$ is done as follows :-

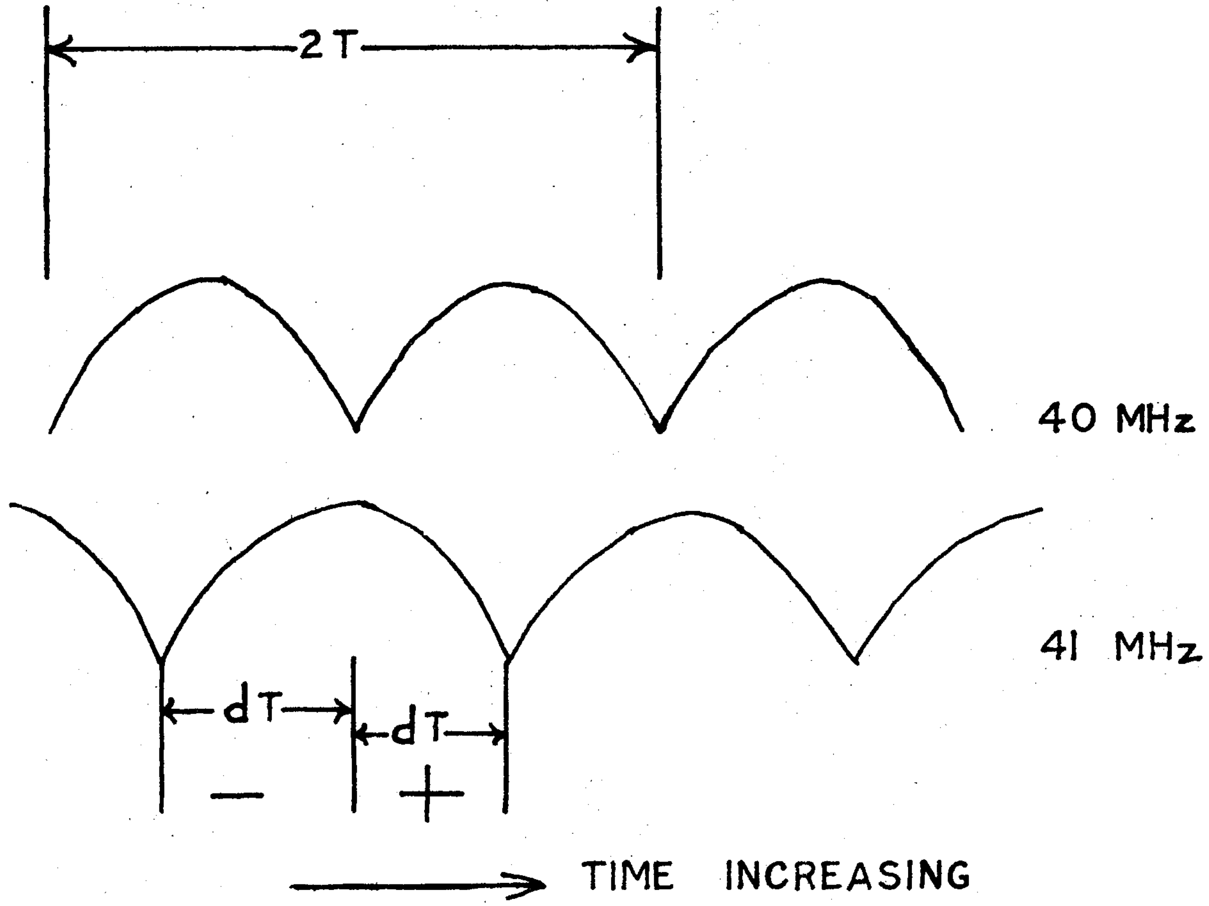

SCALING OF dT AND T FOR CALCULATING $d\Omega$

FIGURE 2·2

2.7.1 Calculation of $\Delta\Omega$

First it is found whether the transit is south-bound or north-bound. Since Ahmedabad is in the northern hemisphere the values of B Cos θ Sec χ increases towards the south of the station. Due to the increase of B Cos θ Sec χ, $\Delta\Omega$ also increases towards the south. So, in a south bound transit $\Delta\Omega$ increases with time and in a north-bound transit $\Delta\Omega$ decreases with time. Normally QT propagation occurs at a time when the sub-satellite latitude is about 29^{o}N. If QT point is seen on the record $\Delta\Omega$ is taken as zero at that time. $\Delta\Omega$ can be written in the form $\Delta\Omega = \delta\Omega + n$, where $\delta\Omega$ is the fraction and 'n' is an integer, which changes by one whenever the Faraday nulls of 40 MHz and 41 MHz coincide. The method of scaling of is illustrated in Fig.2.2.

$$\delta\Omega = \frac{\delta T}{T} \cdot \pi \qquad \text{radians.}$$

δT is scaled off in the positive direction (as shown in figure) if the region under consideration is after the occurrence of QT point. If this region is before the QT point δT is scaled in the negative direction. In Fig.2.3 the values of $\Delta\Omega$ and B Cos θ Sec χ are shown for a south bound transit. In Fig.2.4, the variations of these parameters are shown for a northbound transit. It can be seen that $\Delta\Omega$ becomes zero at the time when B Cos θ Sec χ becomes zero.

2.7.2 Calculation of sub-satellite points and B Cos θ Sec χ

The satellite orbital predictions are received from

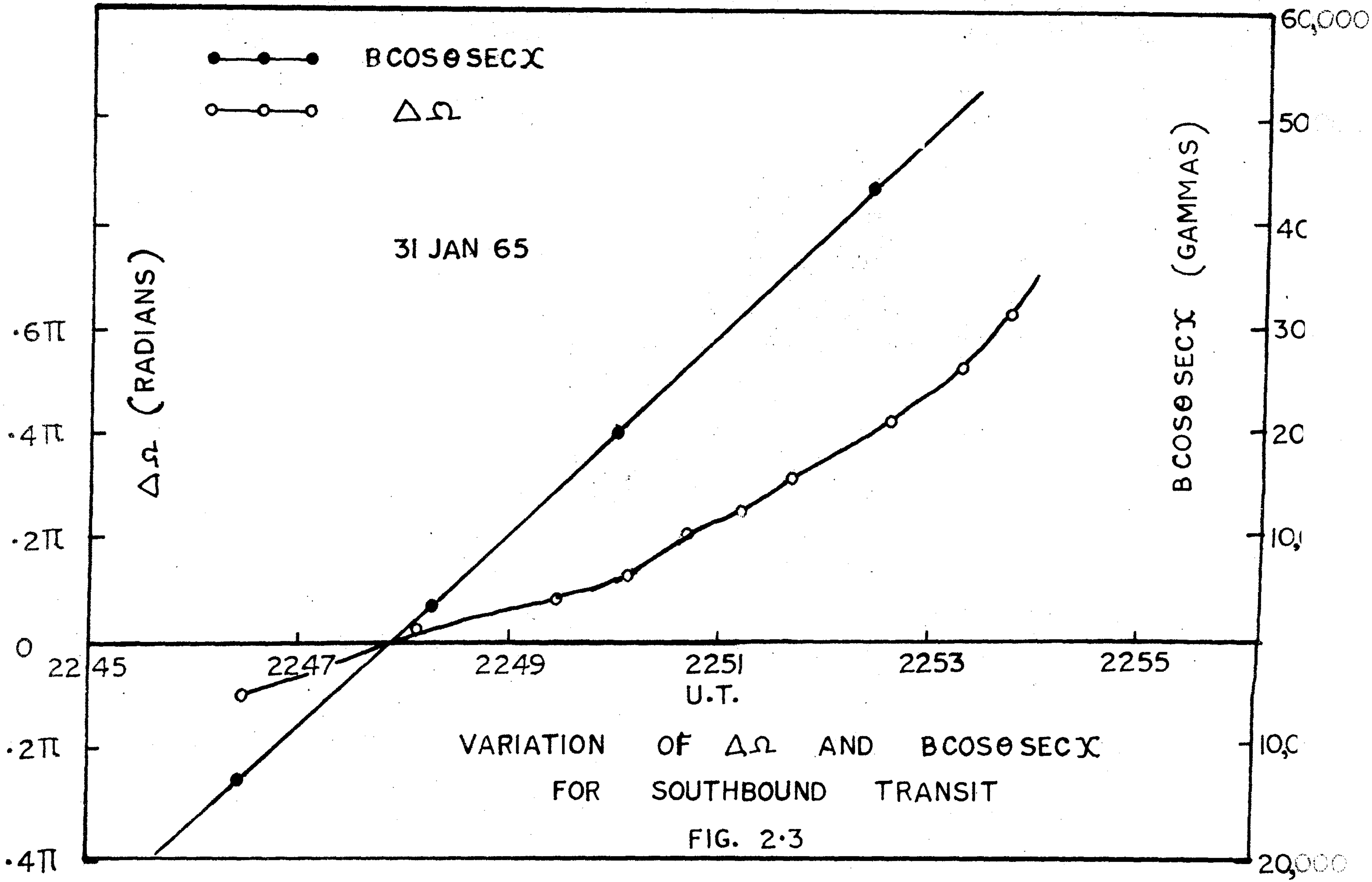

VARIATION OF ΔΩ AND BCOSθSECχ FOR SOUTHBOUND TRANSIT

FIG. 2·3

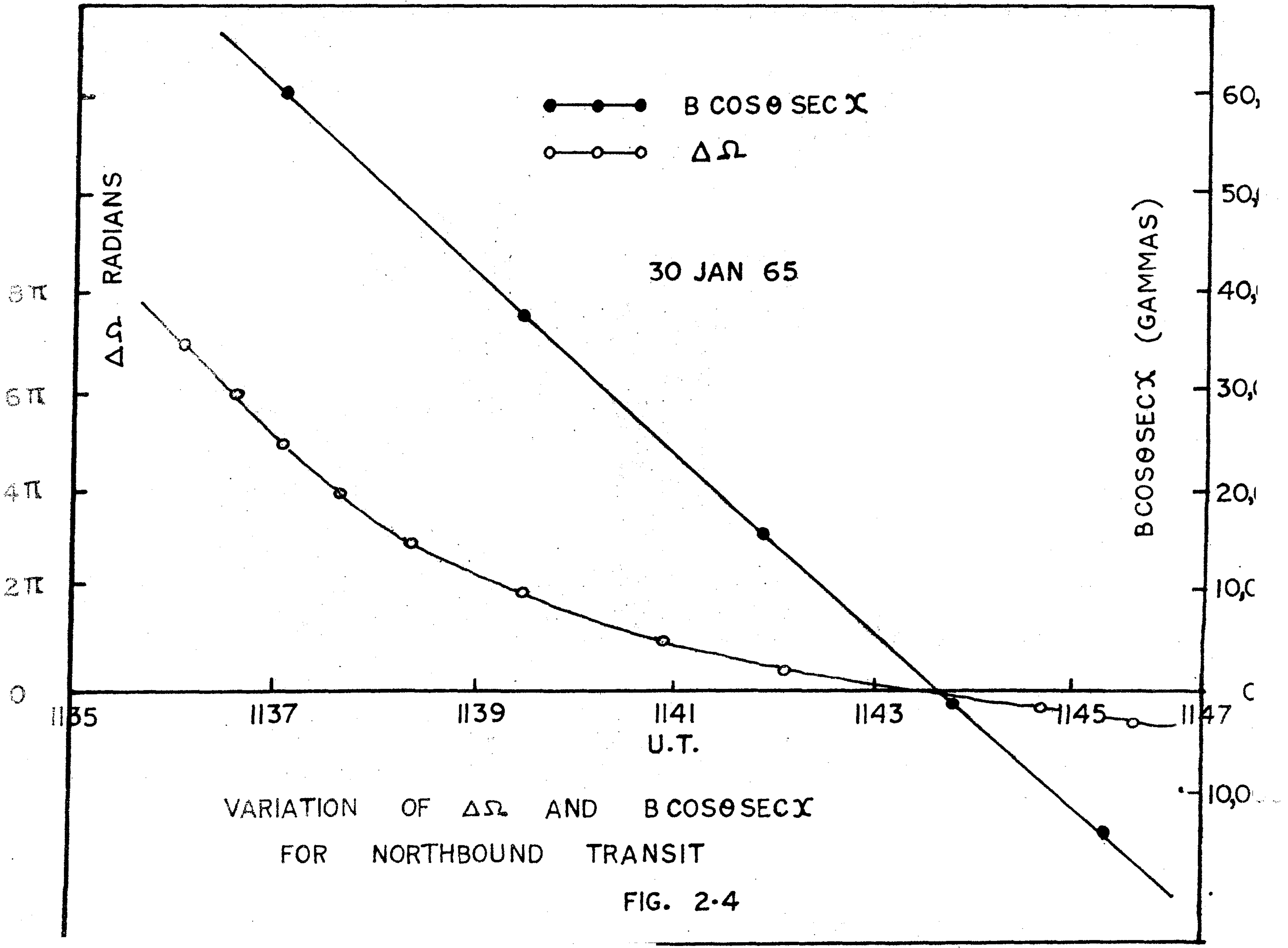

VARIATION OF ΔΩ AND B COS θ SEC χ
FOR NORTHBOUND TRANSIT

FIG. 2·4

Goddard Space Flight Centre, U.S.A. These bulletins are divided into three parts. The first part gives the orbital parameters, the second part gives the equatorial crossing times and the corresponding west longitudes, and the third part gives the time and longitude corrections to be applied to get the crossing times and west longitudes corresponding to each 10^{o} latitude. A computer program has been worked out to use all this information and calculate the geographical position of the satellite at the times when the satellite reaches each latitude between the equator and 40^{o}N latitude.

The values of B Cos θ Sec χ for different satellite heights and sub-satellite points have been provided by Goddard Space Flight Centre, U.S.A. Knowing the sub-satellite point and the height of the satellite, the appropriate values of B Cos θ Sec χ are found from the tables provided by the Goddard Space Flight Centre.

2.8 Second order corrections for closely spaced frequencies method

The Faraday rotation equations have been extended to include second order effects, (Ross, 1965). First order theory is based on straight line propagation and the second order theory takes into account the following departures from this condition:-

(1) The non-uniform distribution of ionisation causes the various rays to be refracted and follow different paths between source and receiver.

(2) Since the medium is anisotropic, the wave normal and ray for a particular mode of propagation do not coincide in direction.

Ross (1965) introduced the following relation correcting the first order equation to

$$\Omega = \frac{K}{f^2}(B \cos\theta \sec\chi)(1+\alpha)\int_0^{h_s} n\, dh \tag{23}$$

Where

$$\alpha = \frac{\bar{X}}{2}\left[\beta + (\beta - 1)G\right]$$

$$\bar{X} = \frac{4.91 \times 10^{-14}}{h'} \cdot \int_0^{h_s} n\, dh$$

$$h' = h_s + R_e(1 - \cos\chi)$$

R_e = Radius of the earth.

$\beta = \frac{\overline{X^2}}{\bar{X}^2}$ = a measure of the non-uniformity of the ionisation distribution over the height of integration.

G = $\tan\theta\,(\tan\theta - Y_1/Y_L)$

Y_1/Y_L = ratio of transverse to longitudinal components of magnetic field.

When second order corrections are included, equation (19) is modified as

$$\Delta\Omega = -2\Omega\,\frac{\Delta f}{f}\,(1+2\alpha)$$

By measuring $\Delta\Omega$ and Ω it is possible to judge whether the second order correction is significant or not. If the correction is insignificant the ratio,

$$\frac{\Omega}{\Delta\Omega} = \frac{f}{2\Delta f} = 20$$

At Ahmedabad, it has been experimentally observed that the ratio $\Omega/\Delta\Omega$ comes out to nearly 20 at the time when the satellite crosses 23°N latitude. In the present analysis, total electron contents have been calculated only for 23°N latitude and the second order corrections have not been applied.

CHAPTER III

EXPERIMENTAL DETAILS

3.1 Description of Ionospheric Beacon Satellite

3.2 Description of the receiving system

3.3 Description of the local time standard and time synchronising

3.4 Schedule for satellite tracking

3.5 Satellite prediction.

CHAPTER III

EXPERIMENTAL DETAILS

The requirements of a beacon satellite for ionospheric studies have been explained in Chapter II. In this chapter, the actual details of the two beacon satellites which were launched by the U.S.A. are described. A description of the system installed at Ahmedabad for receiving the beacon satellite signals have also been described. The method of synchronising the local time standard against standard time signals is explained. The details of Binary Coded Digits (BCD) used in the local time-standard are given in this chapter along with an explanation of the time code.

3.1 Description of Ionosphere Beacon Satellite

The Explorer 22 research satellite, known as Beacon Explorer-B or S-66, was launched by means of a Scout rocket on October 9, 1964 from Vandenberg Air Force Base, U.S.A. The satellite went into orbit with an inclination of 79°, an apogee of 674 miles and a perigee of 546 miles. The initial orbital period was 104.7 minutes.

The Explorer 27 satellite, known as Beacon Explorer-C, was also launched by a similar rocket on April 29, 1965 from the same launching site. This satellite went into orbit with an inclination of 41°, an apogee of 821 miles, and a perigee of 580 miles. The initial period was 108 minutes.

Both the Beacon Explorers are identical in construction. The satellite weighs 116 lbs and consists of an octagonal, cylindrical shell from the sides of which four solar panels extend like wind mill blades. Made of honey comb nylon and fibre-glass, the shell is 12 inches in height and 18 inches in diameter. The solar panels are 10 inches wide and 5.5 feet long and contain twice as many solar cells as are needed for initial power. As the cells deteriorate because of radiation effects, reserve banks of solar cells will be brought into operation. Extending from the ends of opposite solar panels are two 5 feet long whip antennas, which radiate 20.005 Mc/s, 40.01 Mc/s and 41.01 Mc/s frequencies. Two bar magnets 5.75 in long are used for passive orientation of the satellite. They align it along the magnetic field.

To protect the instruments from the large temperature variations, vacuum insulation is provided between the instruments and the satellite shell. When the internal temperature of the space-craft drops below the desired 21^{o}C, any one of the eight thermostats located throughout the satellite triggers an adjacent heater. Centrifugal force causes the weighted anti-spin cables to deploy and allows the four solar panels to erect themselves. The first of these two actions causes the spin rate to be reduced from 160 revolutions per minute to about 40 R.P.M. and the solar panel deployment then lowers the rate to around 3 R.P.M. The rate is then gradually reduced to zero by magnetic anti-spin rods.

The S-66 satellites have three basic transmitting systems. (1) The NASA Ionospheric Beacons at 20, 40, 41 and 360 MHz, (2) the APL Doppler System at 162 and 324 MHz and (3) the telemetry transmitter at 136 MHz. The ionospheric Beacon frequencies are derived from a 5 MHz oscillator, which is enclosed in a package containing a dual oven with high thermal stability. The transmissions are coherent. All the low frequency transmitters radiate 250 m W of power approximately.

A clock marker or timing pulse appears on the 20 MC signal. This modulation is a rectangular pulse, which occurs every 22.018 second. Explorer 22 provides one pulse and Explorer 27 provides two pulses. These timing pulses can be utilised as identification marks for the two satellites. The signal for the timing marks are derived from a tuning fork oscillator with a stability of 1 part in 10^9.

The antennas for 20 MC, 40 MC and 41 MC transmissions consist of whip antennas, 5 feet long, at the end of two oppositely oriented solar panel blades. The signals are linearly polarised.

3.2 Description of the receiving system

Fig.3.1 shows the block diagram of the receiving and recording system. The dipole antennas are erected in the EW direction at a height of $\lambda/4$ from the ground. EW direction has been chosen so that the antenna receiving pattern is symmetrical in the NS direction. Most of the favourable transits are in the north-south direction and it is preferable to have the receiving pattern of the dipole antenna symmetrical in the NS plane. The

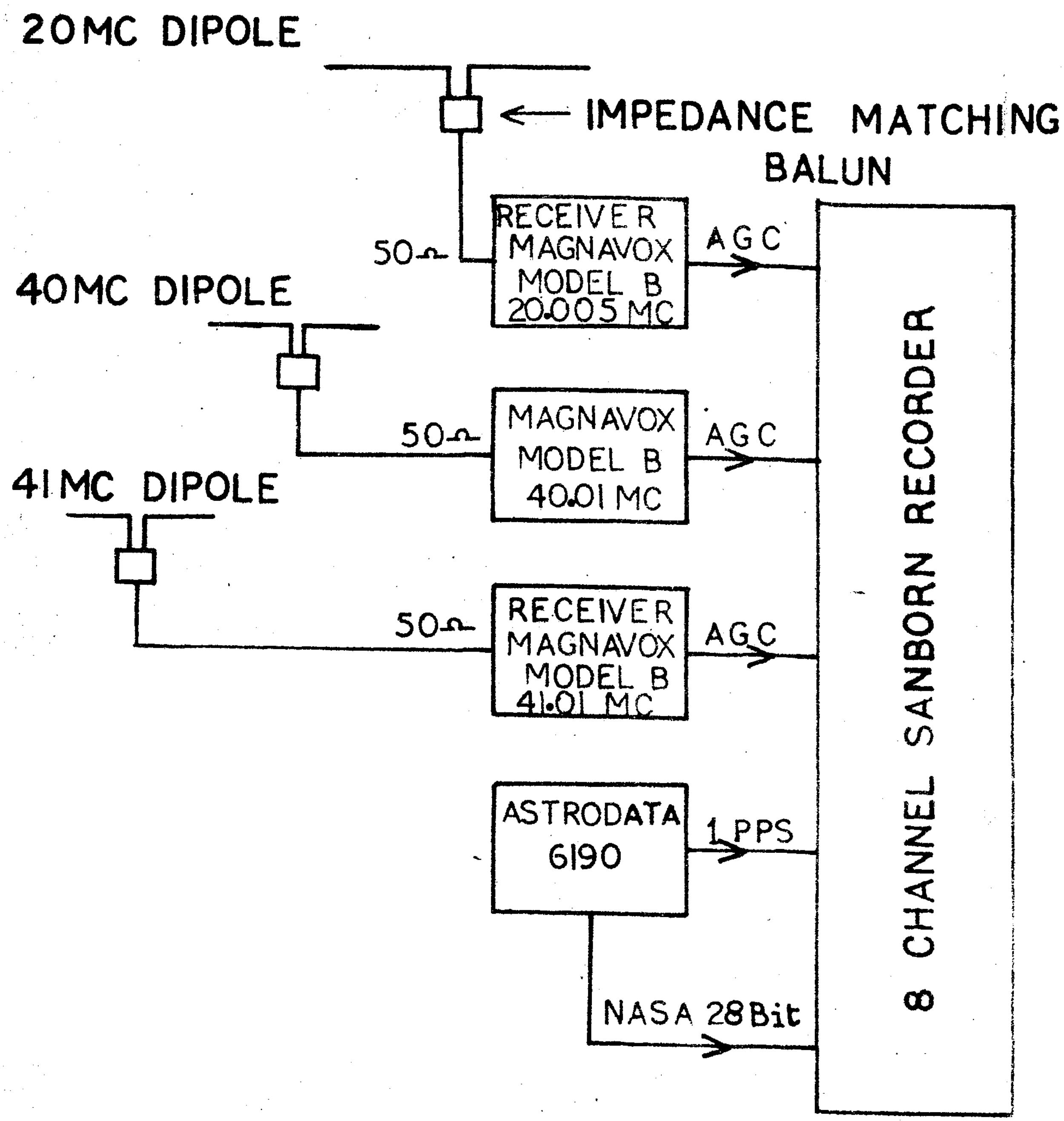

RECEIVING SYSTEM FOR RECORDING SATELLITE SIGNALS AT AHMEDABAD

FIGURE 3·1

receivers have unbalanced inputs with an impedance of 50 Ω. The dipole antenna gives an impedance of 75 Ω (balanced). Impedance matching is achieved by using a wide band "BALUN" matching transformer. This impedance matching transformer is mounted near the antenna itself. Amphenol RG-8/u, coaxial transmission line is used to connect the antenna output to the receiver input.

Fig.3.2 shows the block diagram of the transistorised receiver used for receiving the satellite signals. It is a double conversion receiver employing crystal controlled local oscillators. The pre-amplifier section of the receiver is a fully shielded plug-in unit. By inserting the appropriate pre-amplifier into the front panel of the main receiver, the receiver frequency can be altered. The pre-amplifier plug-in unit contains a single RF stage, a mixer stage and an oscillator stage. This gives an output at 4.790 Mc/s. The RF amplifier provides approximately 35 db gain. The mixer stage has a conversion gain of 5 db.

The front end unit contains the first I.F. stage, the second local oscillator, the second IF amplifier, the second detector and the audio stage. The second local oscillator is crystal controlled at 5245 Kc/s. This stage performs the function of converting the 4.790 MC output of the pre-amplifier into a 455 KC second IF. The automatic gain control (AGC), incorporated into the circuitry, controls the gain such that it is logarithmically related to the magnitude of the incoming signal. The second IF stage has a gain of 90 db. Complete electrical specifications of the receiver are given below :

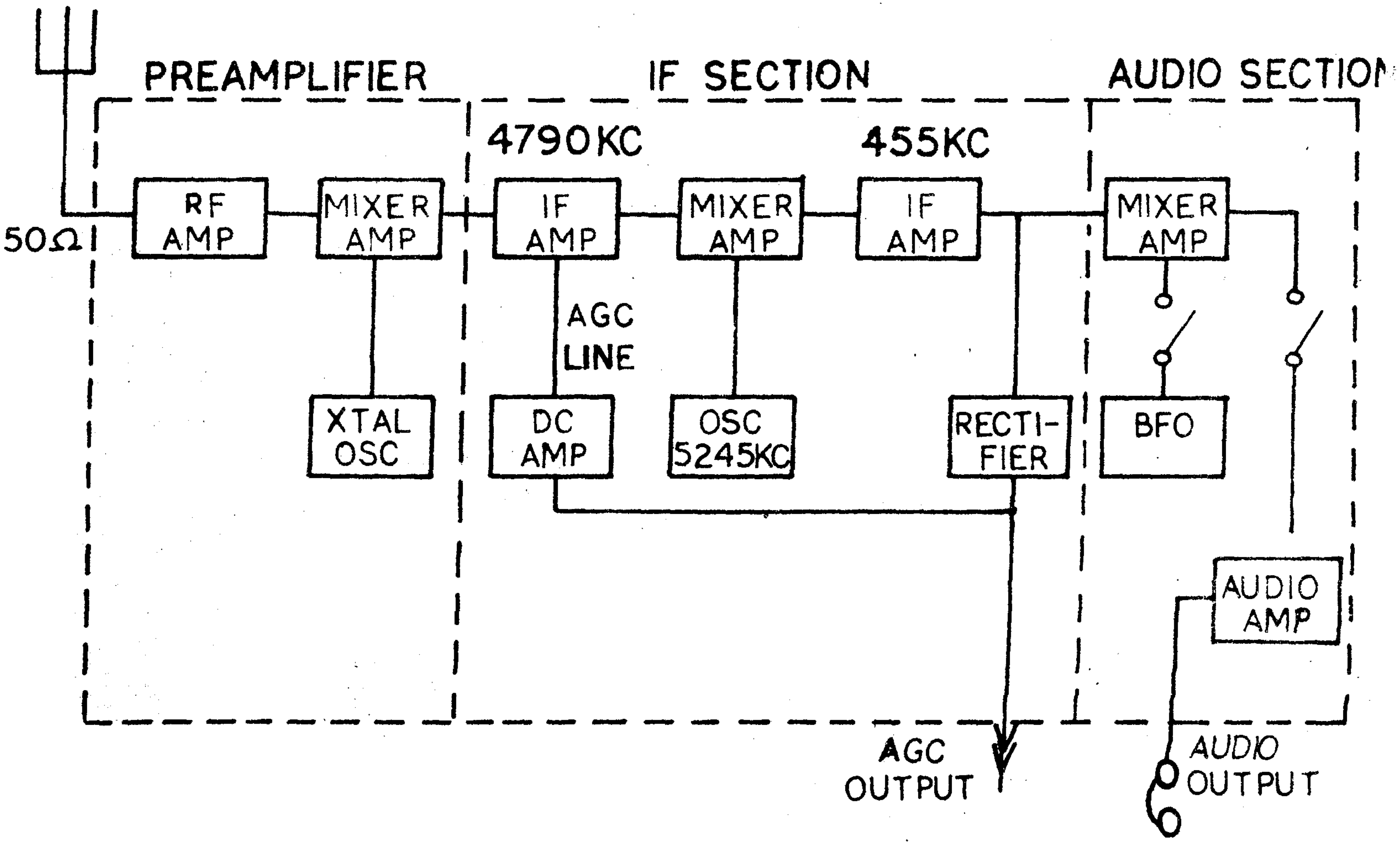

BLOCK DIAGRAM OF THE RECEIVER

FIGURE 3.2

(1) Voltage requirements are + 8.4 V and -12.4 V D.C. The total current drain of each receiver is nominally 15 milli amperes.

(2) The sensitivity of the receiver is -135 dbm.

(3) Bandwidth of the receiver at 3 db points is 2500 CPS.

(4) The AGC output impedance is 15 KΩ and the AGC time constant is 8 milli seconds.

Due to the velocity of the satellite, the signal undergoes Doppler Shift. Consequently the frequency received on the ground gradually changes as the satellite approaches the tracking station and recedes from the tracking station. The 2.5 Kc bandwidth provided for the receivers is sufficient to accommodate the Doppler shift.

The receivers require a positive voltage (+ 8.4) and a negative voltage (-12.6) for the operation. A twin power supply whose voltages can be varied is used as the power supply for the receivers. This unit has two independent D.C. supplies with independent output terminals. The $+^{ve}$ terminal of one of the supplies is connected to the $-^{ve}$ terminal of the other supply and is used as the common terminal for the receiver. With respect to this common terminal the positive and negative DC voltages are taken from the Power Supply and fed to the receivers.

The AGC output of the receiver is fed to DC amplifier manufactured by Sanborn Company. The DC amplifier drives the galvanometer of Sanborn Strip Chart recorder. The frequency response of the recording system is from 0 to 50 cycles. The strip chart recorder used for the experiment has 8 channels. At a time, 5 channels are used. Once the paper is completed, it is rewound and used again. Two channels are used twice by shifting the position of the stylus. These two channels are used for recording the time marks only. The chart speed of the recorder can be varied from 0.25 mm/sec to 100 mm/sec. Depending on the rate of fading of the signal, the chart speed is adjusted at the time of transit. The overall gain of the whole system is approximately 145 db.

Amplitude calibration is not necessary for Faraday rotation analysis. Since the AGC of receiver has logarithmic response, amplitude calibration is necessary for studying the signal scintillations. A standard signal generator (HP 608D), manufactured by Hewlett Packard, U.S.A., is used for calibrating the recording system.

3.3 Description of the time standard and time synchronisation

Since the satellites move with very high velocity it is necessary to have a time standard, which is correct upto a fraction of a second with respect to standard time signals. At Ahmedabad, a time standard manufactured by the Astrodata Company has been used. This time standard gives an output of 1 pulse per second, which is derived from a crystal controlled 1 MHz oscillator having very high stability.

Many countries broadcast standard time signals in the H.F. band. The frequencies allotted for time signals are 2.5 MC, 5 MC, 10 MC, 15 MC, 20 MC and 25 MC. At Ahmedabad 10 MC and 15 MC transmissions from Japan or HaWaii(WWVH) are used for synchronising the local time standard. The time standard is adjusted to an accuracy of a fraction of a millisecond and is never allowed to have an error more than about 100 milli second at the time of recording a satellite transit.

Fig.3.3 shows the block diagram of the system adopted for synchronising the time standard with respect to the standard time signal transmissions. Motorola R - 390 receiver was used for receiving J.J.Y. or WWVH time signal transmission at 10 MC or 15 MC. During day time 15 MC and during night time 10 MC transmissions were used. Every 5 minutes both these stations announce Japan standard time and Hawaii standard time respectively. In addition to the time announcement, the carrier has 1 pulse per second modulation also. The audio output of R-390 receiver, which gives standard one pulse per second, is fed to the Y input of a Tektronix oscilloscope. The time base of the oscilloscope is put into external trigger mode and is then triggered by the one pulse per second output of the local Astrodata time standard. If the Astrodata time is ahead of the standard time, then one pulse per second output of R-390 can be seen on the oscilloscope time base. The local time standard is then adjusted so that the triggering pulse coincides with the standard time signal pulse. By adjusting the sweep interval of the oscilloscope it is possible to see the

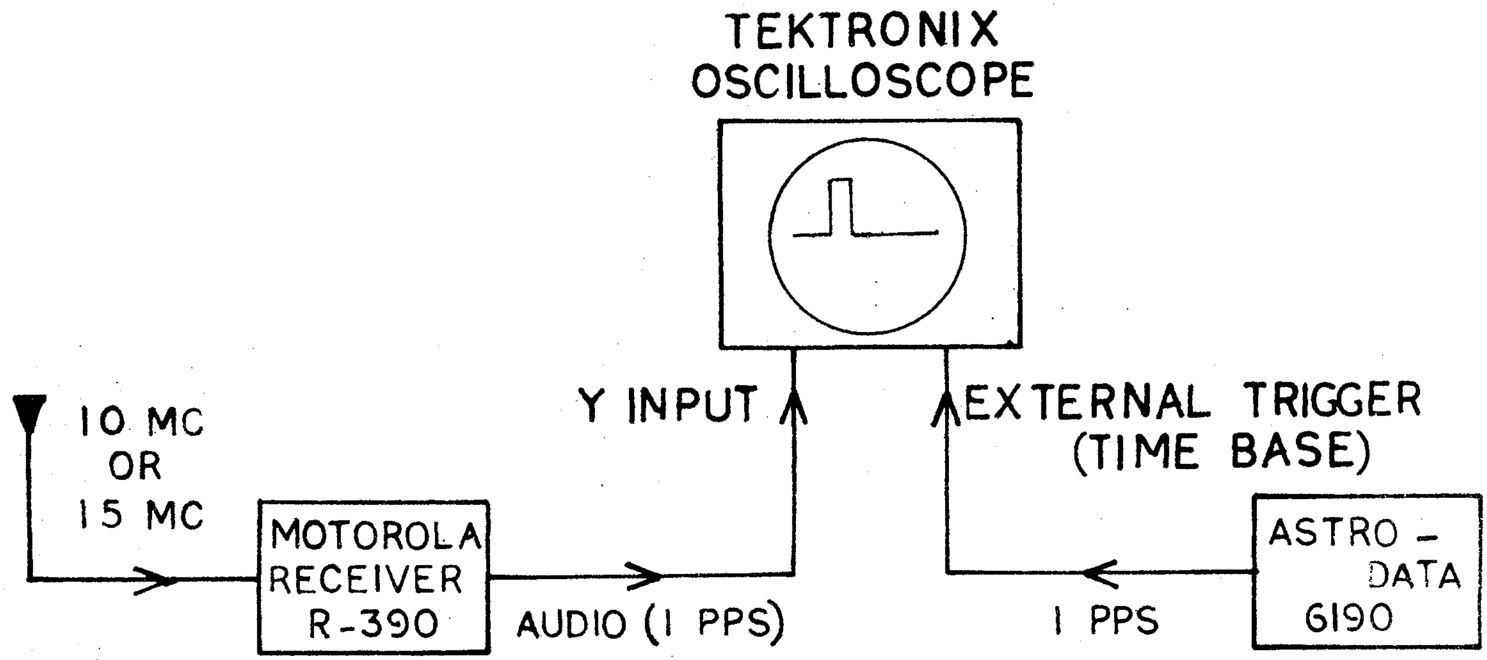

FIGURE 3.3

SYSTEM USED AT AHMEDABAD FOR SYNCHRONISING LOCAL TIME STANDARD (ASTRODATA MODEL 6190) AGAINST JJY OR WWVH TIME SIGNALS two pulses clearly even when the time difference between them is about a milli second. The Astrodata time standard used at Ahmedabad is found to be quite accurate and does not drift by more than 1 milli second per day. The time standard is fed by AC mains supply, which is quite reliable at Ahmedabad. Every week the local time standard is checked against JJY or WWVH.

In addition to one pulse per second, Astrodata gives coded outputs also. Fig.3.4 gives the NASA 28 Bit Code, which is in binary coded decimal form. The code is composed of a reference marker and seven sub-code words describing Time-of-year in minutes, hours and days. Each sub-code is in binary coded decimal fashion. The leading edges of all pulses are precisely spaced at 0.5 second intervals. The "time frame" is completed by index markers occurring every 5 seconds.

Fig.3.4 shows one complete frame of the time code. One frame is completed in one minute. In the figure, the frame is split into two parts. The lower portion shows the former half (30 seconds) and the upper portion shows the latter half (30 seconds) of one complete frame. Two narrow pulses, (A) and (B), indicate the beginning of each frame. In the figure, the time increases from A to B. After each 5 seconds, the 5th second identification pulse (wide pulse) can be seen. The time codes are given in the former half of the frame. After each 5th second mark, the time code is given. The code starts with the unit digit of minute and ends with the hundredth digit of number of days.

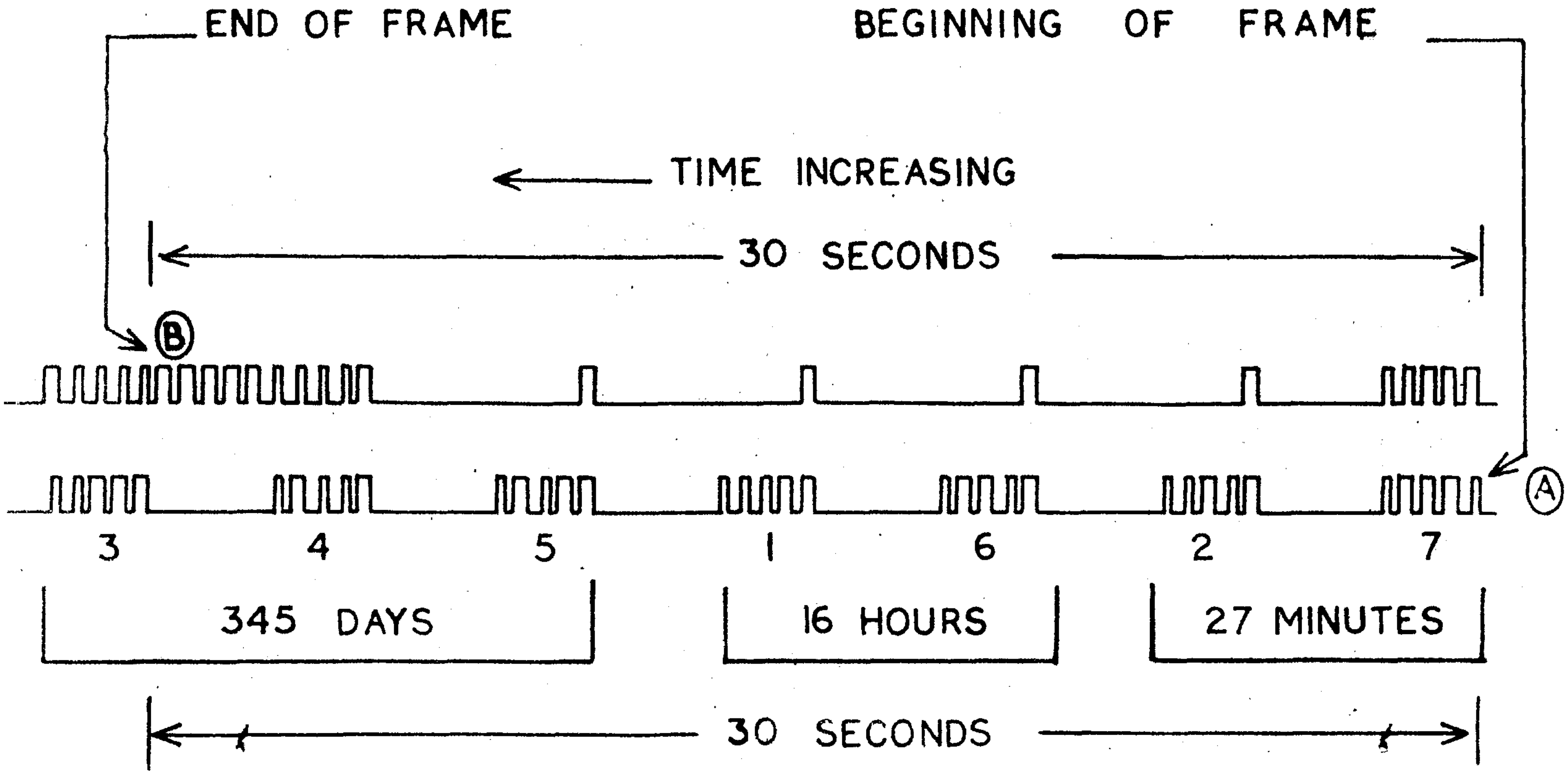

ONE MINUTE FRAME OF ASTRODATA TIME-CODE

NASA 28 BIT CODE

FIGURE 3.4

In the example shown in Fig.3.4, the time given by the code is 16 hours 27 minutes. The number of the day given by the code, is 345. So, the time code identifies the numbers 7, 2, 6, 1, 5, 4 and 3 in the order. The number of the day are counted from the 1st of January. Each digit is given by a group of 4 binaries. The numbers can be read-off very easily. In order to see the pulses clearly the chart speed must be at least 2.5 mm/sec.

The method of reading the binary coded digits is illustrated in Fig.3.5. The system gives either a wide pulse or a narrow pulse as shown in the figure. By noting the stages which give narrow and wide pulses, the number can be made out. Fig.3.5 shows the configuration of the pulses in the group of four binaries in order to give the numbers from 0 to 9. By noting the number given by each of the seven groups in a minute frame, it is possible to find out the time at any point on the record.

3.4 Schedule for satellite tracking

For programming the routine schedule for tracking the satellite, it is necessary to know the time when the satellite comes over the tracking station and the maximum elevation angle of the satellite at the time of closest approach. Depending on the maximum elevation angle, it is decided whether a particular transit is to be followed or not. During the period of observation, only the transits, which gave more than 30° elevation, were tracked for Faraday rotation studies. In order to study the satellite signal scintillations at night, this limit of elevation angle was brought down to about 20°.

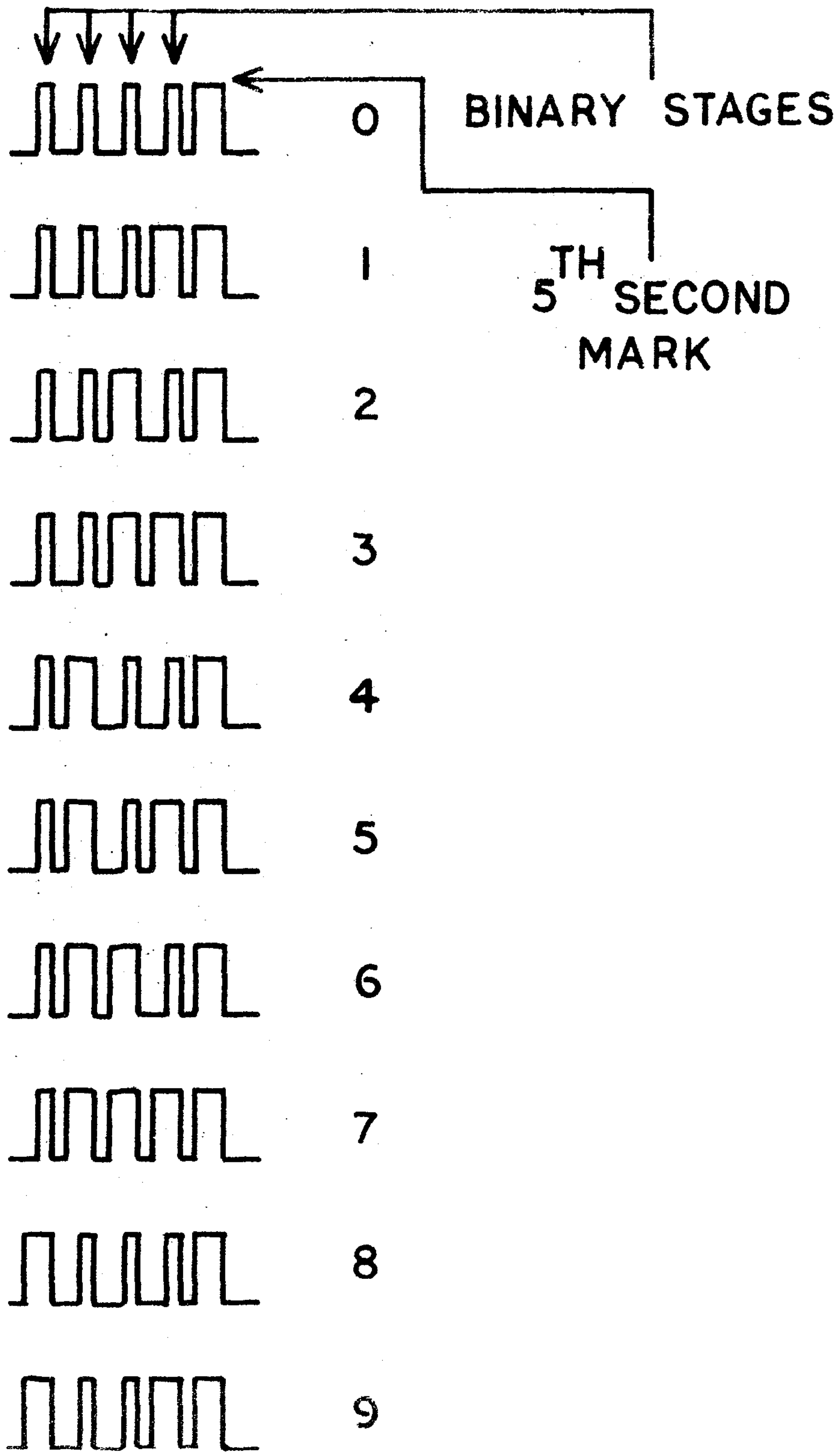

ILLUSTRATION OF
BINARY CODED DIGITS

3.5 Calculation of satellite prediction

In section 2.7 of Chapter II, the details of NASA satellite orbital bulletins have been given. The calculation of sub-satellite points is also described. Knowing the sub-satellite point and the height of the satellite, it is possible to calculate the azimuth, elevation and slant range of the satellite. These parameters are essential if the receiving antenna is to be pointed towards the satellite. Fixed dipole antennae had been used for the Faraday rotation experiments and so it was not necessary to know the position of the satellite very accurately for tracking it. Still, the elevation, azimuth and slant range of the satellite were calculated and were used for deciding the transits that were to be followed.

CHAPTER IV

ELECTRON CONTENT OVER AHMEDABAD

CHAPTER IV

ELECTRON CONTENT OVER AHMEDABAD

The method of analysis adopted at Ahmedabad for calculating the total electron content upto the satellite altitude has been described in section 2.6 of Chapter II. The result of these calculations are presented in this chapter. At the time of a satellite transit, normally an ionogram is also taken. This ionosonde is located near the satellite tracking station. These bottom side ionograms are used for comparing the top side of the ionosphere with the bottom side.

4.1 Diurnal and seasonal variations of total electron content (N_T)

Because of the relative motion of the satellite and earth, one measurement of electron content per day, on the average, is obtained when the satellite passes near the observing station in a northward direction. Another measurement is made when the satellite again passes near the station in a southward direction. With two satellites in orbit it was possible to make four measurements per day. As a consequence of the precession of the satellite orbit the times of passage receded on the average from day to day and it was possible to sweep through a 24 hour period more than once within a season of 4 months. All the observations made in each season have been grouped together.

The values of total electron content determined at various hours for summer, winter and equinox are shown in Figs. 4.1, 4.2 and 4.3 respectively. The diurnal variation of N_T can be seen in all the three seasons. Since the observations were made on different days, the N_T values exhibit scatter showing the variability of the ionosphere. A mean curve can still be drawn through the scatter points. The maximum value of N_T occurs at about 14 hours in winter and summer and at about 16 hours in equinox. The total electron content starts falling after sun set to a pre-dawn minimum and then starts rising after sun rise to the day time maximum. The rate of increase seems to taper off between 09 hours and 10 hours in winter, between 08 hours and 09 hours in equinox and between 07 hours and 08 hours in summer. The day time maximum value is about 2 x 10^{17}/meter^2 in winter, 3.2 x 10^{17}/meter^2 in summer and 3.8 x 10^{17}/meter^2 in equinox. The night time minimum value of N_T is about 0.16 x 10^{17}/meter^2 in winter and summer and 0.14 x 10^{17}/meter^2 in equinox. It can be seen that the day time maximum undergoes more seasonal change than the night time minimum. The diurnal range is about 12 in winter, 20 in summer and 27 in equinox.

4.2 Rate of loss of electrons at night

The rate of change of electron density at a given height is determined by

$$\frac{\partial n}{\partial t} = q - \beta n - \mathrm{div}(nV) \qquad (1)$$

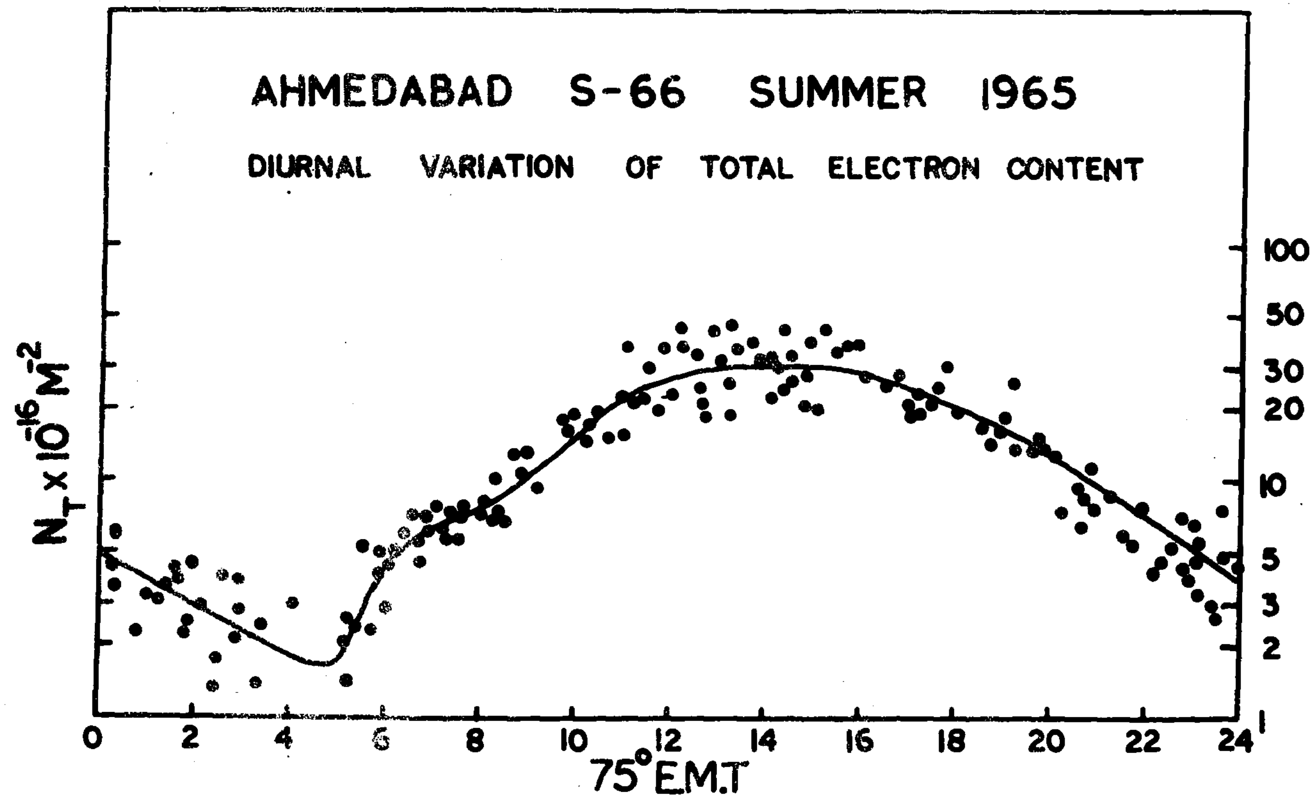
AHMEDABAD S-66 SUMMER 1965
DIURNAL VARIATION OF TOTAL ELECTRON CONTENT
$N_T \times 10^{-16} M^{-2}$
100
50
30
20
10
5
3
2
1
0
2
4
6
8
10
12
14
16
18
20
22
24
75° E.M.T

FIG. 4·1

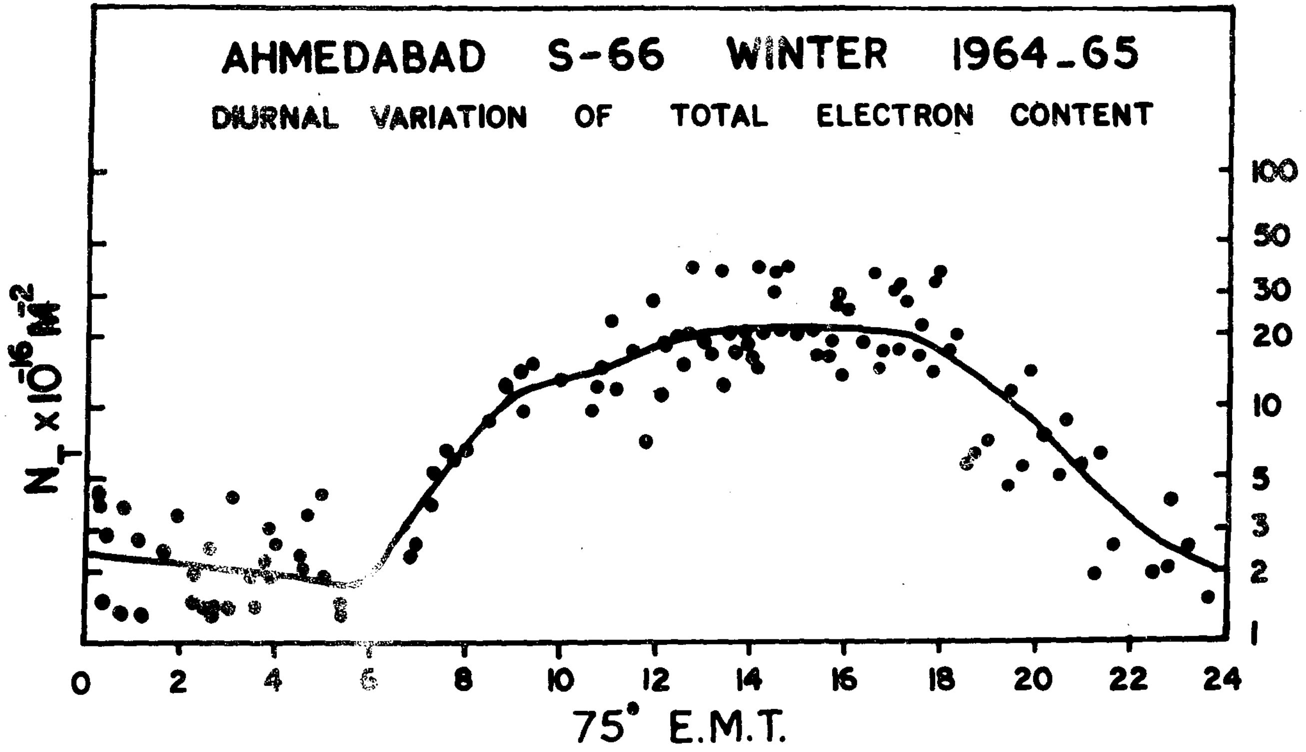
AHMEDABAD S-66 WINTER 1964-65
DIURNAL VARIATION OF TOTAL ELECTRON CONTENT
$N_T \times 10^{-16} M^{-2}$
100
50
30
20
10
5
3
2
1
0 2 4 6 8 10 12 14 16 18 20 22 24
75° E.M.T.

FIG. 4·2

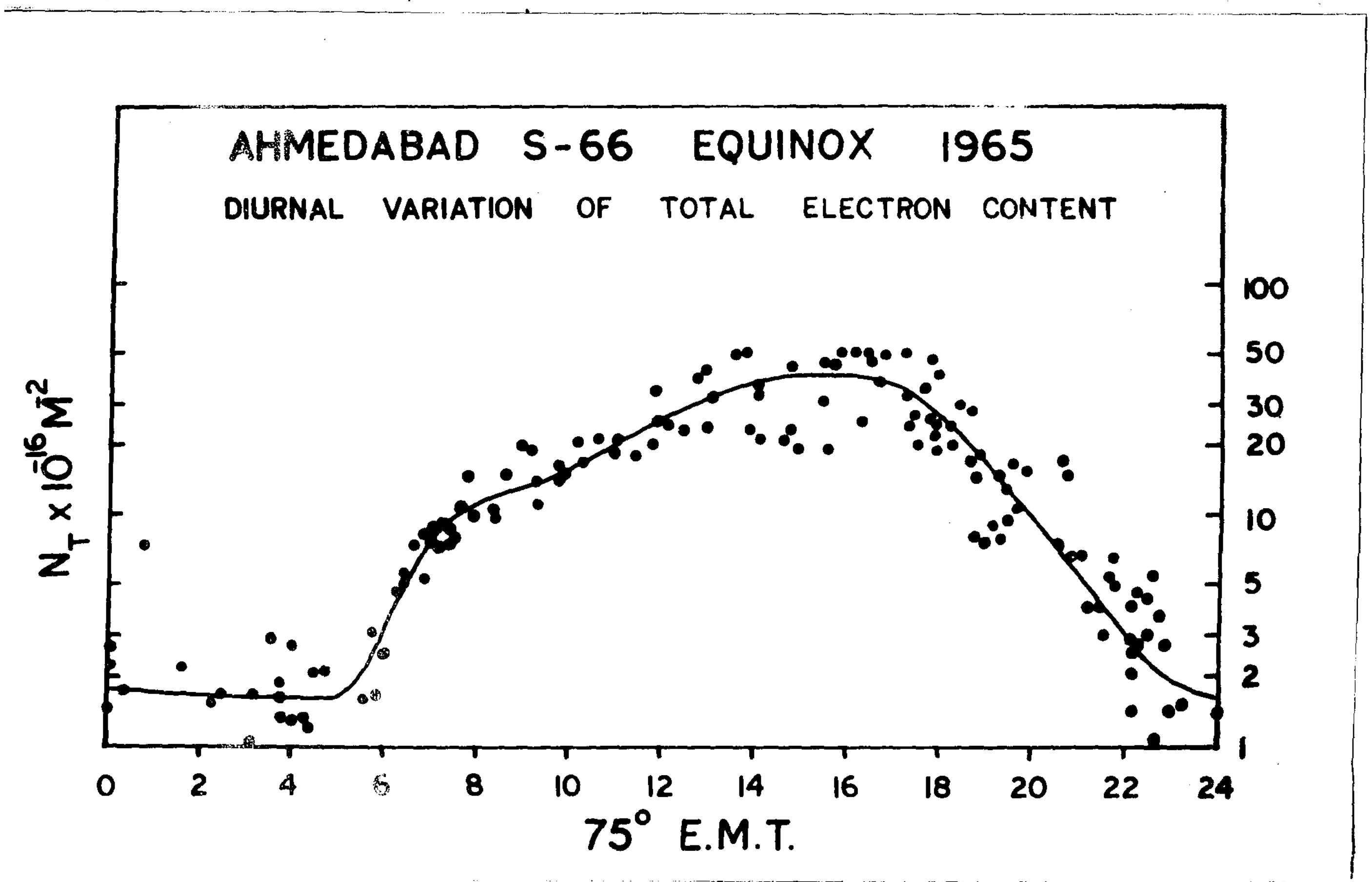
AHMEDABAD S-66 EQUINOX 1965
DIURNAL VARIATION OF TOTAL ELECTRON CONTENT
$N_T \times 10^{-16} M^{-2}$
100
50
30
20
10
5
3
2
1
0
2
4
6
8
10
12
14
16
18
20
22
24
75° E.M.T.

FIG. 4·3

where q is the number of electrons produced per unit volume per second, β is the effective attachment coefficient and V is the velocity of transport of electrons. The loss process has been written in the form of βn because most of the loss of ionisation at night takes place in the lower F region where the attachment process is predominant.

The rate of change of total content is obtained by integrating equation (1) over all heights, viz. the surface of an infinite vertical cylinder of unit cross section. This gives

$$\frac{dN_T}{dt} = \frac{\partial\left(\int_0^\infty n\,dh\right)}{\partial t} = \int_0^\infty q\,dh - \int_0^\infty \beta\,n\,dh - \int_0^\infty \mathrm{div}\,(nV)\,dh$$

If the velocity of transport is entirely vertical, the net transport of electrons out of the cylinder is zero,

$$\int_0^\infty \mathrm{div}(nV)\,dh = 0$$

Therefore
$$\frac{dN_T}{dt} = \int_0^\infty q\,dh - \int_0^\infty \beta n\,dh \qquad (2)$$

Thus at night time, when q is zero

$$\frac{dN_T}{dt} = -\int_0^\infty \beta\,n\,dh = -\bar{\beta}\int_0^\infty n\,dh = -\bar{\beta}\,N_T$$

where $\bar{\beta}$ is some mean value of β. It follows that

$$N_T(t) = N_T(t=0)\,\exp(-\bar{\beta}t)$$

The night time portions of the curves of log N_T in Figs.4.1, 4.2 and 4.3 are almost linear showing that N_T falls exponentially during night time. These portions of the diurnal curves have been used for calculating the values of $\bar{\beta}$. The value of $\bar{\beta}$ comes to about 1.3×10^{-4}/sec in equinox, 1.2×10^{-4}/sec in winter and 0.8×10^{-4}/sec in summer.

4.3 Variation of maximum electron density (n_{max})

Since the major fraction of the total electron content occurs in the region of maximum electron density, the values of n_{max} are also determined at the times of satellite transits. At the time of a transit if ionogram is not available then interpolation is done using the available ionograms. n_{max} is calculated from the formula $n_{max} = 1.24\ (f_oF_2)^2 \times 10^{10}$ electrons/(Metre)^3 where f_oF_2 is the critical frequency of the F layer. The values of n_{max} for summer winter and equinox are plotted in figures 4.4, 4.5 and 4.6 respectively. It can be seen that the maximum electron density also exhibits the features which are present in the total electron content. Between 07 hours and 10 hours, the decrease in the rate of increase can be seen in n_{max} also.

4.4 Variation of bottom side (N_b) and top side(N_a) electron contents

By subjecting the ionograms to true height analysis it is possible to calculate the electron content below the height of maximum electron density. The bottom side content (N_b) is substracted from the total content and the top side content (N_a) is determined. The values thus calculated are plotted in Figs.4.7, 4.8 and 4.9 respectively. The day time maximum value of N_a is about 2×10^{17}/meter^2 in summer, 1.2×10^{17}/meter^{2}in

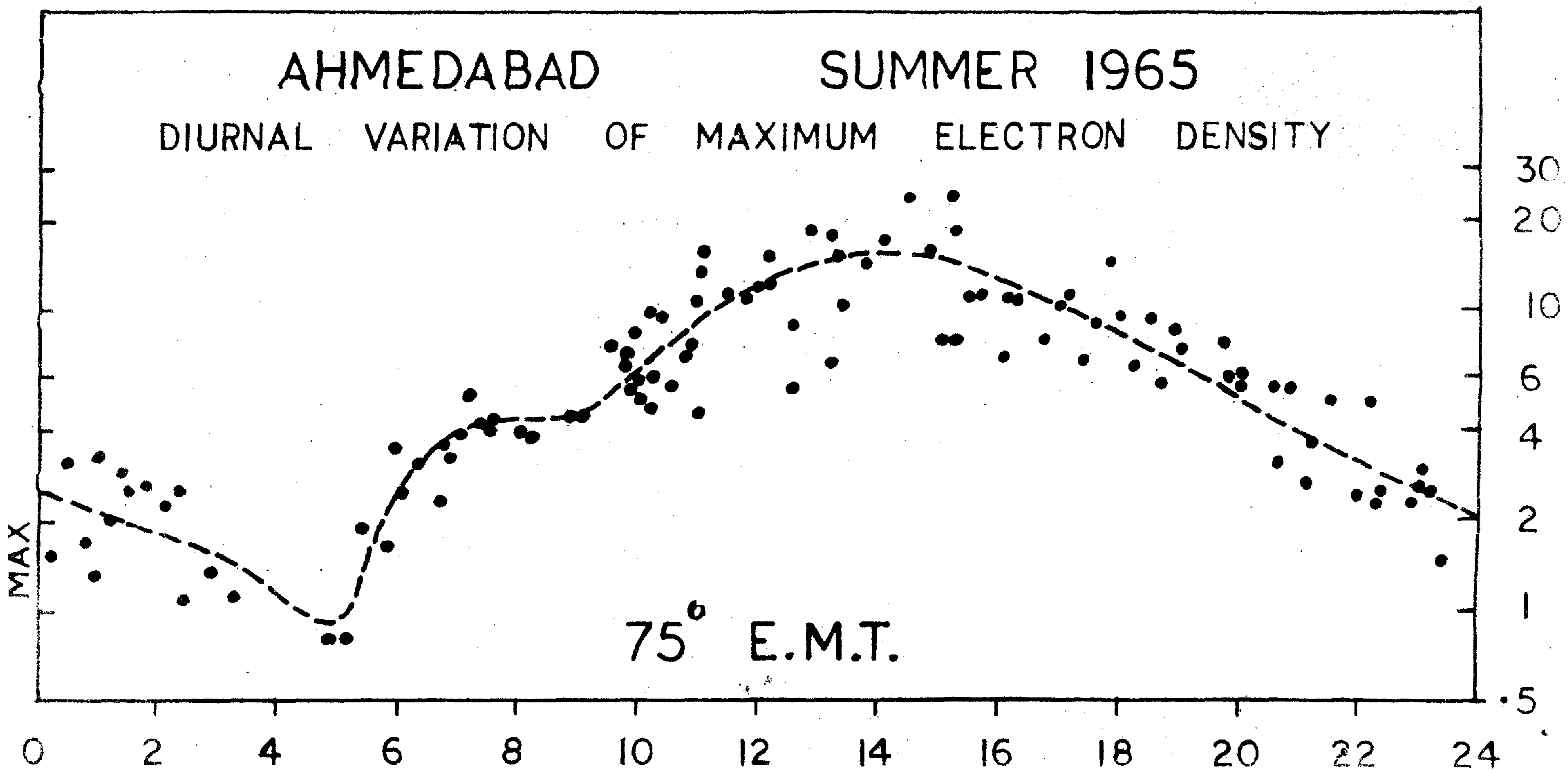
AHMEDABAD SUMMER 1965
DIURNAL VARIATION OF MAXIMUM ELECTRON DENSITY
75° E.M.T.
MAX
30
20
10
6
4
2
1
.5
0
2
4
6
8
10
12
14
16
18
20
22
24

FIGURE 4.4

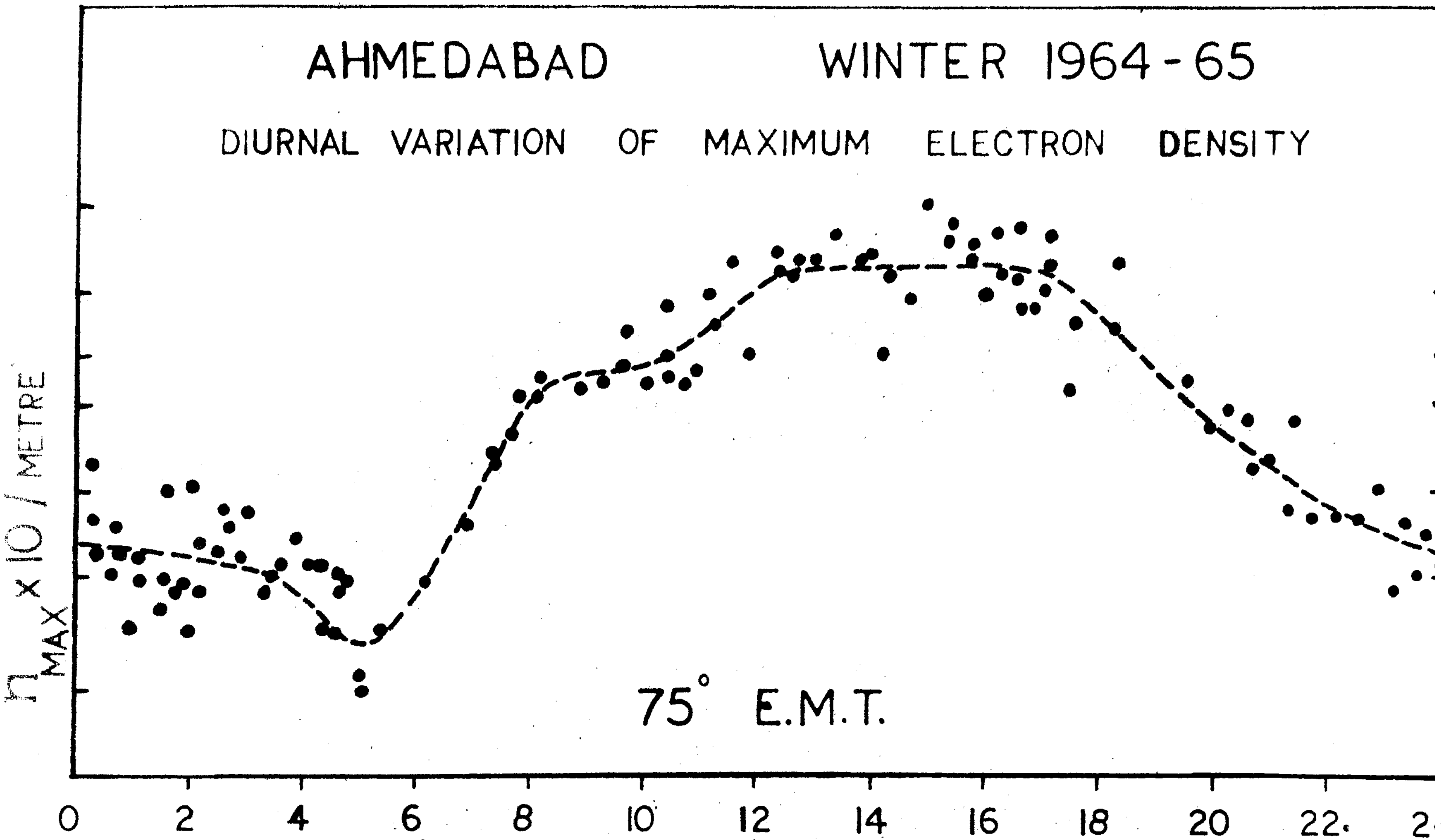

AHMEDABAD WINTER 1964-65
DIURNAL VARIATION OF MAXIMUM ELECTRON DENSITY
75° E.M.T.
n MAX x 10 / METRE
0
2
4
6
8
10
12
14
16
18
20
22
2

FIGURE 4.5

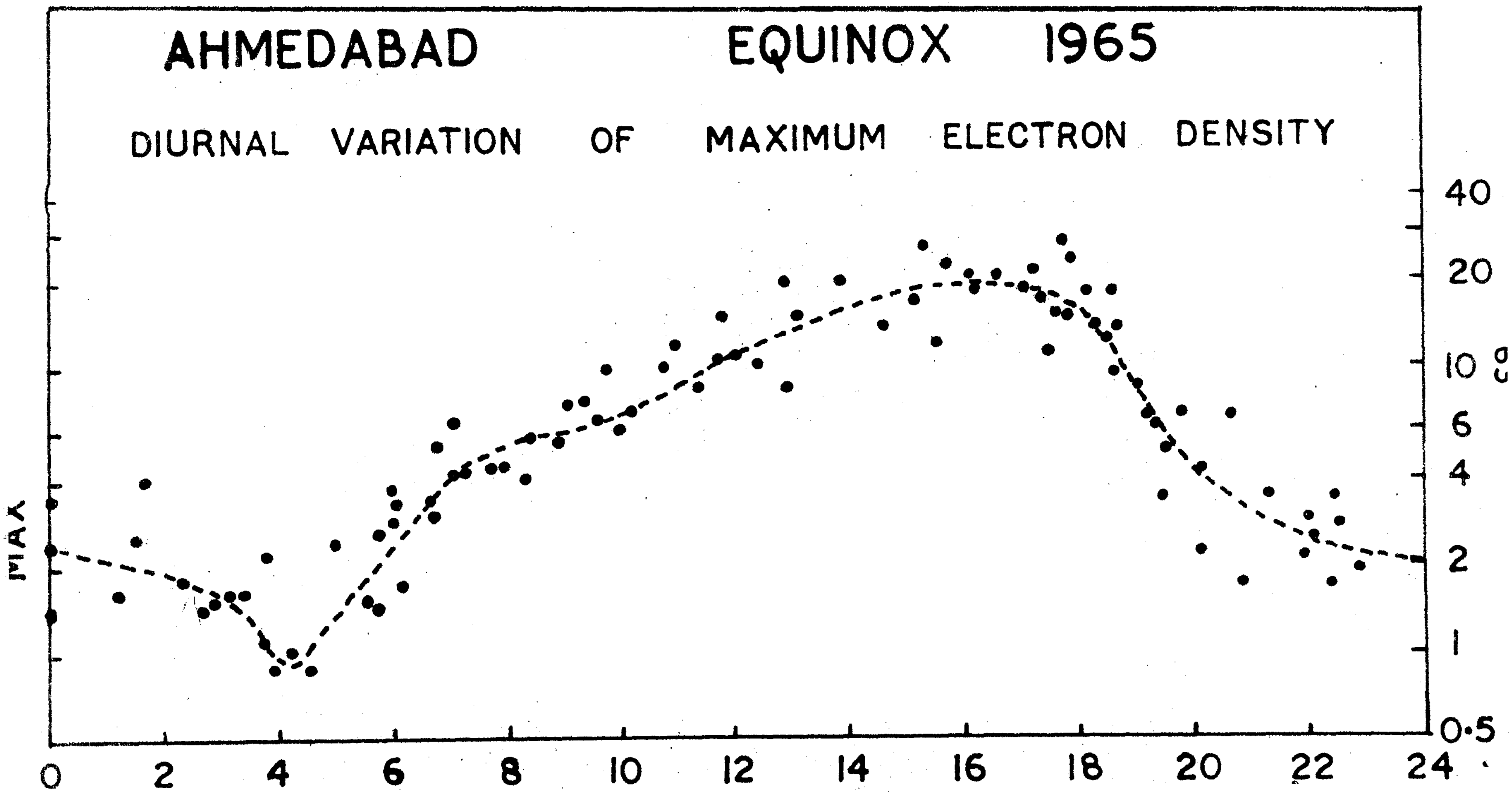

FIGURE 4·6 75° E.M.T.

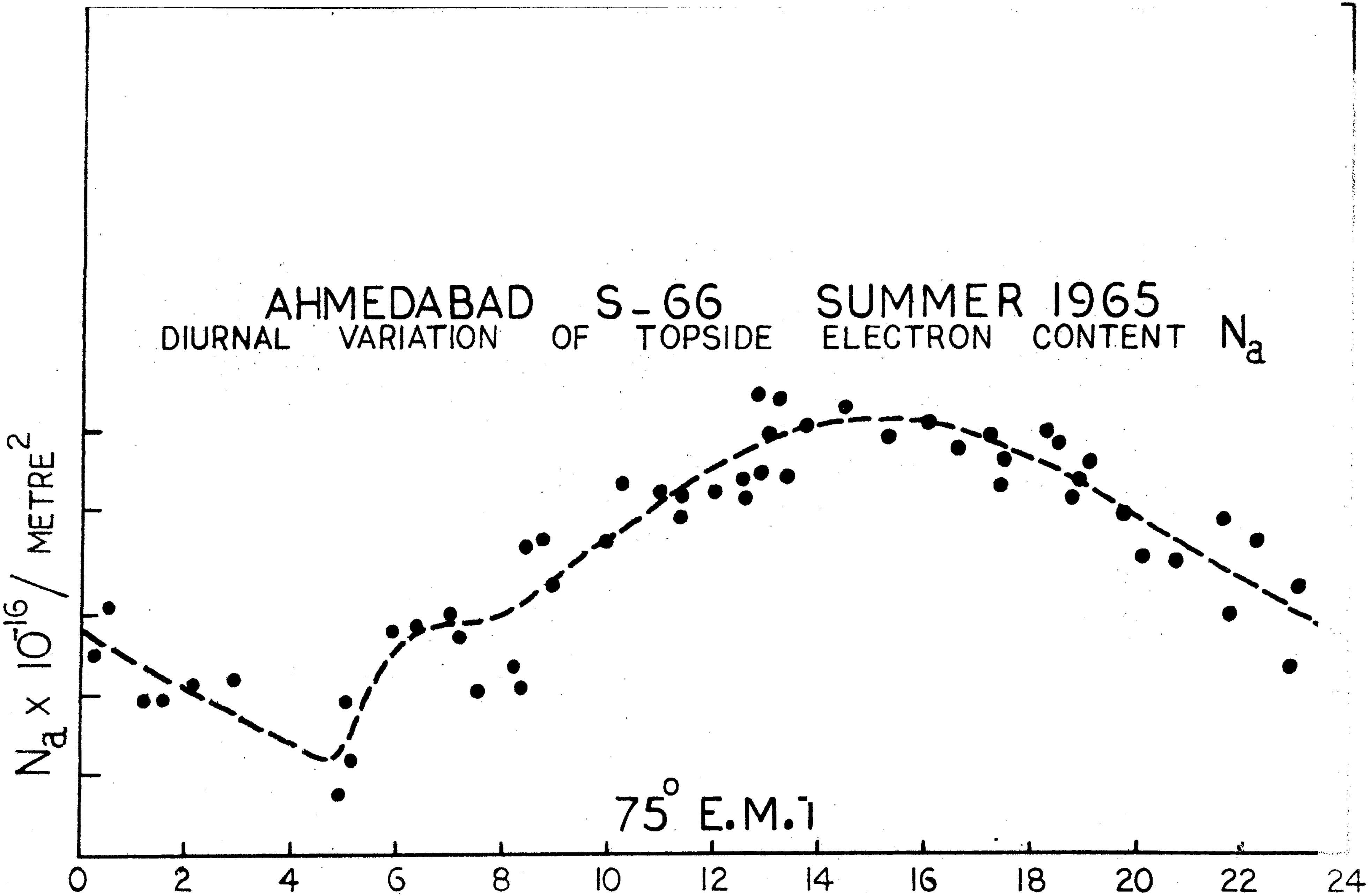
AHMEDABAD S-66 SUMMER 1965
DIURNAL VARIATION OF TOPSIDE ELECTRON CONTENT N_a
$N_a \times 10^{-16}$ / METRE^2
75° E.M.T
0
2
4
6
8
10
12
14
16
18
20
22
24

FIGURE 4.7

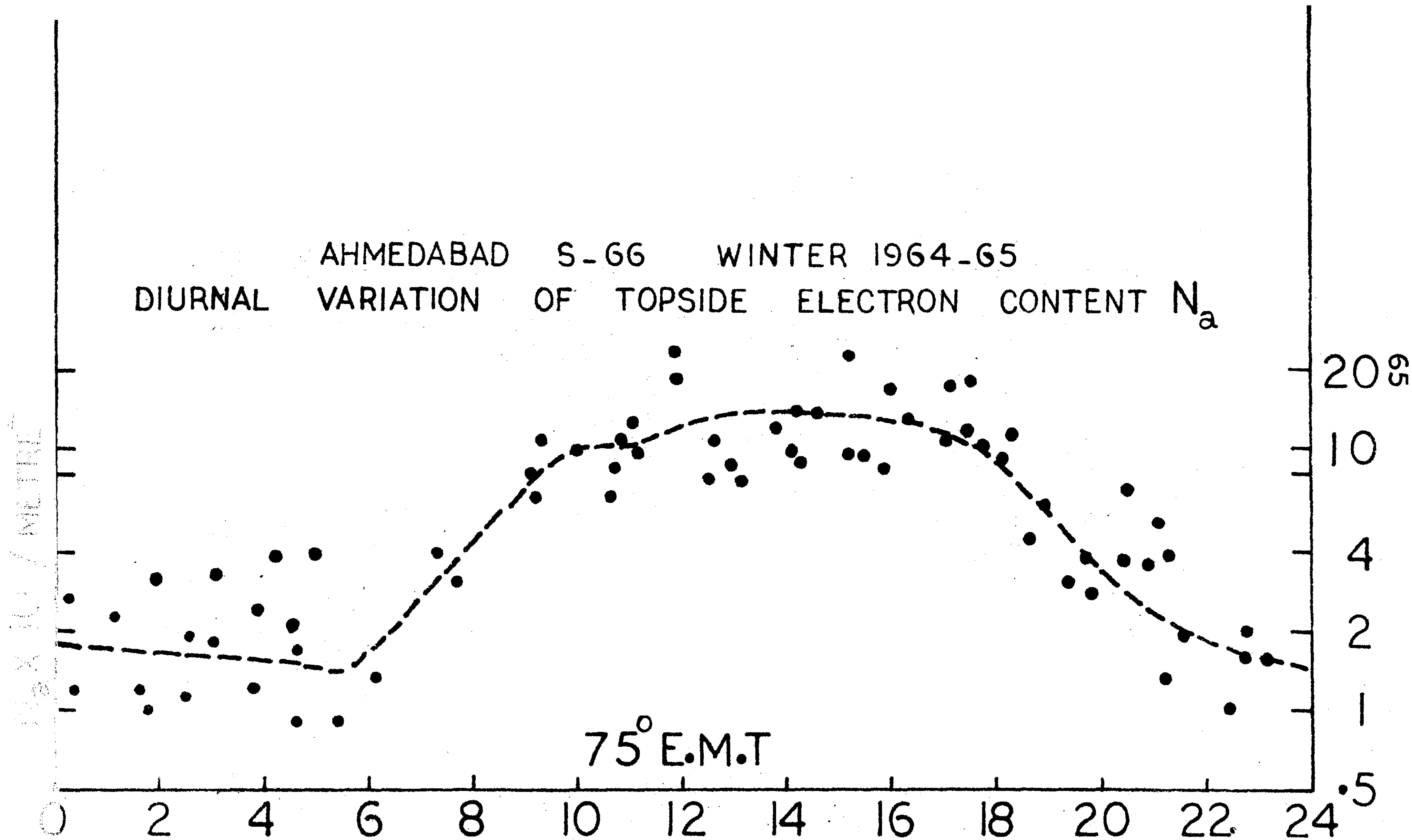
AHMEDABAD S-66 WINTER 1964-65
DIURNAL VARIATION OF TOPSIDE ELECTRON CONTENT N_a
75° E.M.T
0 2 4 6 8 10 12 14 16 18 20 22 24
20 10 4 2 1 .5
65

FIGURE 4.8

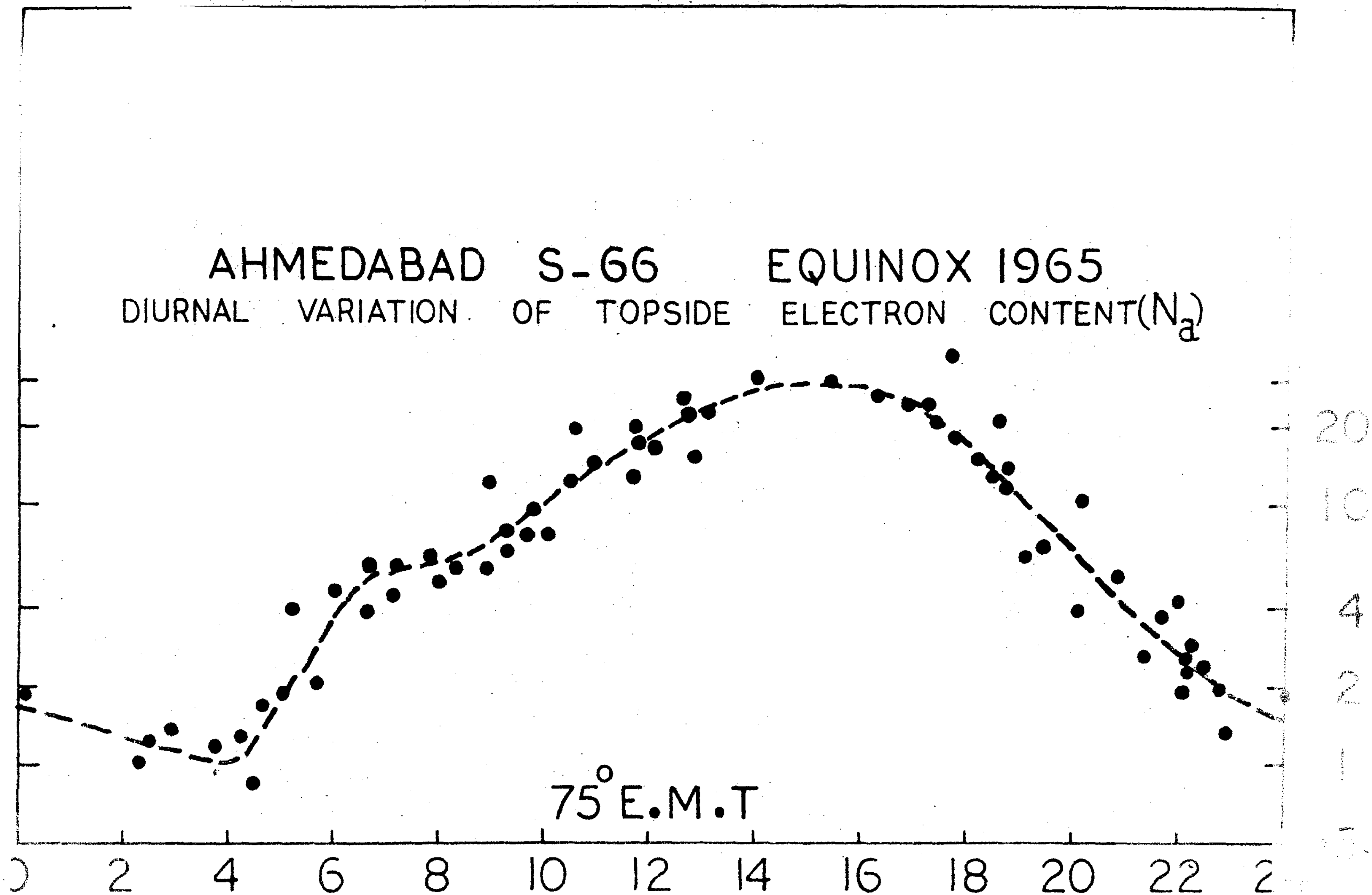
AHMEDABAD S-66 EQUINOX 1965
DIURNAL VARIATION OF TOPSIDE ELECTRON CONTENT(N_a)
75° E.M.T
20
10
4
2
1
0
2
4
6
8
10
12
14
16
18
20
22

FIGURE 4.9

winter and 2.4 x 10^{17}/meter^2 in equinox. The night time minimum value of N_a is about 0.14 x 10^{17}/meter^2 in winter and 0.12 x 10^{17}/meter^2 in summer and equinox. The bottom side electron content (N_b) values are shown in Figs.4.10, 4.11 and 4.12. The day time maximum value of N_b is about 1.3 x 10^{17}/meter^2 in summer, 0.8 x 10^{17}/meter^2 in winter and 1.4 x 10^{17}/meter^2 in equinox. The minimum value at night is about 0.03 x 10^{17}/meter^2 in summer and equinox and 0.02 x 10^{17}/meter^2 in winter.

4.5 Diurnal and seasonal variation of equivalent slab thickness (T)

The equivalent slab thickness of the ionosphere is given by $T = N_T/n_{MAX}$

This parameter is evaluated from the satellite results in conjunction with the n_{max} values obtained from ionosonde observations. Wright (1960) proposed that F region might be represented by part of a Chapman region with a scale height of about 100 km. For a Chapman distribution of electrons Wright has shown that

$$N_T = 4.13\ H\ n_{max} \qquad (2)$$

$$N_a = 2.82\ H\ n_{max} \qquad (3)$$

$$N_b = 1.31\ H\ n_{max} \qquad (4)$$

Where N_a and N_b are the integrated electron contents above and

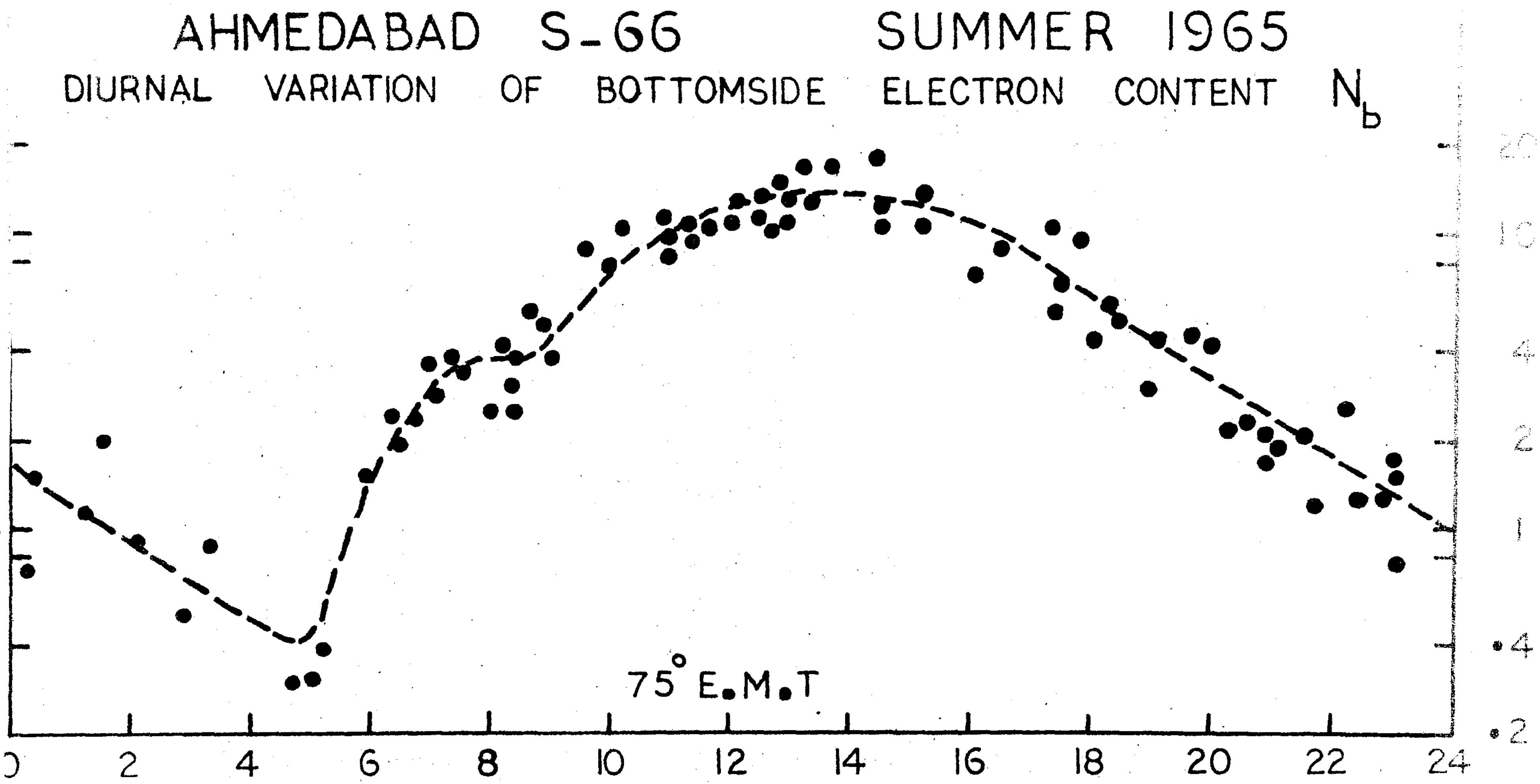
AHMEDABAD S-66 SUMMER 1965
DIURNAL VARIATION OF BOTTOMSIDE ELECTRON CONTENT N_b
75° E.M.T
0
2
4
6
8
10
12
14
16
18
20
22
24
1
2
4
10
20
•4
•2

FIGURE 4.10

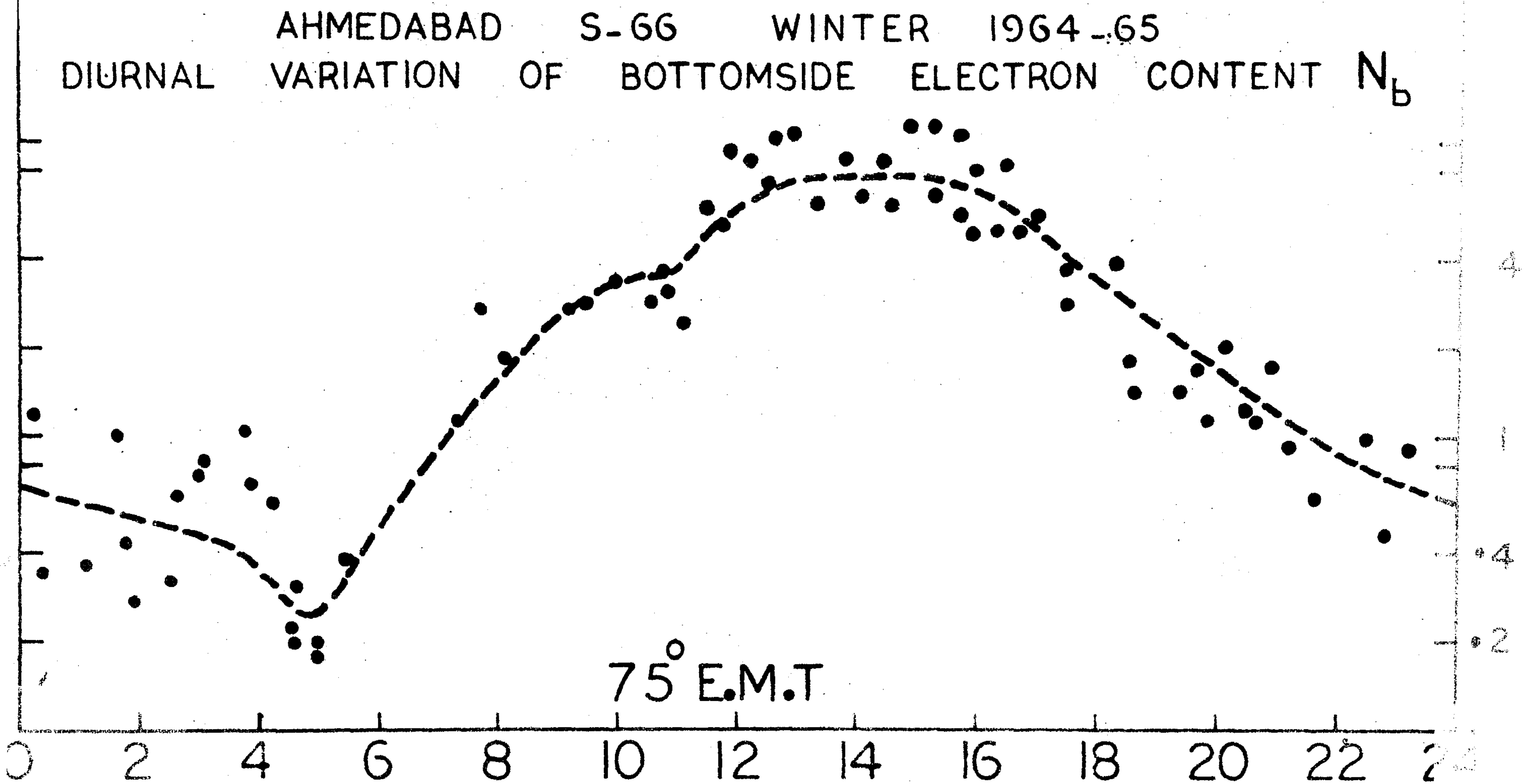
AHMEDABAD S-66 WINTER 1964-65
DIURNAL VARIATION OF BOTTOMSIDE ELECTRON CONTENT N_b
4
1
·4
·2
75° E.M.T
0
2
4
6
8
10
12
14
16
18
20
22
24

FIGURE 4·11

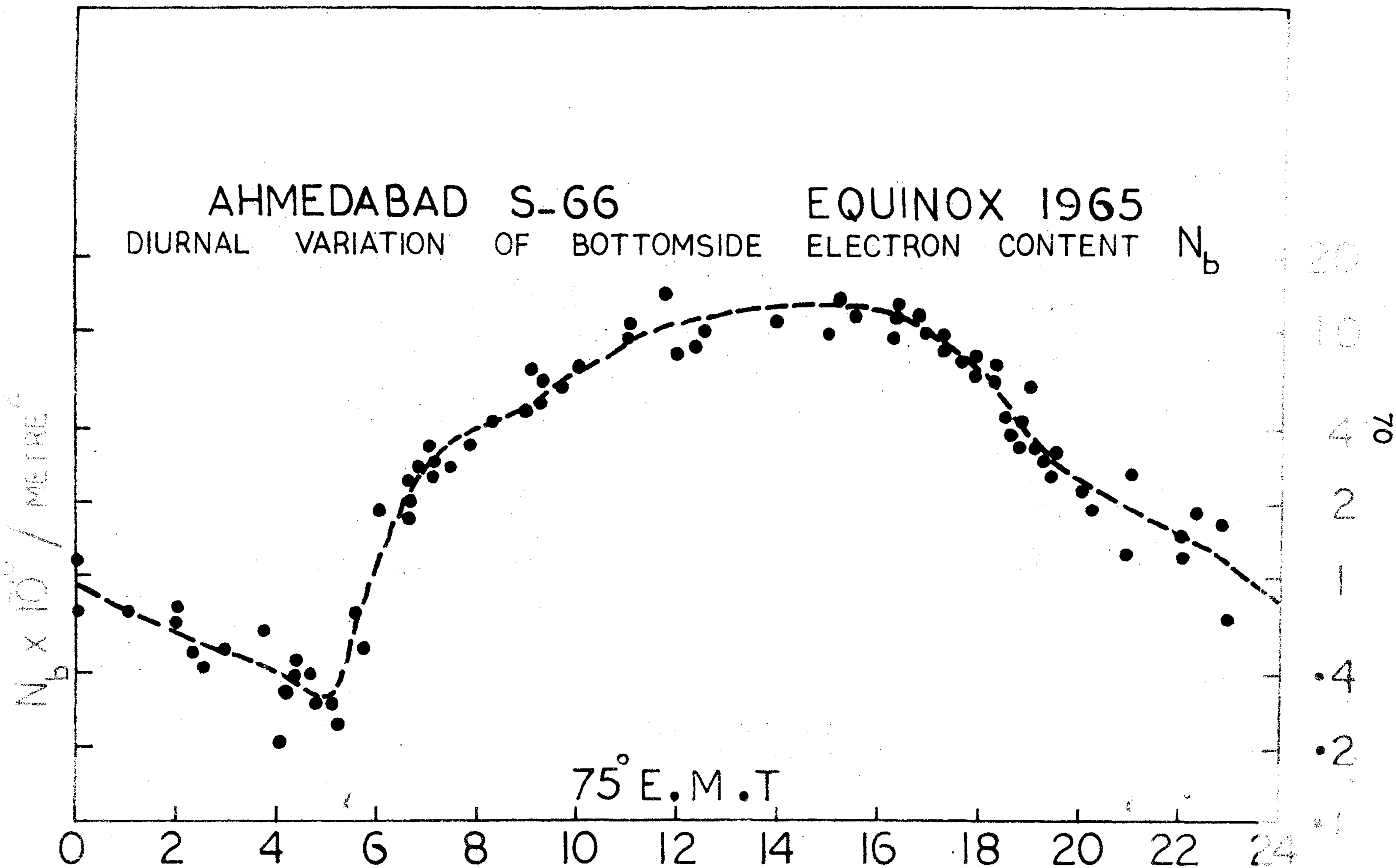
AHMEDABAD S-66 EQUINOX 1965
DIURNAL VARIATION OF BOTTOMSIDE ELECTRON CONTENT N_b
$N_b \times 10^{16}$ / METRE^2
20
10
4
2
1
·4
·2
·1
75° E.M.T
0 2 4 6 8 10 12 14 16 18 20 22 24

FIGURE 4.12

below maximum electron density level (h_{max}) and H is the scale height. Following this hypothesis τ has been used by a number of investigators as a temperature indicator at midday in the ionosphere. (Ross, 1960; Hibberd, 1964; Bhonsle et al, 1965). Chapman model assumes that electrons and ions are in thermal equilibrium. A theory without such a restriction is the diffusion transport theory developed by Yeh and Flaherty (1966). They have proposed a hybrid layer made up of a diffusion transport layer above the peak and a Chapman layer below the peak. They have also shown the dependence of slab thickness on electron to ion temperature ratio. The values of τ in summer, winter and equinox have been shown in Figs.4.13, 4.14 and 4.15 respectively. The simultaneous values of h_mF_2 have also been shown in these figures. During winter, τ exhibits very large values before ground sun rise. This anomalous increase is not seen clearly in summer. Equinox months show slightly large values of τ around the same time. From the figures it can be seen that the height of maximum electron density also increases in the early morning hours. At Huancayo, an equatorial station, Blumle (1962) observed an increase in the τ values around layer sun rise. It can be seen from the Figs.4.13, 4.14 and 4.15 that the τ values increase after sun rise. The day time maximum occurs after mid-day hours in winter and around mid-day hours in summer and equinox. The maximum day time thickness for the period 1964-65 is approximately 225 km. in winter, 235 km. in equinox and 250 km. in summer. The corresponding h_mF_2 values also show a maximum after mid-day hours in winter and around mid-day hours

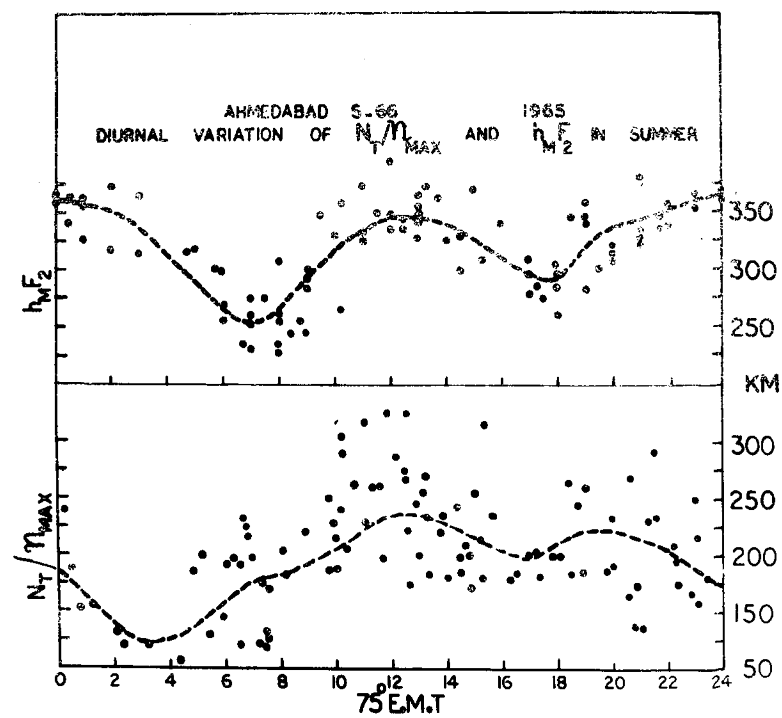
AHMEDABAD S-66 1965
DIURNAL VARIATION OF N_T/n_{MAX} AND h_MF_2 IN SUMMER
h_MF_2
350
300
250
KM
N_T/n_{MAX}
300
250
200
150
50
0 2 4 6 8 10 12 14 16 18 20 22 24
75°E.M.T

FIG. 4·13

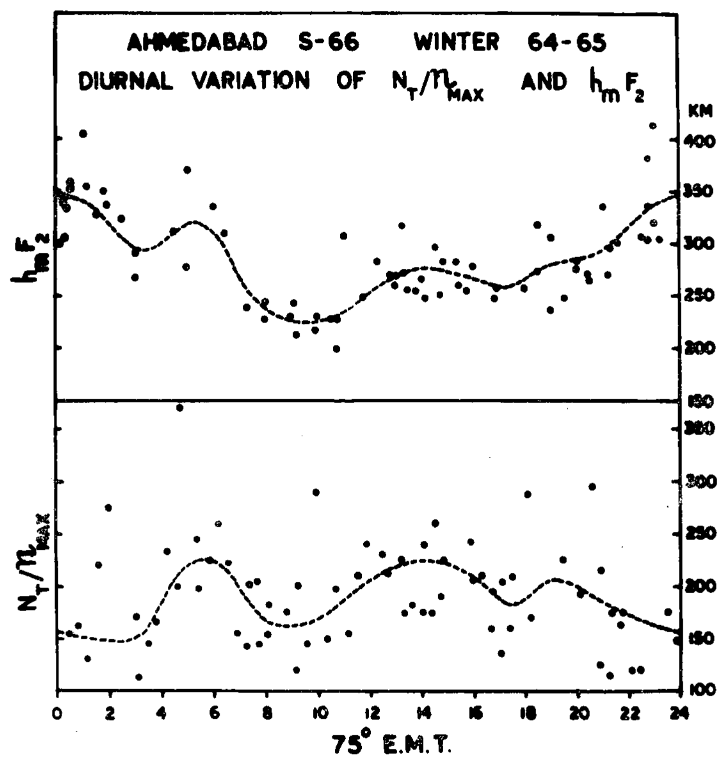
AHMEDABAD S-66 WINTER 64-65
DIURNAL VARIATION OF N_T/n_{MAX} AND h_mF_2
KM
400
350
300
250
200
150
h_mF_2
300
250
200
150
100
N_T/n_{MAX}
0 2 4 6 8 10 12 14 16 18 20 22 24
75° E.M.T.

FIG. 4·14

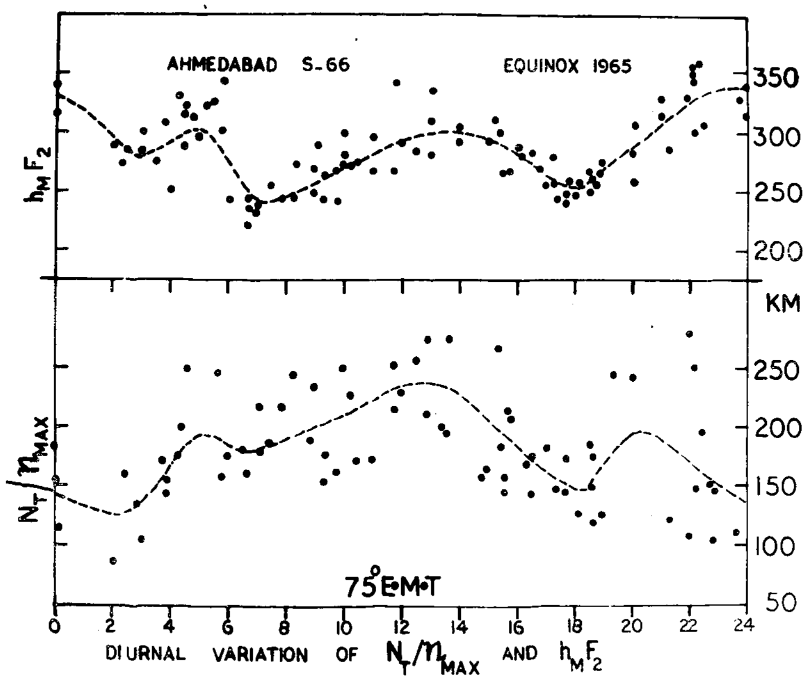
AHMEDABAD S-66
EQUINOX 1965
$h_M F_2$
350
300
250
200
KM
250
200
150
100
50
N_T/n_{MAX}
75°E.M.T
0
2
4
6
8
10
12
14
16
18
20
22
24
DIURNAL VARIATION OF N_T/n_{MAX} AND $h_M F_2$

FIG. 4.15

in summer and equinox. The day time maximum of h_mF_2 during the observational period is about 275 km in winter, 300 km in equinox and 350 km in summer. In all the three seasons, it can be seen that τ and h_mF_2 have similar variation during day time. After sun set, while h_mF_2 increases towards mid night τ does not show similar variations. Between 18 hours and 22 hours the thickness parameter shows large values. This feature can be seen in all the seasons. In the case of h_mF_2, this increase is not seen.

4.6 Diurnal and seasonal variation of the ratio of topside electron content to bottom side electron content(N_a/N_b)

Ratio of the electron content N_a above the height of maximum electron density to the content N_b below this height has been introduced by Evans (1956) as a simple and convenient measure of the electron distribution in the ionosphere. If the ionosphere were isothermal and had Chapman's distribution of electron density the ratio N_a/N_b would be equal to 2.15. (Wright, 1960). Using the diffusion transport theory Pound and Yeh (1966) have shown that the ratio N_a/N_b will have a value of 3.12 during summer night and 3.33 during winter night.

In Figs.4.16, 4.17 and 4.18 the data for 1964-65 have been plotted separately for summer, winter and equinox. The diurnal variation of this ratio can be seen in all the seasons. Compared to the day time values the night time values of N_a/N_b are higher. In winter and equinox, N_a/N_b exhibits large values

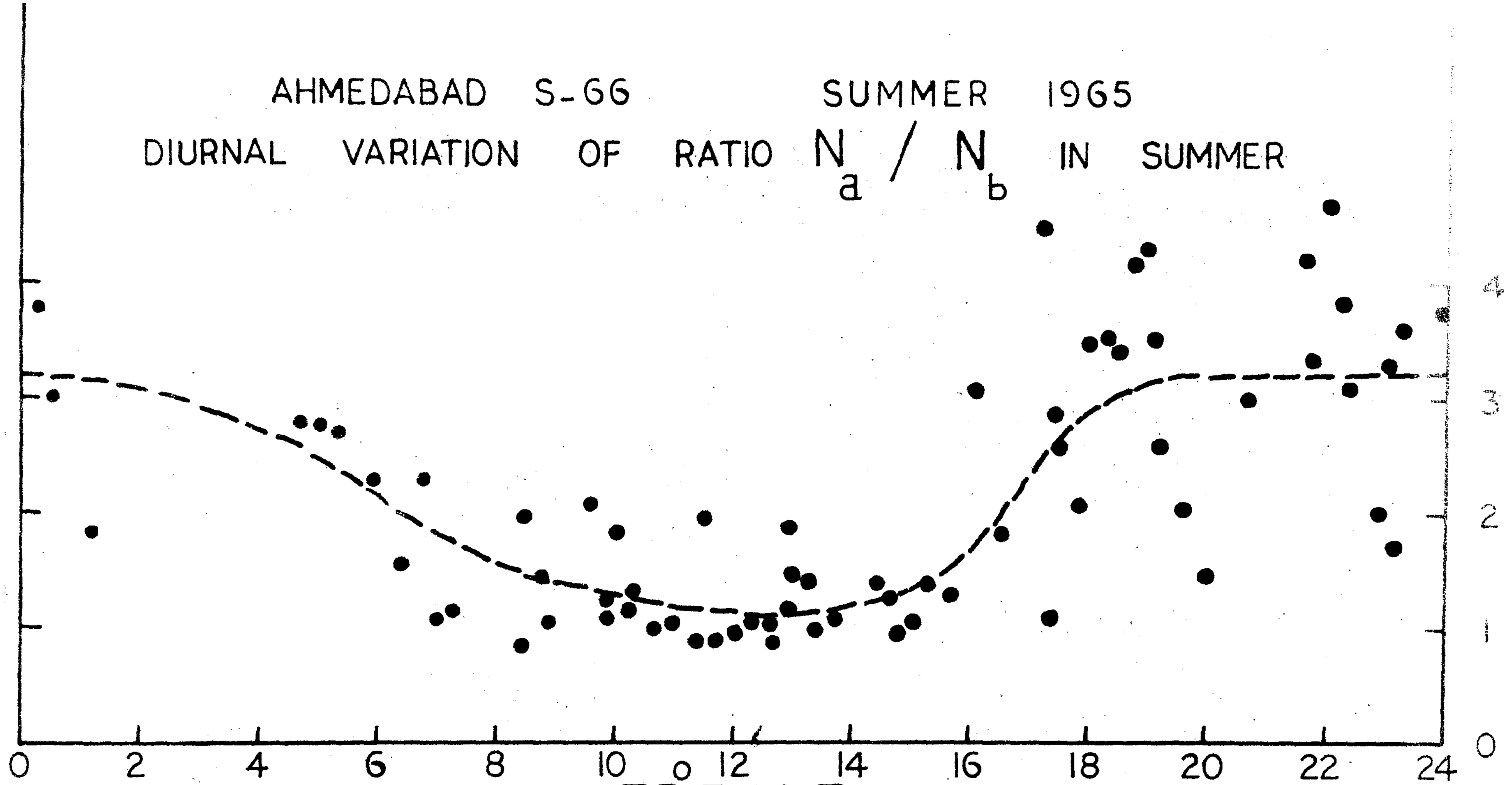

FIGURE 4.16 75°E.M.T

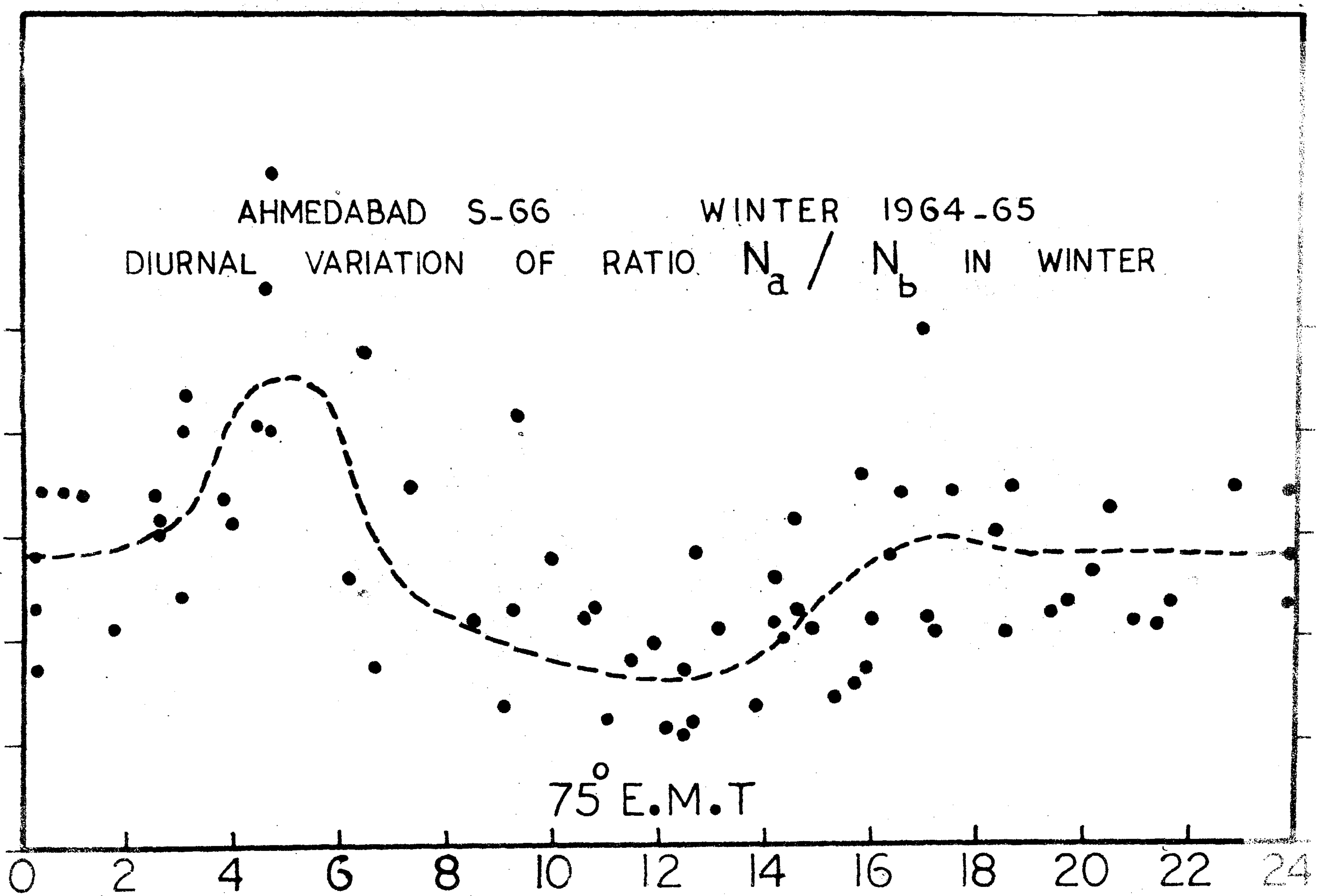

AHMEDABAD S-66 WINTER 1964-65
DIURNAL VARIATION OF RATIO N_a / N_b IN WINTER
1
2
3
4
5
75° E.M.T
0
2
4
6
8
10
12
14
16
18
20
22
24

FIGURE 4.17

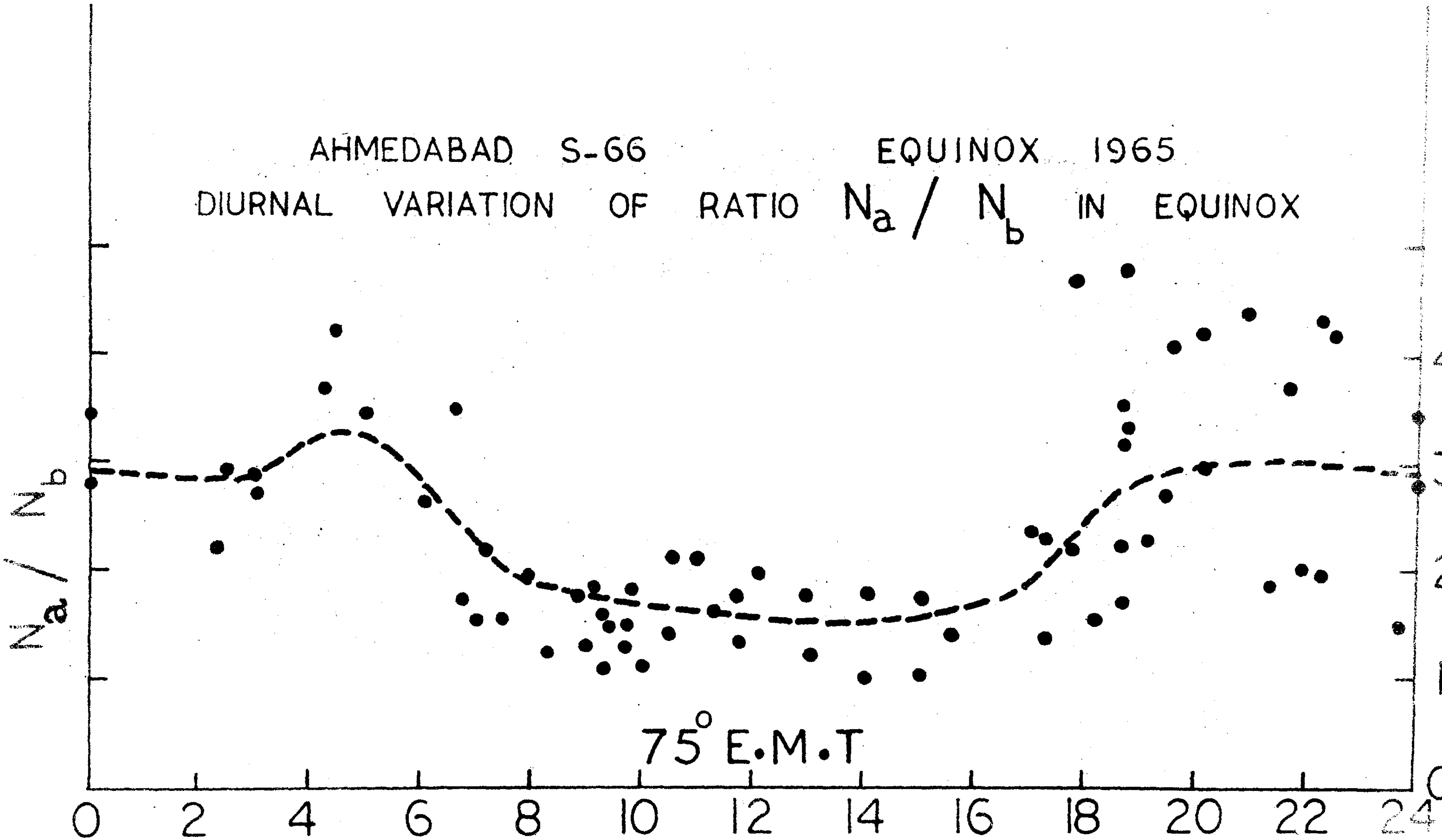
AHMEDABAD S-66
EQUINOX 1965
DIURNAL VARIATION OF RATIO N_a / N_b IN EQUINOX
N_a / N_b
75° E.M.T
0
1
2
3
4
0 2 4 6 8 10 12 14 16 18 20 22 24

FIGURE 4.18

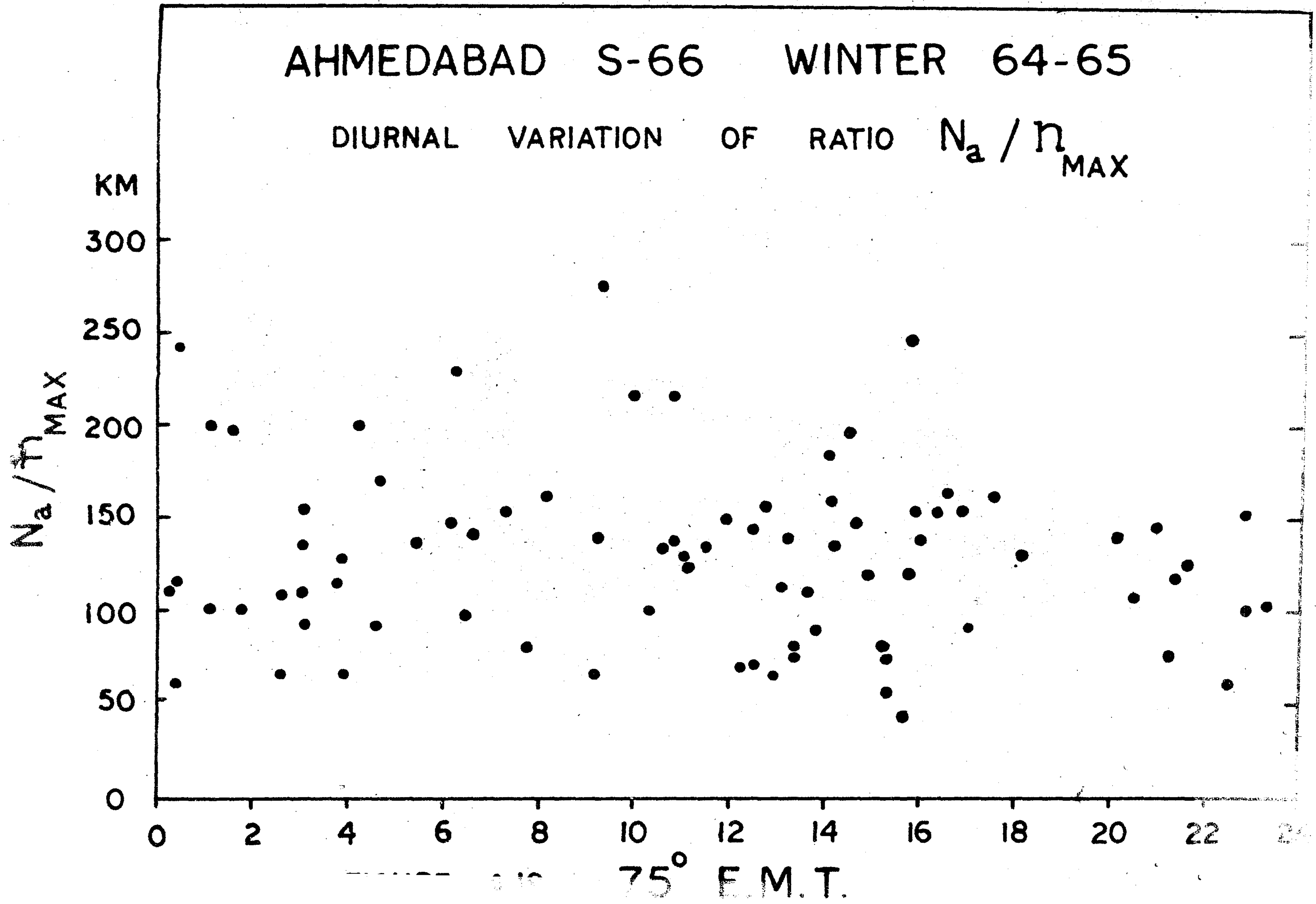

AHMEDABAD S-66 WINTER 64-65
DIURNAL VARIATION OF RATIO N_a / n_{MAX}
KM
300
250
200
150
100
50
0
N_a / n_{MAX}
0
2
4
6
8
10
12
14
16
18
20
22
75° E.M.T.

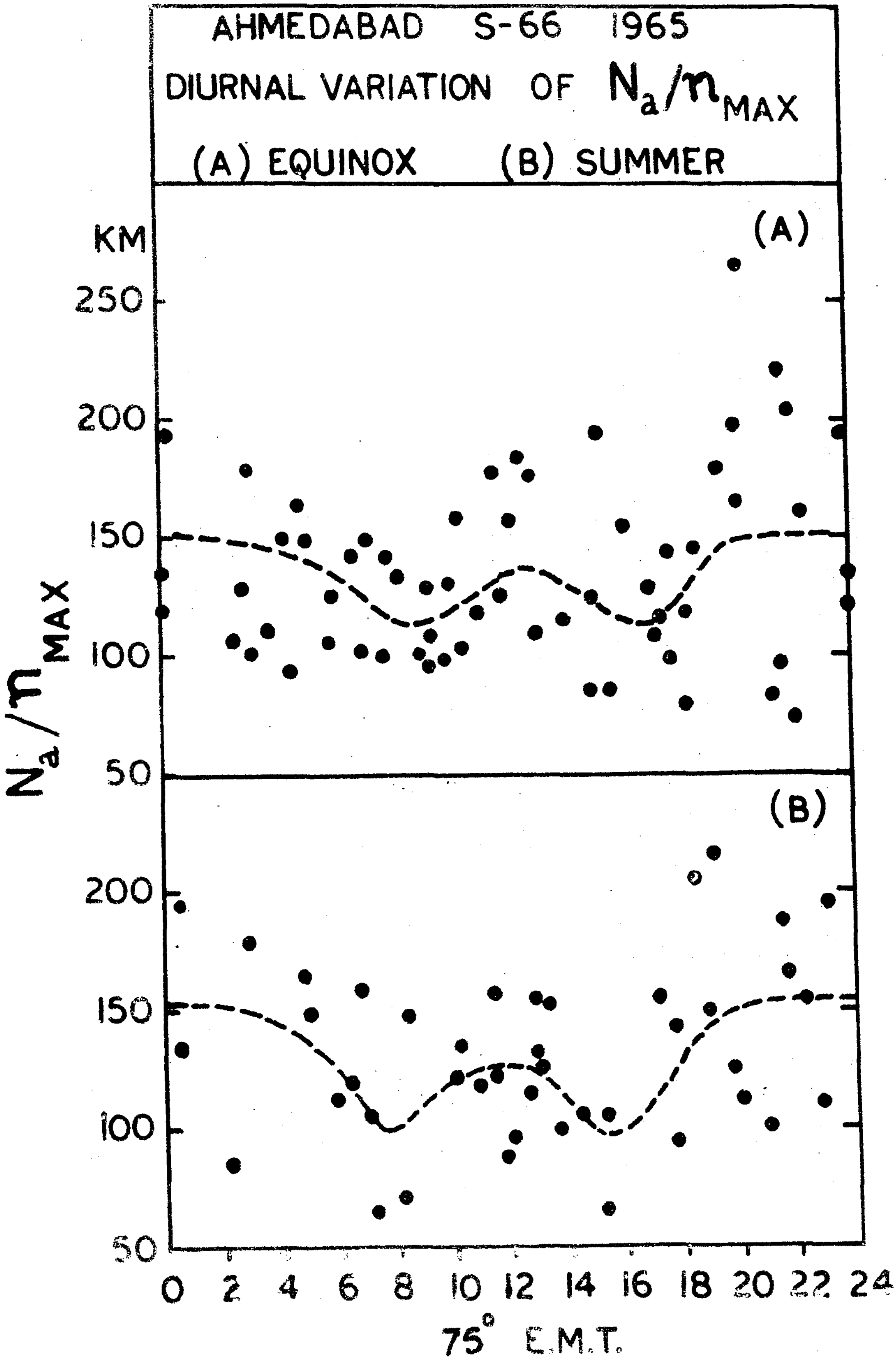
AHMEDABAD S-66 1965
DIURNAL VARIATION OF N_a/n_{MAX}
(A) EQUINOX (B) SUMMER
(A)
(B)
KM
250
200
150
100
50
N_a/n_{MAX}
0 2 4 6 8 10 12 14 16 18 20 22 24
75° E.M.T.

FIGURE 4.20

before ground sun rise. In summer, this feature is not very evident. The mid-day minimum value of N_a/N_b is about 1.4 in summer, 1.5 in equinox and 2.0 in winter. The night time steady value before mid-night is about 3.2 in summer, 3.0 in equinox and 2.9 in winter. After mid-night the ratio does not remain steady.

4.7 Diurnal and seasonal variation of N_a/n_{max}

The winter values of N_a/n_{max} are plotted in Fig.4.19. It can be seen that the diurnal variation of this parameter is not clear in winter. The summer and equinox values are shown in Fig.4.20. The diurnal variation is found to be more evident in equinox and summer. After sun set N_a/n_{max} increases in these two seasons and attains a steady value of about 150 km during the night. After sun rise this ratio decreases to a lower value and then starts increasing to a mid-day maximum. Again it starts decreasing after mid-day and reaches a low value before sun set.

4.8 Discussion

A summary of the electron content results for summer and winter has been given in Table I. It can be seen that during 1964-65, the day time maximum values of N_T, N_a, N_b and n_{max} in summer are higher than the corresponding values in winter. In middle latitudes, during periods of high solar activity the day time maximum values of N_T are higher in winter than in summer (Ross, 1960; Yeh and Swenson, 1961). This seasonal effect is

Table I

Season	$N_T \times 10^{-17}$/metre^2			$N_a \times 10^{-17}$/metre^2			$N_b \times 10^{-17}$/metre^2			$n_{max} \times 10^{-12}$/metre^3		
	Max.	Min.	Range	Max.	Min.	Range	Max.	Min.	Range	Max.	Min.	Range
Summer	3.2	0.16	20	2.0	0.12	17	1.3	0.034	38	1.4	0.09	15
Winter	2.0	0.16	12	1.2	0.14	9	0.8	0.024	33	1.2	0.07	17

less pronounced during periods of lower solar activity (Hibberd, 1964). In the present observations over Ahmedabad, during minimum solar activity conditions, the winter anomaly is not seen.

The summer to winter ratios of N_T, N_a, N_b and n_{max} are shown in Table II. Maximum electron density increased by about 17 % from winter to summer. At the same time topside content and bottom side content increased by about 60 %. Since the electron content is related to n_{max} and H, the larger increase of electron content from winter to summer may be attributed to the increase of temperature and the throwing up of ionizable constituents in summer.

Table II

Ionospheric Parameter	Summer to winter ratio	Percentage change
N_T	1.60	60 %
N_a	1.67	67 %
N_b	1.63	63 %
n_{max}	1.17	17 %

The occurrence of a peak in τ near sun rise has been reported by many investigators (Evans and Taylor, 1961; Lawrence et al, 1963; Titheridge, 1964). This has been explained by the fact that sun-rise occurs earlier at greater heights so that the ionisation above the peak of F layer will have considerably increased by the time the electron density at the peak begins to increase (Titheridge, 1964). Also, measurements of electron temperature T_e, made by Bowles et al (1962) using incoherent back scatter technique and by the Ariel satellite (Willmore et al, 1962) show ~~the~~ evidence of a significant departure from thermal equilibrium between electrons and ions near sunrise. Blumle (1962) attributed this increase in T to the departure from thermal equilibrium between the electrons and ions near sunrise.

The results of ratio N_a/N_b are given in Table III. The day time value of N_a/N_b in winter is nearer to the value of 2.15 given by Wright (1960) for Chapman distribution. In equinox and summer this day time value is still lower. In all the seasons the night time values of N_a/N_b are higher than the day time values. The following qualitative explanation of the diurnal variation of N_a/N_b has been proposed by Hibberd and Ross (1966). During most of the day time the vertical distribution of ionisation may be taken as that of a Chapman region, except for the additional ionisation in the E and F_1 region. The presence of E and F_1 region ionisation could cause the day time value of N_a/N_b to be rather lower than the Chapman value of 2.15.

Table III

Season	Ratio N_a/N_b	
	Day time	Night time
Summer	1.4	3.2
Winter	2.0	2.9
Equinox	1.5	3.0

The effective attachment coefficient $\overline{\beta}$ for a middle latitude station has been determined by Hibberd and Ross (1966). They get a value of about 0.8 x 10^{-4}/Sec. The present results show higher values of $\overline{\beta}$ in winter and equinox. The summer value of $\overline{\beta}$ over Ahmedabad comes out to be the same as the middle latitude value given by Hibberd and Ross. From the results of Lawrence et al (1963) for 1958-59, Hibberd and Ross have obtained a value of $\overline{\beta}$ of the order of 0.9 x 10^{-4}/Sec.

CHAPTER V

IONOSPHERIC ELECTRON CONTENT AND EQUIVALENT SLAB THICKNESS IN RELATION TO SOLAR AND MAGNETIC ACTIVITY

5.1 Introduction

5.2 Dependence of daytime N_T on solar flux

5.3 Dependence of night time N_T on solar flux

5.4 Dependence of daytime N_T/n_{max} on solar flux

5.5 Dependence of daytime N_T on magnetic activity

5.6 Dependence of night time N_T on magnetic activity

5.7 Dependence of daytime N_T/n_{max} on magnetic activity

5.8 Dependence of night time N_T/n_{max} on magnetic activity

5.9 Dependence of daytime and night time values of N_a/N_b on magnetic activity

5.10 Dependence of daytime and night time values of h_pF_2 on magnetic activity

5.11 Discussion.

CHAPTER V

IONOSPHERIC ELECTRON CONTENT AND EQUIVALENT SLAB THICKNESS IN RELATION TO SOLAR AND MAGNETIC ACTIVITY

5.1 Introduction

It is well known that the critical frequency, f_oF_2, of the F_2 layer varies markedly with the solar cycle. Bhonsle et al (1965) found the solar cycle dependence of N_T the total electron content up to about 1000 km over middle latitudes for sunspot numbers higher than 40. Yeh and Flaherty (1966) extended these observations to sunspot numbers less than 40. Hibberd and Ross (1966) have examined the relationship between 10.7 cm solar flux and total electron content over middle latitudes. Over low latitudes, these effects have not been studied in detail. In this Chapter, the dependence of N_T and N_T/n_{max} on 10.7 cm solar flux and the effect of moderate magnetic activity (defined by A_p index) on electron content have been studied and the results are presented. Before examining the data for such effects the reasons for not studying the magnetic storm variations may be mentioned. Since the satellite technique provides only a few measurements in a day, it is not possible to follow the effects of individual magnetic disturbances throughout its life. Further, the ionosphere fluctuates from day to day even under magnetically quiet conditions and it is often difficult to decide whether a change observed in a short interval of time is really related to the storm or is a random variation. Because of such draw-backs in the technique of investigation, storm time variations could not be studied in detail. Instead, the dependence of N_T, N_T/n_{max}, N_a/N_b and h_pF_2 on moderate magnetic activity defined by A_p is studied.

5.2 Dependence of daytime N_T on solar flux

In Fig.5.1 the values of N_T measured between 12 hours and 16 hours are plotted against the daily values of 10.7 cm solar flux. In order to get over the effect of diurnal variation, the time around mid-day hours has been chosen. The N_T values have been plotted separately for summer, winter and equinox. In all the seasons it can be seen that N_T increases linearly with 10.7 cm solar flux. In winter, N_T seems to increase at a slow rate till the solar flux reaches a value of about 100 units, and beyond this, it increases with solar flux at a faster rate. In summer and equinox, this transition at the solar flux value of about 100 units is not noticeable. The change of N_T per unit of 10.7 cm solar flux is about $0.04 \times 10^{+17}$ in summer and 0.054×10^{17} in equinox. In winter, this is about 0.02×10^{17} when the solar flux is below 100 units, and 0.06×10^{17} unit flux, above 100 units.

The value of the logarithmic gradient, $\frac{\partial N_T/\partial s}{N_T(100)}$ comes out to be 0.025 in winter and 0.01 in summer and equinox.

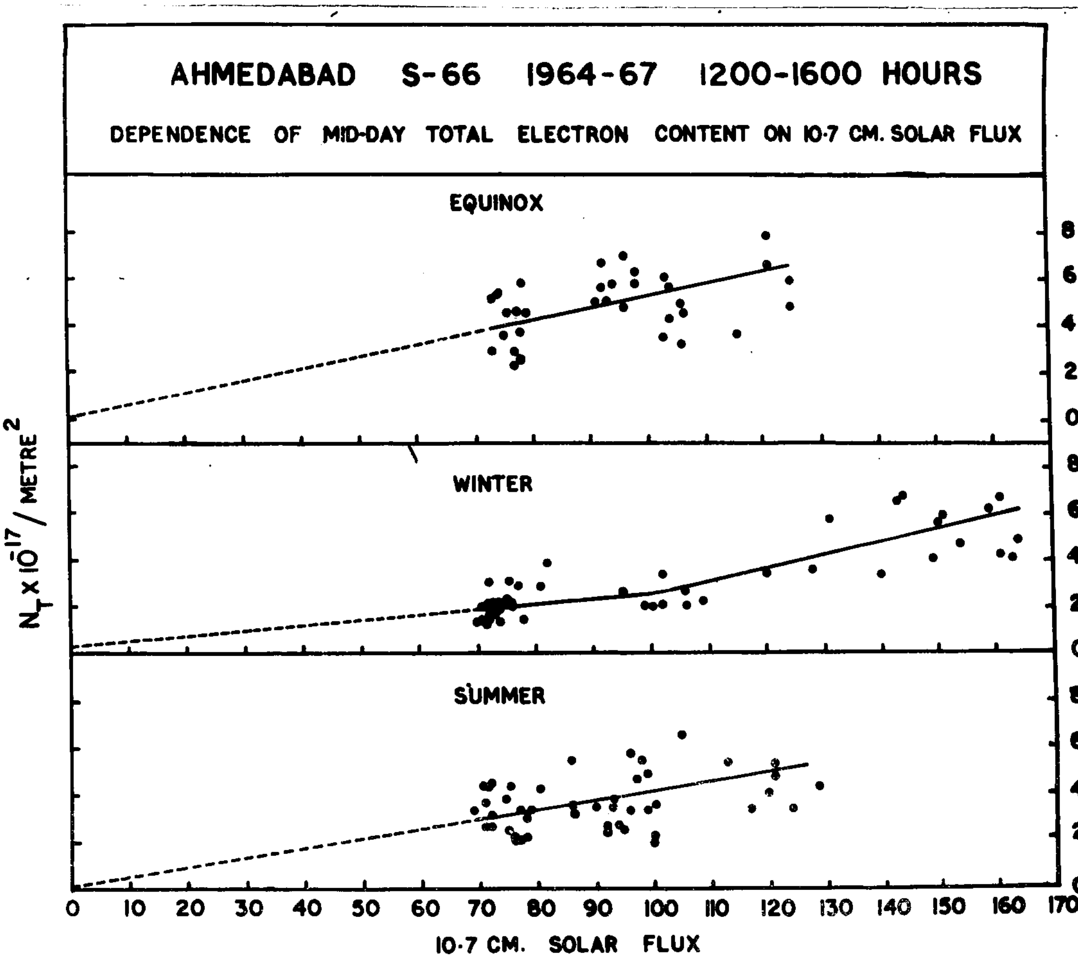

Fig.5.1 Dependence of afternoon (12-16 hrs) total electron content on 10.7 cm solar flux.

5.3 Dependence of night-time N_T on solar flux

Between 23 hours and 03 hours N_T remains nearly steady. The values of N_T measured during this part of the night have been used for studying the effect of solar flux at night. In Fig.5.2, the night-time values of N_T have been plotted against the daily values of 10.7 cm solar flux separately for summer, winter and equinox. In all the seasons, night-time N_T also seems to have a linear dependence on solar flux. The rate of increase with solar flux seems to be nearly the same in all the seasons. N_T increases at the rate of about 0.007×10^{17} per unit flux. The night-time logarithmic gradient comes out to be about 0.02.

5.4 Dependence of daytime N_T/n_{max} on solar flux

It is generally accepted that solar extreme ultra-violet radiation is an important source responsible for the heating of the F region (Hunt and van Zandt, 1961). Satellite drag measurements show that the thermopause temperature and hence the neutral perticle densities at F region heights vary linearly with the solar activity (Nicolet, 1963). Since the average equivalent slab thickness, N_T/n_{max}, is an indicator of scale height and electron-ion mean temperature, it must have positive correlation with solar flux. In Fig.5.3, the daytime values of N_T/n_{max} are plotted against the daily values of 10.7 cm solar flux. It can be seen that there is linear relationship between N_T/n_{max} and 10.7 cm solar flux (S). The rate of increase

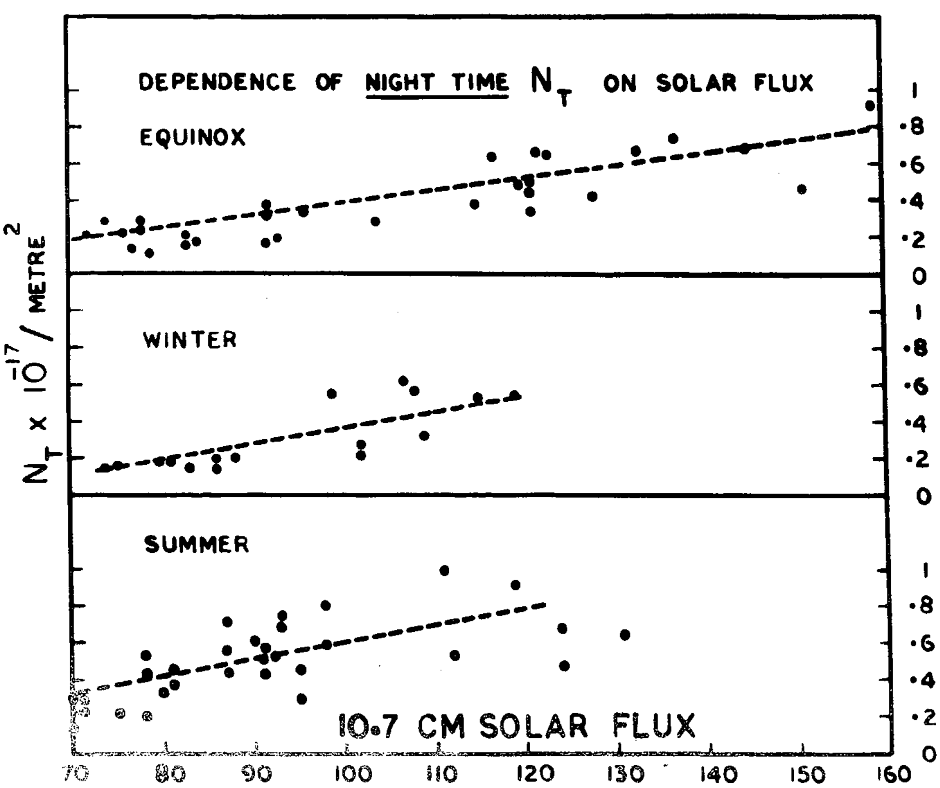

Fig.5.2 Dependence of night time (23-03 hrs) total electron content on 10.7 cm solar flux

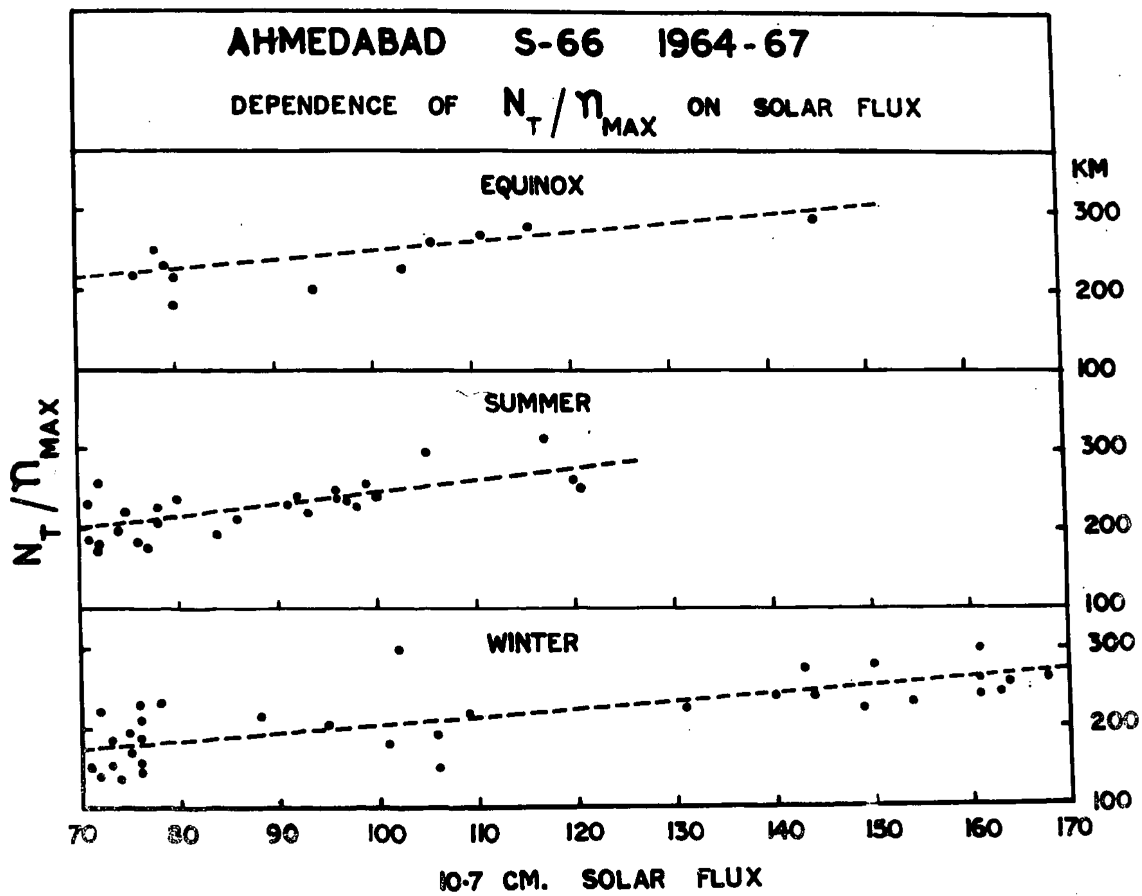

Fig.5.3 Dependence of daytime N_T/n_{max} on 10.7 cm solar flux

of τ per unit flux is about 1 km in winter 1.2 km in equinox and 1.5 km in summer. The empirical linear relationship between and S may be written as

$$\tau \text{ (km)} = 175 + 1.0 \text{ (S-70) for winter}$$

$$\tau \text{ (km)} = 210 + 1.2 \text{ (S-70) for equinox}$$

$$\tau \text{ (km)} = 200 + 1.4 \text{ (S-70) for summer.}$$

5.5 Dependence of daytime N_T on moderate magnetic activity

In Fig.5.4, the day-time values of N_T have been plotted against the daily values of A_p separately for summer, winter and equinox. In summer and equinox, the total electron content decreases with increase in magnetic activity. In winter there is probably a similar effect but it is not clear.

5.6 Dependence of night-time N_T on magnetic activity

In Fig.5.5, the values of N_T measured between 23 hours and 03 hours are plotted against A_p index separately for summer, winter and equinox. It can be seen that N_T increases with magnetic activity. In summer the figure shows more scatter. A whole-year plot is also given in Fig.5.6. It thus appears that while the total electron content decreases with increase in magnetic activity in the afternoon hours it increases with increase in A_p in the late night hours.

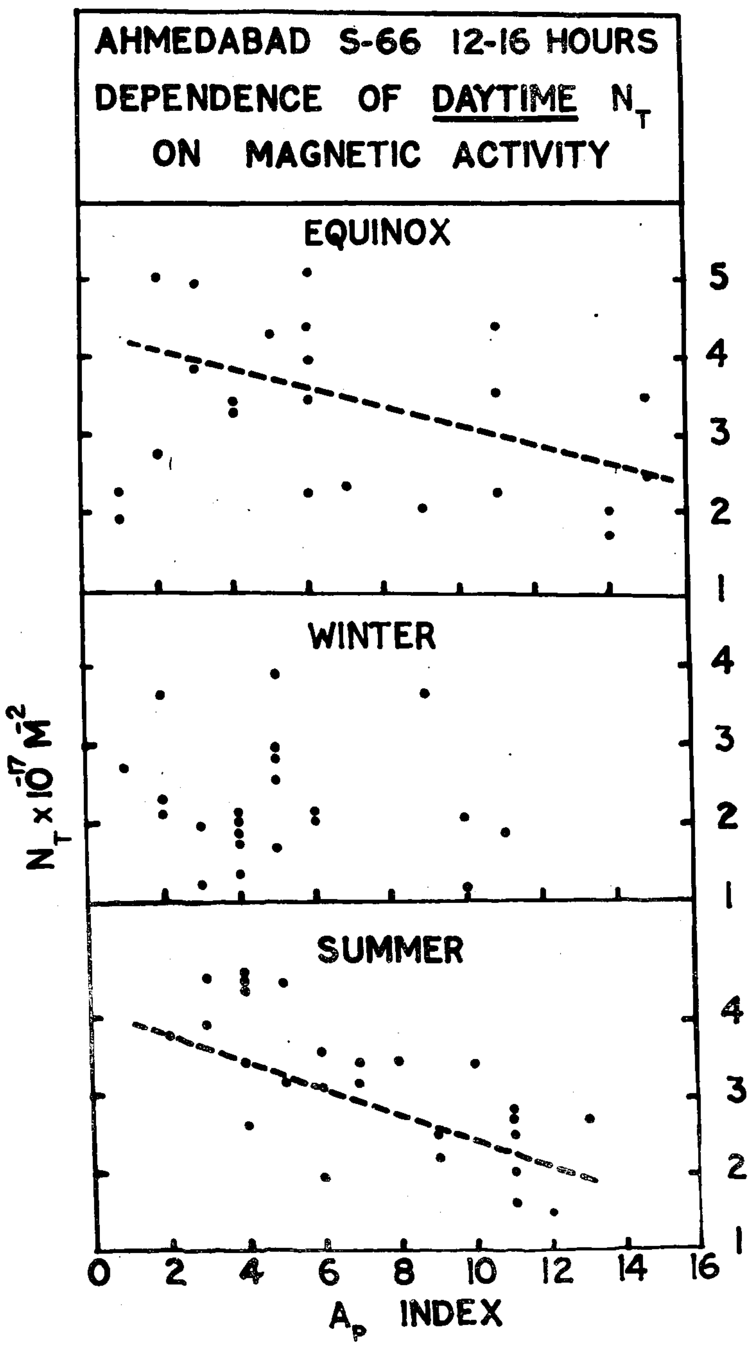
AHMEDABAD S-66 12-16 HOURS
DEPENDENCE OF DAYTIME N_T
ON MAGNETIC ACTIVITY
EQUINOX
WINTER
SUMMER
$N_T \times 10^{-17} M^{-2}$
A_p INDEX
0 2 4 6 8 10 12 14 16
1 2 3 4 5

FIG. 5·4

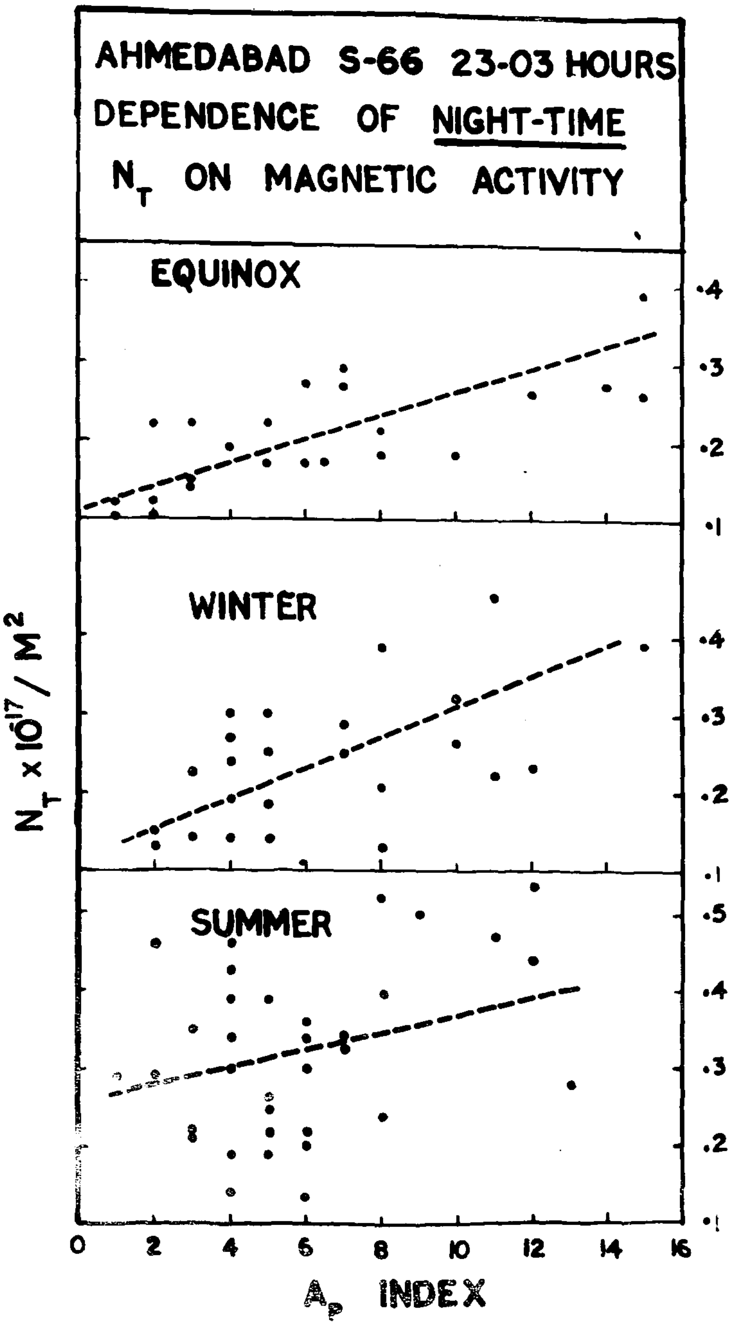

AHMEDABAD S-66 23-03 HOURS
DEPENDENCE OF NIGHT-TIME
N_T ON MAGNETIC ACTIVITY
EQUINOX
WINTER
SUMMER
$N_T \times 10^{17} / M^2$
·1 ·2 ·3 ·4
·1 ·2 ·3 ·4
·1 ·2 ·3 ·4 ·5
0 2 4 6 8 10 12 14 16
A_p INDEX

FIG. 5·5

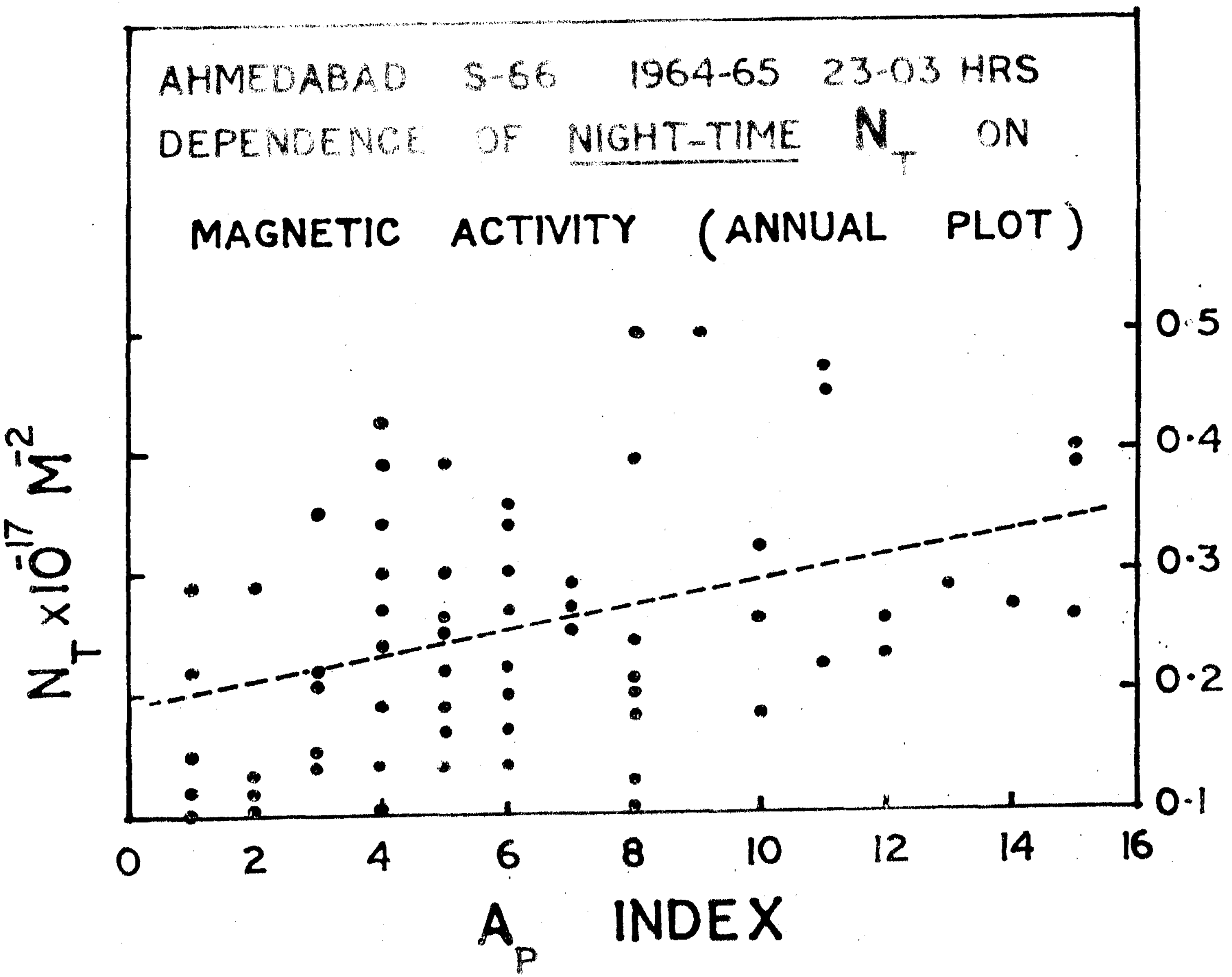
AHMEDABAD S-66 1964-65 23-03 HRS
DEPENDENCE OF NIGHT-TIME N_T ON
MAGNETIC ACTIVITY (ANNUAL PLOT)
$N_T \times 10^{-17}$ M^{-2}
0·5
0·4
0·3
0·2
0·1
0
2
4
6
8
10
12
14
16
A_P INDEX

FIG. 5·6

5.7 Dependence of day-time slab thickness (τ) on magnetic activity

Since the diurnal variation of τ is small, the day-time values have been used for studying the effect of magnetic activity. In Fig.5.7, the day-time values of N_T/n_{max} have been plotted against A_p index separately for summer, winter and equinox. In winter, τ increases with increase in A_p. In equinox this effect is not so pronounced. In summer, τ does not show any clear dependence on A_p.

5.8 Dependence of night-time N_T/n_{max} on magnetic activity

In Fig.5.8, the night-time values of N_T/n_{max} have been plotted against A_p index separately for summer, winter and equinox. In summer and equinox night-time N_T/n_{max} increases with increase in A_p values. In winter night, N_T/n_{max} does not seem to depend on magnetic activity.

5.9 Dependence of day-time and night-time values of N_a/N_b on magnetic activity

The day-time and night-time values of N_a/N_b have been studied separately. In Fig.5.9, the day-time values of N_a/N_b have been plotted against A_p index separately for summer, winter and equinox. In summer N_a/N_b decreases with increase in A_p index. In equinox the ratio does not seem to depend on magnetic activity. In winter the ratio increases with A_p index.

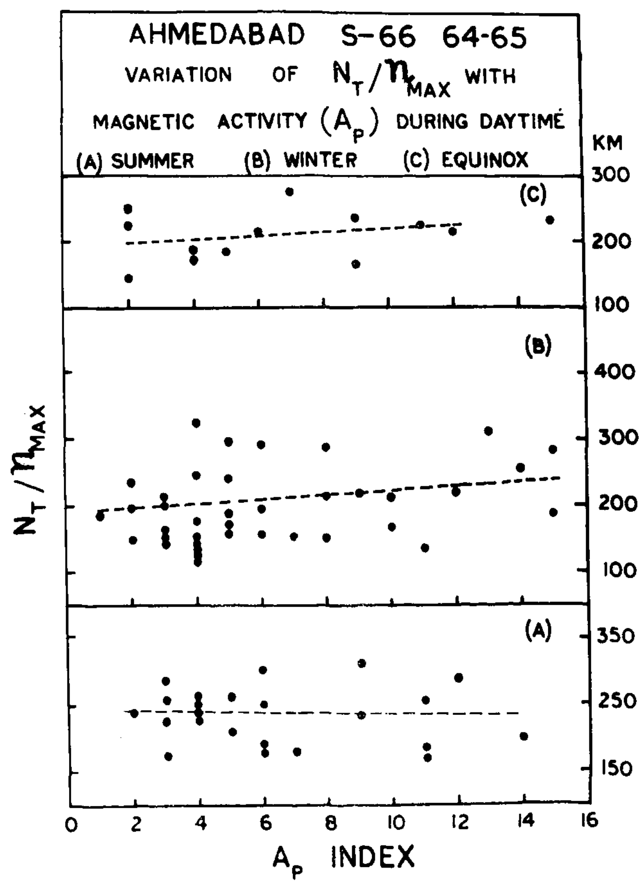
AHMEDABAD S-66 64-65
VARIATION OF N_T/n_{MAX} WITH
MAGNETIC ACTIVITY (A_p) DURING DAYTIME
(A) SUMMER (B) WINTER (C) EQUINOX
KM
300
200
100
400
300
200
100
350
250
150
(C)
(B)
(A)
N_T/n_{MAX}
0
2
4
6
8
10
12
14
16
A_p INDEX

FIG. 5·7

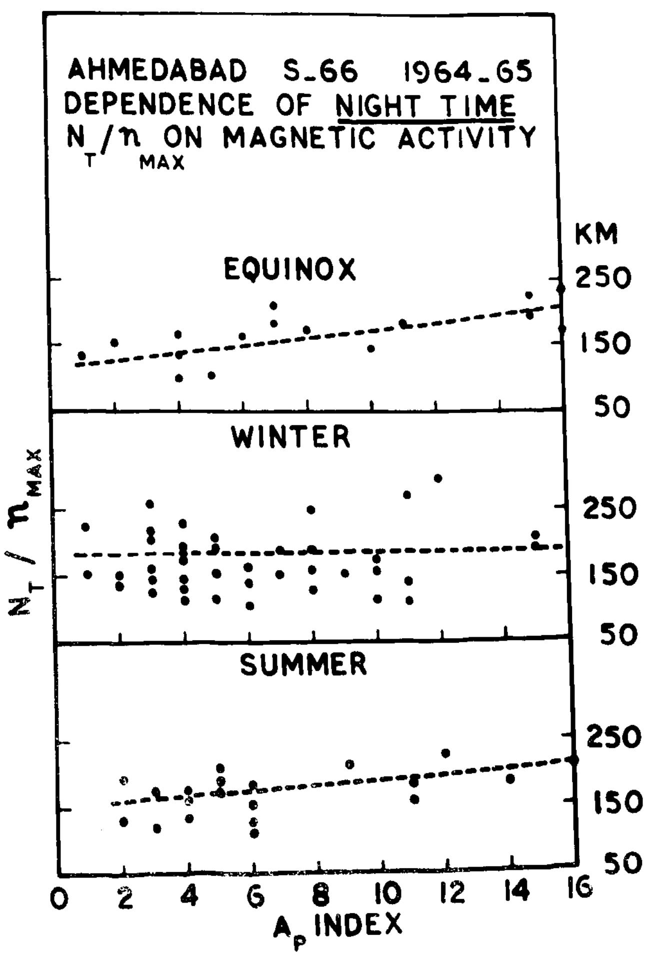
AHMEDABAD S-66 1964-65
DEPENDENCE OF NIGHT TIME
N_T/n_MAX ON MAGNETIC ACTIVITY
KM
EQUINOX
250
150
50
WINTER
250
150
50
SUMMER
250
150
50
N_T / n_MAX
0 2 4 6 8 10 12 14 16
A_P INDEX

FIG. 5·8

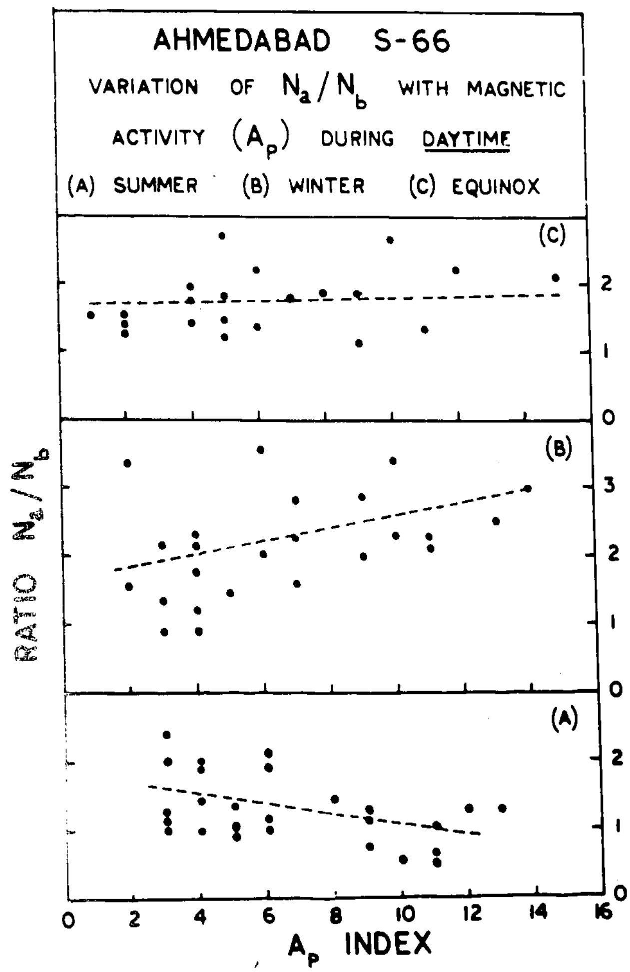
AHMEDABAD S-66
VARIATION OF N_a/N_b WITH MAGNETIC ACTIVITY (A_p) DURING DAYTIME
(A) SUMMER (B) WINTER (C) EQUINOX
(C)
(B)
(A)
RATIO N_a/N_b
0
1
2
3
0
2
4
6
8
10
12
14
16
A_p INDEX

FIG. 5.9

The night-time values of N_a/N_b have been shown in Fig.5.10. These values are plotted against A_p index separately for summer, winter and equinox. Since the ratio becomes very large early in the morning, these values have not been included. It can be seen that in equinox the night-time values of N_a/N_b also do not seem to depend on magnetic activity. While the night-time ratio increases with A_p in summer, it decreases in winter.

5.10 Dependence of day-time and night-time values of h_pF_2 on magnetic activity

Since the electron content variations are connected with the changes in the height of maximum electron density, the dependence of mid-day and mid-night values of h_pF_2 on magnetic activity has also been studied. Fig.5.11 shows the dependence of mid-day h_pF_2 on A_p. In winter and equinox, mid-day h_pF_2 does not seem to depend on magnetic activity.

In Fig.5.12 the values of h_pF_2 at 22 hours have been plotted against A_p index separately for summer, winter and equinox. In winter, night-time h_pF_2 increases with A_p. In summer and equinox, night-time h_pF_2 does not seem to depend on magnetic activity.

5.11 Discussion

In Fig.5.1, the best fitting straight lines have been drawn and these lines have been extended to zero solar flux. It

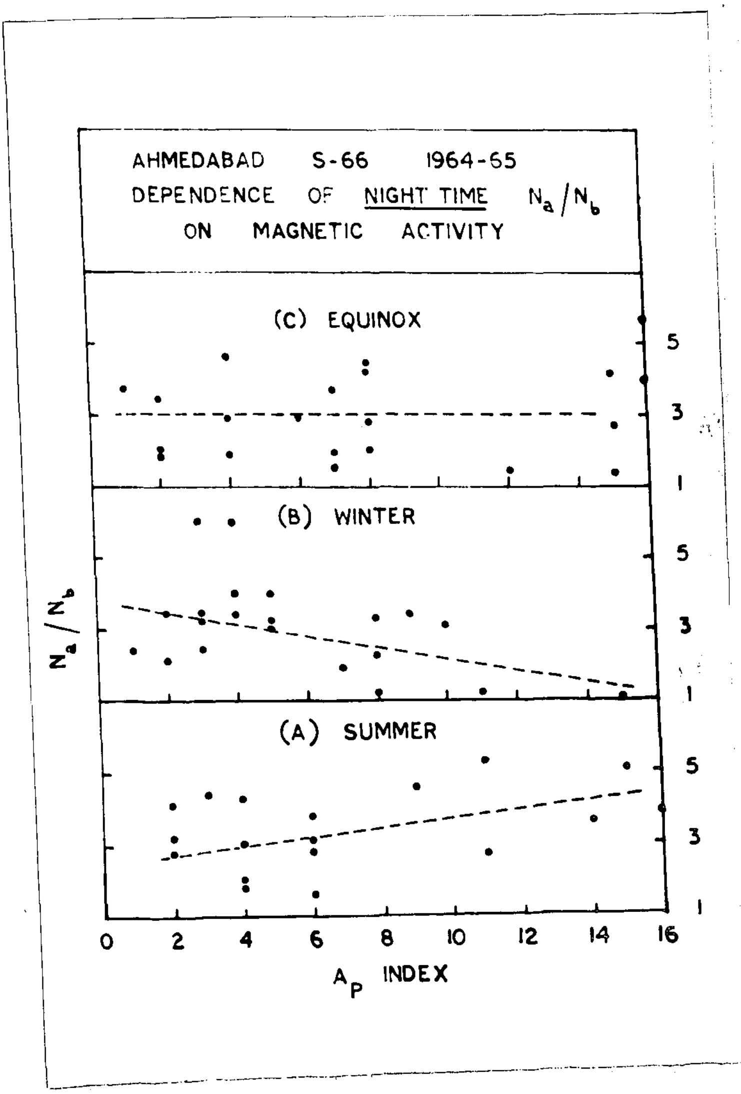
AHMEDABAD S-66 1964-65
DEPENDENCE OF NIGHT TIME N_a/N_b
ON MAGNETIC ACTIVITY
(C) EQUINOX
(B) WINTER
(A) SUMMER
N_a/N_b
1
3
5
0
2
4
6
8
10
12
14
16
A_p INDEX

FIG. 5.10

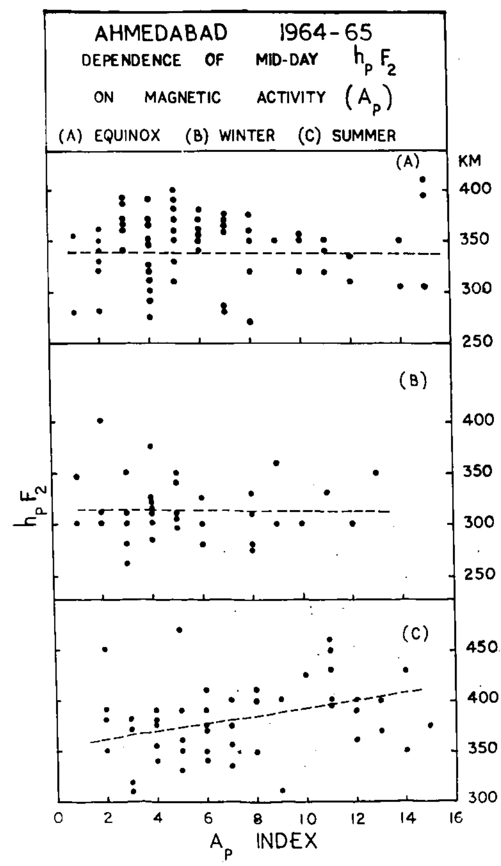

AHMEDABAD 1964-65
DEPENDENCE OF MID-DAY $h_p F_2$
ON MAGNETIC ACTIVITY (A_p)
(A) EQUINOX (B) WINTER (C) SUMMER
(A)
KM
400
350
300
250
(B)
400
350
300
250
(C)
450
400
350
300
$h_p F_2$
0 2 4 6 8 10 12 14 16
A_p INDEX

FIG. 5·11

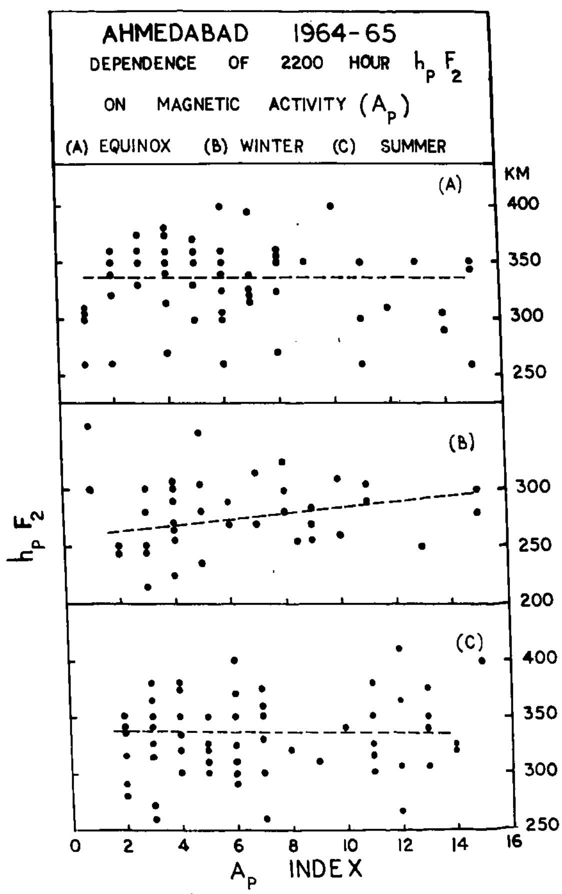
AHMEDABAD 1964-65
DEPENDENCE OF 2200 HOUR h_pF_2
ON MAGNETIC ACTIVITY (A_p)
(A) EQUINOX (B) WINTER (C) SUMMER
KM
(A)
400
350
300
250
(B)
300
250
200
(C)
400
350
300
250
h_pF_2
0 2 4 6 8 10 12 14 16
A_p INDEX

FIG. 5·12

can be seen that in all the seasons the line passes through the origin. Taylor (1966) has reported that the winter line intercepts the solar flux axis at a point significantly away from the origin. This might have been due to the fact that there were no observations corresponding to solar flux values less than 100 units. In the present result also it can be seen that the winter line which fits the observations corresponding to solar flux values higher than 100 units intercepts the x axis at a point away from the origin. If the change in the slope of the line in the region of solar flux less than 100 units is taken into account, the winter line also passes through the origin.

An approximate linear relationship between N_T and sunspot number has been found by Bhonsle et al (1965) for sunspot numbers larger than 40. Yeh and Flaherty (1966) have extended these observations to sunspot numbers less than 40. They find that the linear dependence breaks down when the sunspot number falls below 40. At Ahmedabad in winter, a change in the linear relationship between N_T and S can be seen when the solar flux falls below 100 units. In summer and equinox, this feature is not noticeable even though there are observations corresponding to solar flux values between 70 units and 130 units. Somayajulu et al (1966) have shown that N_T over Delhi is independent of solar flux when the flux is less than 80 units. From Fig.5.1 it can be seen that N_T over Ahmedabad definitely shows an increase with flux even in the region of solar flux less than 80 units.

Bhonsle et al (1965) have determined an empirical relationship between τ in middle latitudes and the mean sunspot number ($\bar{R}$). Over middle latitudes, the rate of increase of τ with sunspot number is about 1 km in winter, 1.2 km in equinox and 1.35 km in summer. These values have been normalised by Bhonsle et al (1965). After normalising they get a coefficient of 0.005 in all the seasons. Normalising is done by dividing the rate of change of τ by the value of τ corresponding to zero sunspot number. In the present result over Ahmedabad also, it can be seen that the rate of change of τ with solar flux is minimum in winter and maximum in summer. If these values are normalised by dividing the rate of change of τ by the value of τ corresponding to solar flux of 70 units, the coefficient comes out to be about 0.006 in winter and equinox and 0.007 in summer. Since the measurements have been made within a limited range of solar flux the values of these coefficients determined by this analysis are to be treated with caution.

The variation of middle latitude N_T with 10.7 cm solar flux has been studied by Hibberd (1964). He has calculated the rate of change of N_T with flux (S) for summer and winter. In summer and winter he finds $\partial N_T/\partial S$ to be 0.028×10^{17} and 0.038×10^{17} respectively. Over Ahmedabad, $\partial N_T/\partial S$ seems to be higher. From the results of Hibberd, it can be seen that the logarithmic gradient, $\frac{\partial N_T/\partial S}{N_T(100)}$, is nearly the same in winter and summer. Over Ahmedabad this is about 0.01 in summer and equinox and about 0.026 in winter. In winter the middle and low latitude results show the same value of logarithmic gradient of N_T.

Ross (1960), Yeh and Swenson (1961) and de Mendonca (1962) have shown that electron content figures are depressed following a magnetic storm. Ross has shown an inverse dependence of N_T upon ΣK_p for the previous 24 hours during the months of June, July and August 1959. Over middle latitude Ross (1960) and Garriott (1960) have found no systematic dependence during the winter months. Our results over Ahmedabad are also in confirmity with these middle latitude results. Lyon (1965) has also found that the middle latitude N_T is inversely dependent upon the magnetic activity index in summer months and not in winter months.

In summer and winter, day-time and night-time values of N_a/N_b exhibit opposite dependence on magnetic activity. In summer, while the day-time values of N_a/N_b decrease with A_p the night time values increase with A_p. In winter, day-time shows positive correlation and night-time shows negative correlation.

Summer and winter also behave differently. During day time it can be seen that N_a/N_b decreases with A_p in summer and increases with A_p in winter. In the night also this seasonal effect can be seen. Night-time value of N_a/N_b increases with A_p in summer and decreases with A_p in winter. It can also be noticed that when h_pF_2 increases with magnetic activity N_a/N_b decreases. A summary of the results has been provided in Table I.

Table 1

Changes of N_T and related parameters with increase in A_p

Parameter	Summer	Winter	Equinox
	Day-time		
N_T	Negative	Uncertain	Negative
N_T/n_{max}	Nil	Positive	Positive
N_a/N_b	Negative	Positive	Nil
h_pF_2	Positive	Nil	Nil
	Night-time		
N_T	Positive	Positive	Positive
N_T/n_{max}	Positive	Nil	Positive
N_a/N_b	Positive	Negative	Nil
h_pF_2	Nil	Positive	Nil

CHAPTER VI

SATELLITE SIGNAL SCINTILLATIONS

CHAPTER VI

SATELLITE SIGNAL SCINTILLATIONS

6.1 Introduction

Radio signals from Beacon Satellites have been used to study the small scale inhomogeneities in the electron density of the ionosphere. These irregularities, when present, cause scattering of radio waves propagated through them, resulting in irregular patterns of signal strength on the ground. Radio scintillation is a random time variation of the amplitude and phase of a radio wave which has propagated through a region of ionospheric inhomogeneities. Generally speaking, diffraction effects of ionospheric inhomogeneities in refractive index give rise to scintillations.

Radio scintillation is analogous to visual star scintillation or twinkling. In both cases the variations are caused by irregularities in the dielectric constant of the atmosphere. Air density irregularities are always present in the troposphere and it is these irregularities which cause optical scintillation. However, at radio wave-lengths greater than about 30 cm the dielectric constant of the ionosphere becomes significantly larger than the dielectric constant of the troposphere. There is reason to believe that ionospheric irregularities are responsible for radio scintillation.

6.1.1 Radio Star Scintillation

Radio signals from "stars" were discovered by Karl Jansky in 1932. In 1946 it was discovered that the intensity of the radio signal received from the strong radio source in Cygnus was variable (Hey, Parsons and Phillips, 1946). The development of the correct explanation of this phenomenon was closely parallel with the development of the explanation of optical star scintillation. It was first believed that the variations were due to fluctuations in the source itself (Hey et al, 1946). Later experimental evidence proved this explanation wrong. As with light, it is not possible to interpret completely the signal strength record of scintillation. The variation could be caused by the motion of a fixed pattern of radio signal strength past the antenna, or by changes in an unmoving pattern of signal strength or both. To study scintillation-producing irregularities in detail it is necessary to study the distribution of signal strength over the ground, its motions and its changes. To do this, data from several points on the ground are necessary. Using a pair of receivers spaced 3.9 Km apart, recordings of the signals from Cygnus were found to be similar (50 to 95 percent correlated). For a spacing of 20 km, "No detailed correlation could be found" (Smith, 1950; Little and Lovell, 1950). Thus it was first revealed that radio star scintillation must be introduced somewhere in the earth's atmosphere.

6.1.2 Satellite Scintillation

On October 5, 1957, the first artificial satellite, Sputnik I, was launched. The 20 MHz and 40 MHz beacon signals from the transmitters on board were observed to scintillate rapidly and irregularly, at rates of the order of several fluctuations per second (Kraus and Albus, 1958; Warwick, 1958). Observations in Australia (Slee, 1958) suggested a correlation between scintillations of satellite signals and radiation from cosmic sources, though this suggestion was not supported by a report from Alaska (Parthasarathy and Reid, 1959). Later, many reports have been published on satellite scintillation over middle and high latitudes. Relatively few results have been published of observations made in low latitudes.

6.1.3 Comparison of radio star and satellite scintillation

Radio star scintillation studies cannot give an instantaneous picture of the latitudinal variation of the irregularities. On the other hand, the fast moving earth satellites can provide a "snap shot" of the irregularities in the ionosphere. Radio star scintillation studies cannot accurately locate the height of the scintillation-producing irregularities. Artificial earth satellites offer several good ways of measuring the height of the irregularities. The easiest method is to observe the variation of average scintillation index with satellite height. Using this method it has been reported that most of the irregularities are within the following height ranges: 200 to 400 Km at Baker Lake (Swenson and Yeh, 1961); 270 to 325 Km at Cambridge, England (Kent, 1959); 250 to 650 Km at College Alaska (Basler and Dewitt, 1962).

Since the satellite velocity is much greater than the drift velocity of the ionospheric irregularities, the ground velocity of the pattern is determined only by the satellite velocity, satellite height and irregularity height. By determining the velocity of the irregularity pattern on the ground, it is possible to measure the irregularity height.

6.1.4 Scope of the present investigation

Since the advent of artificial satellites, a large amount of data has been collected over middle and auroral latitudes and the effects of ionospheric irregularities on satellite signals have been studied. Relatively, low latitude scintillations have not been studied in detail. In the present investigation the role of sporadic E ionisation in producing satellite signal scintillations has been emphasised and studied in some detail. The movements of the boundary of F region irregularities as seen by satellite signal scintillations has also been studied. The dependence of scintillation depth on zenith angle has been determined. The diurnal variation of the occurrence of scintillation over low latitudes has also been shown.

6.2 Scintillation depth and scintillation rate

Different measures of scintillation depth have been used in observations of radio star and satellite scintillations. When radio waves are received from a satellite, the deflection of the recorder is normally proportional to the amplitude of the wave. It is therefore convenient to use a measure of the scintillation depth. This is taken as the ratio of the deviation of the amplitude from the mean amplitude to the mean amplitude. The deviation may be the mean deviation or the root mean square deviation.

The receiving system used in the present work has been described in Chapter III. Since the transmission and reception are plane polarised, the amplitude scintillations are super-imposed on Faraday fading. A sample record is shown in Fig.6.1. The maximum (I_X) and minimum (I_N) amplitudes of scintillation have been scaled as shown in Fig.6.1. I_X and I_N are scaled at the time of maximum amplitude of each Faraday fade. The scintillation depth is calculated from the formula

$$S = (I_X - I_N)/(I_X + I_N) \qquad (1)$$

where S is the scintillation depth.

The scintillation rate is given by the number of fades per second. The frequency response of the strip chart recorder is 48 cycles/second and the A.G.C. time constant of the receiver is 8 milli second. The receiving system is capable of recording fast scintillations. The limitation is due to low chart speeds which had to be used in order to reduce the consumption of chart paper. The 40 MHz scintillation rate could be revolved even with slow chart speeds. For each transit, the scintillation rates have been determined at intervals of 30 seconds.

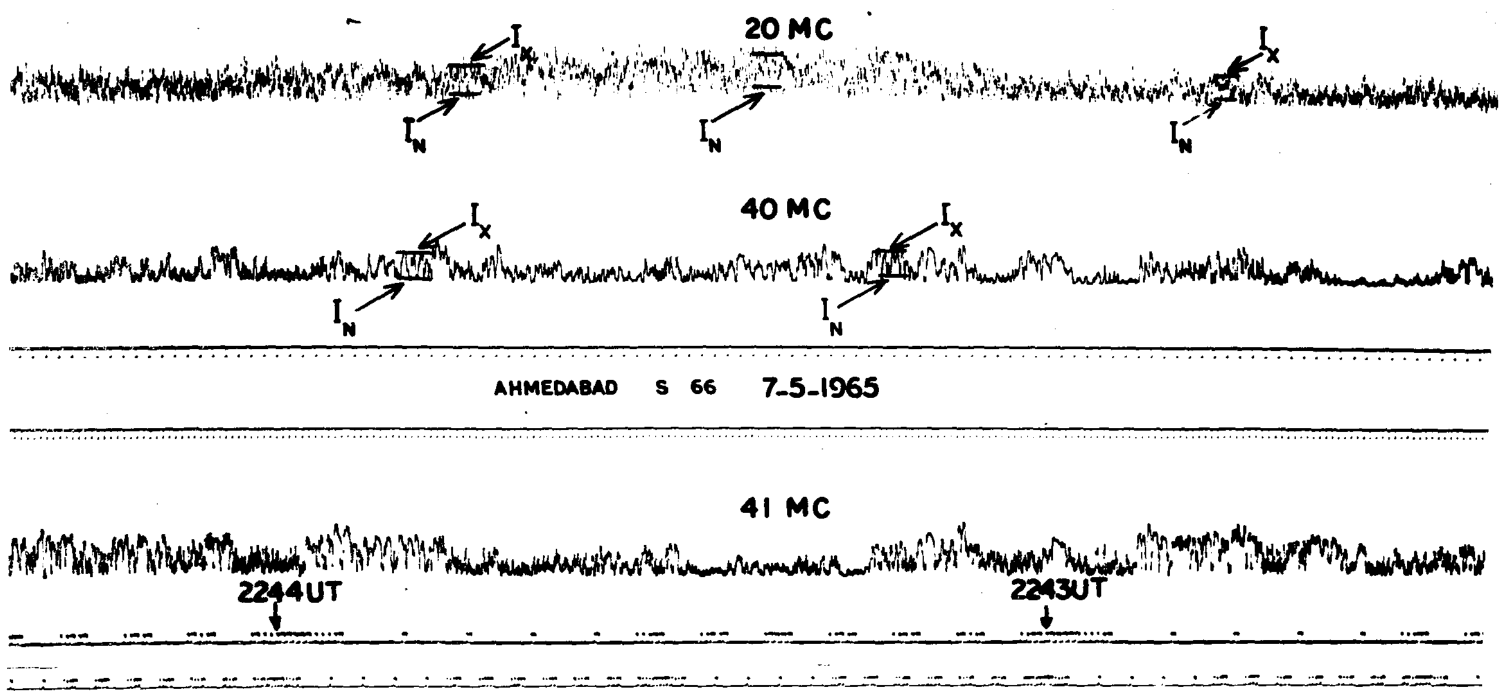

Fig.6.1 Figure illustrating the scaling of I_x (maximum) and I_N (minimum) levels of scintillation.

6.3 Dependence of scintillation on sporadic E ionisation

Fig.6.2 shows the amplitude of satellite signals recorded at 1455 hours U.T. on May 25, 1965. It can be seen that the amplitude of the scintillations mask the regular Faraday fading also. The ionogram taken at the time of this transit on 25th May is shown in Fig.6.3. The presence of strong sporadic E ionisation can be seen on the ionogram. It can also be noted that the F layer trace on the ionogram does not exhibit scattered echoes. Such examples of satellite transits, which gave amplitude scintillations in the presence of sporadic E ionisation alone, have been studied separately. In Fig.6.4 the average scintillation rate of 40 MHz signals have been plotted against f_xE_s, which is the maximum frequency of the sporadic E trace as seen on the ionogram. It can be seen that the scintillation rate increases with f_xE_s. Each value of scintillation rate is the mean value of about 25 readings taken at intervals of 30 seconds during each transit.

The values of scintillation depth have also been calculated for the transits, which gave scintillations in the presence of sporadic E alone. As mentioned earlier, the scintillation depth is calculated at the time of maximum amplitude of each Faraday fade. These values are plotted and the value corresponding to the time when the satellite crossed 23^{o}N latitude is determined. In Fig.6.5 these values of scintillation depths at 20 MHz and 40 MHz have been plotted against the corresponding values of f_xE_s. It can be seen that

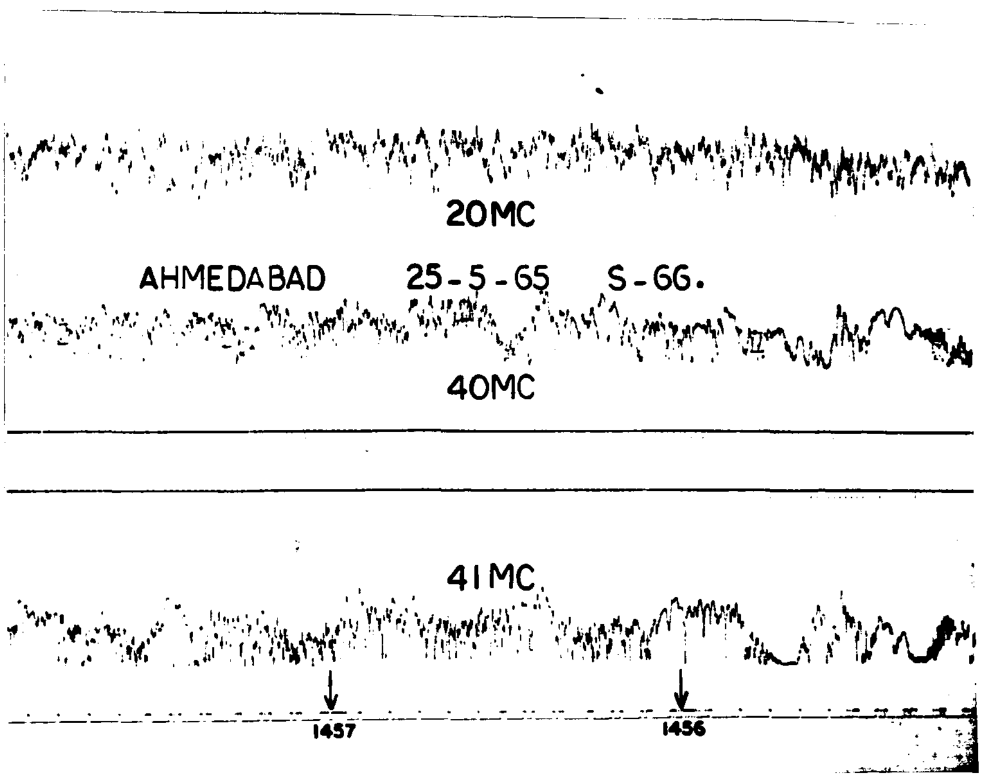

FIG. 6.2
SATELLITE SIGNAL SCINTILLATIONS IN THE PRESENCE OF SPORADIC-E-ONLY

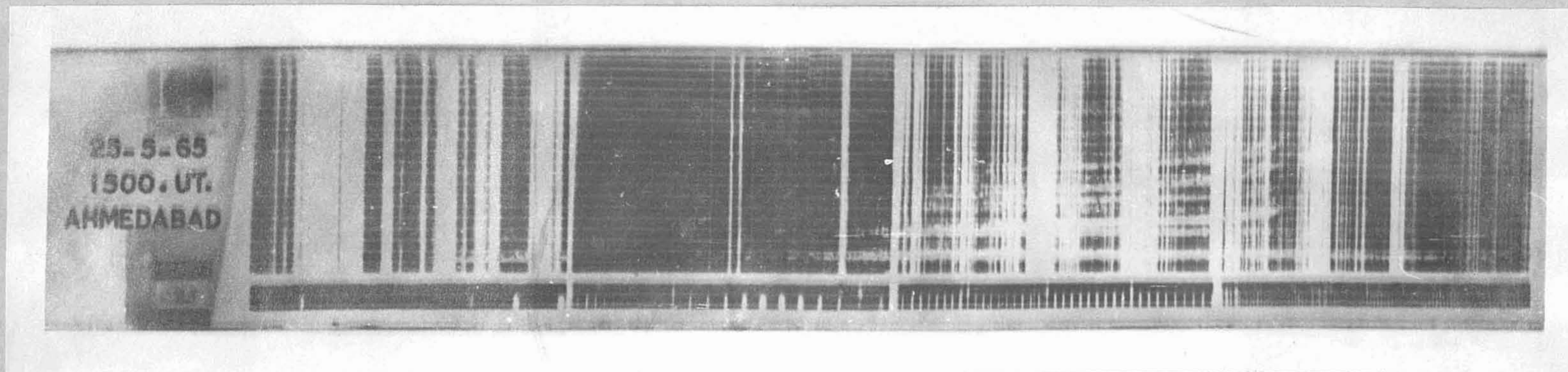

Fig.6.3 Ionogram taken at the time of satellite transit, which gave scintillations.

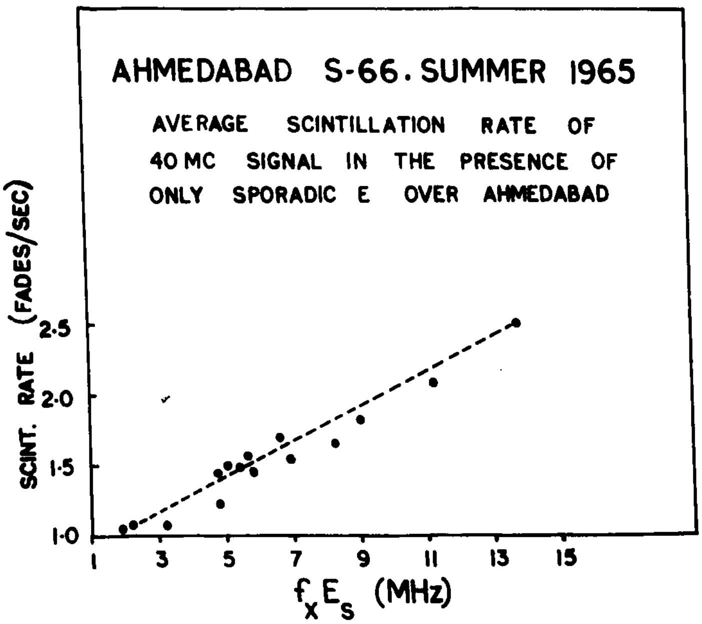
AHMEDABAD S-66. SUMMER 1965
AVERAGE SCINTILLATION RATE OF
40 MC SIGNAL IN THE PRESENCE OF
ONLY SPORADIC E OVER AHMEDABAD
SCINT. RATE (FADES/SEC)
2·5
2·0
1·5
1·0
1
3
5
7
9
11
13
15
$f_x E_s$ (MHz)

FIG. 6·4

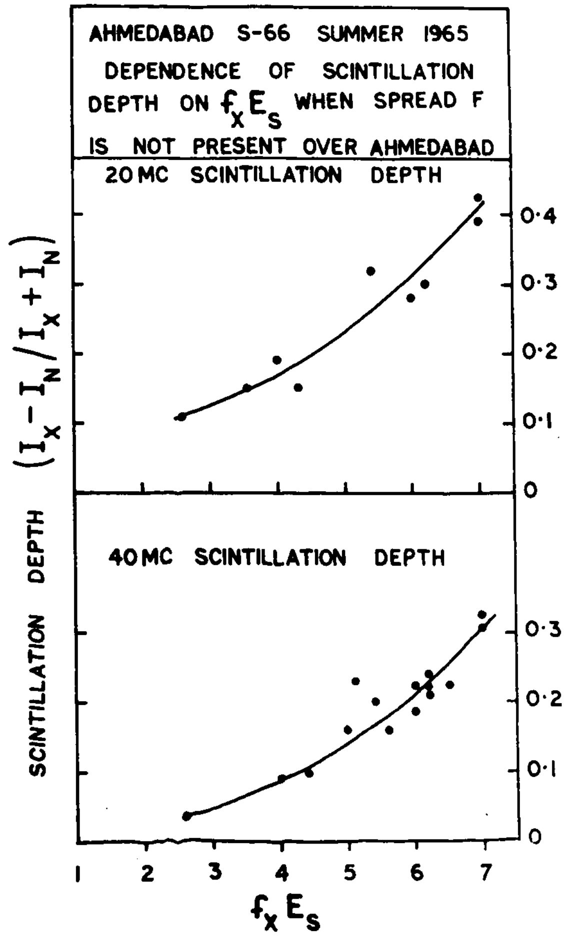
AHMEDABAD S-66 SUMMER 1965
DEPENDENCE OF SCINTILLATION DEPTH ON $f_x E_s$ WHEN SPREAD F IS NOT PRESENT OVER AHMEDABAD
20 MC SCINTILLATION DEPTH
40 MC SCINTILLATION DEPTH
SCINTILLATION DEPTH $(I_X - I_N / I_X + I_N)$
0·4
0·3
0·2
0·1
0
1
2
3
4
5
6
7
$f_x E_s$

FIG. 6·5

scintillation depth at 20 MHz is larger than the corresponding depth at 40 MHz. With f_xE_s, 40 MHz scintillation depth seems to increase at a faster rate than the 20 MHz depth. From Fig.6.5 it seems that the scintillation depth increases exponentially with f_xE_s. In Fig.6.6, these values have been plotted on logarithmic scale. The points show a reasonable straight line dependence. An empirical relationship between scintillation depth and f_xE_s has been determined. The following relationships have been found :-

$$S_{20} = 0.02\ (f_xE_s)^{1.5} \qquad (2)$$

$$S_{40} = 0.006\ (f_xE_s)^{2.0} \qquad (3)$$

where S_{20} and S_{40} are the values of scintillation depths at 20 MHz and 40 MHz respectively. From the exponential part of the equations it can be seen that the scintillation depth at 40 MHz increases with f_xE_s at a faster rate. In Fig.6.7, the ratios of 20 MHz scintillation depth to 40 MHz scintillation depth are plotted against f_xE_s. The individual values of 20 MHz and 40 MHz scintillation depths have been taken from the mean curves of Fig.6.5. It can be seen from Fig.6.7 that the ratio decreases with increasing value of f_xE_s. The relationship between ratio of scintillation depths and f_xE_s seems to be of the form

$$R = C + K\ (E_s)^{-n} \qquad (4)$$

where R is the ratio of scintillation depths and E_s is the value of f_xE_s.

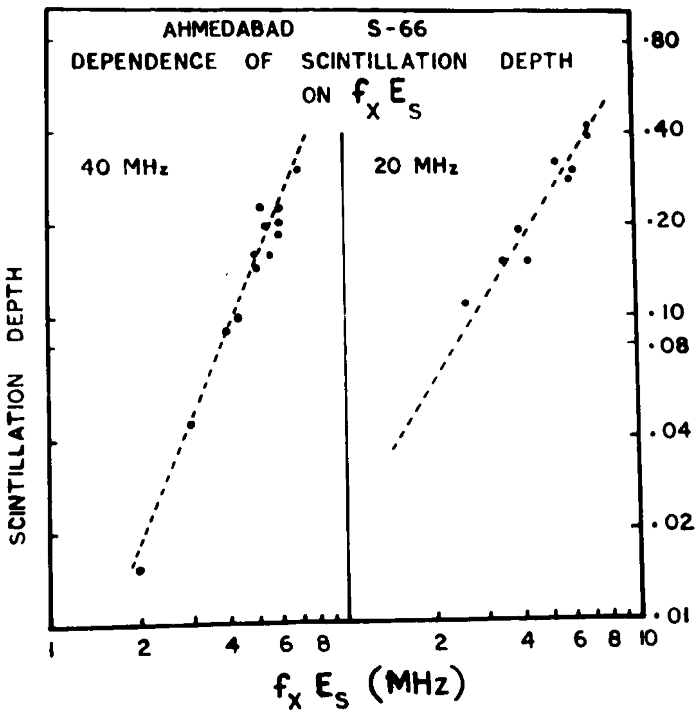
AHMEDABAD S-66
DEPENDENCE OF SCINTILLATION DEPTH ON $f_x E_s$
40 MHz
20 MHz
SCINTILLATION DEPTH
·80
·40
·20
·10
·08
·04
·02
·01
1
2
4
6
8
2
4
6
8
10
$f_x E_s$ (MHz)

FIG. 6·6

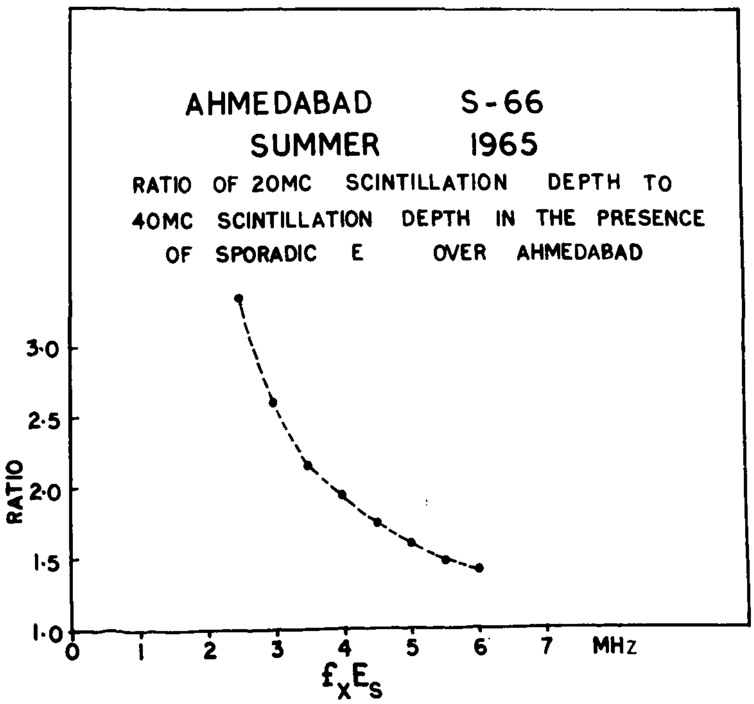
AHMEDABAD S-66
SUMMER 1965
RATIO OF 20MC SCINTILLATION DEPTH TO 40MC SCINTILLATION DEPTH IN THE PRESENCE OF SPORADIC E OVER AHMEDABAD
RATIO
3·0
2·5
2·0
1·5
1·0
0
1
2
3
4
5
6
7
MHz
f_xE_s

FIG. 6.7

On differentiating equation (4) with respect to E_s, we get

$$\frac{dR}{dE_s} = (-nk)\,(E_s)^{-(n+1)} \tag{5}$$

Taking logarithms on both sides

$$\text{Log}\,\frac{(dR)}{dE_s} = \log(-nk) - (n+1)\log(E_s)$$

Plot of $\log\left(\frac{dR}{dE_s}\right)$ against $\log(E_s)$ must give a straight line. In Fig.6.8, $\frac{dR}{dE_s}$ is plotted against E_s on logarithmic scale. The points fall in a reasonable straight line. From the slope of this line, the value of 'n' is determined. It comes out to be -1.75. The relationship between R and f_xE_s is given by the empirical formula, $R = 0.8 + 13.3\,(E_s)^{-1.75}$. For large values of f_xE_s, the ratio of 20 MHz scintillation depth to 40 MHz scintillation depth seems to approach unity.

6.4 Scintillation boundary

In some of the night time records, a type of scintillation which stops abruptly at some latitude is noticed. This phenomenon occurs in all the seasons. An example of a southbound satellite transit illustrating the scintillation boundary is shown in Fig.6.9. The change over from intense scintillation to regular Faraday fading can be seen clearly. Similar transitions have also been reported to occur at Cambridge, England (Kent, 1959);

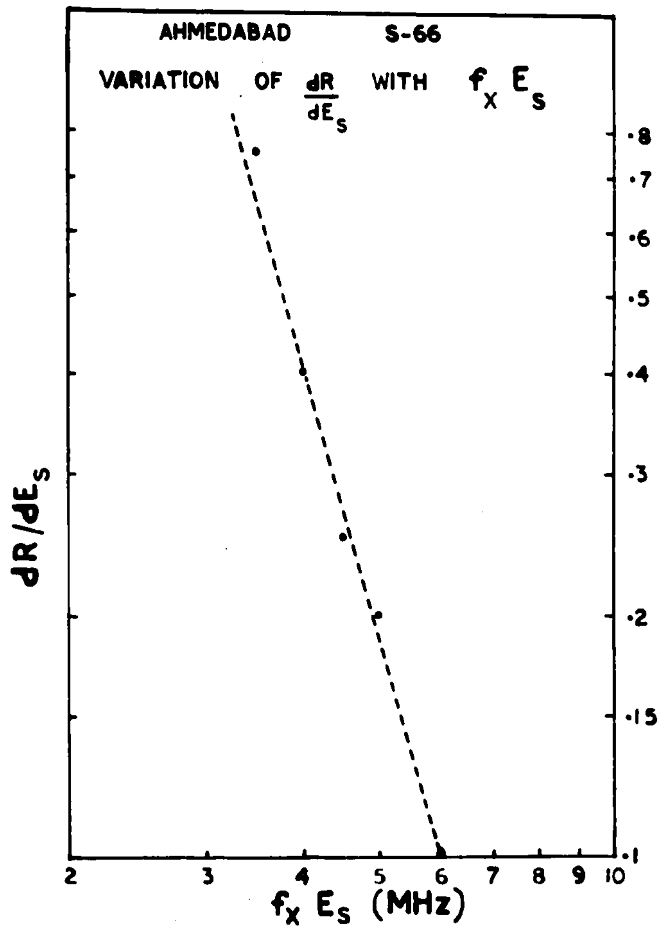
AHMEDABAD S-66
VARIATION OF $\frac{dR}{dE_s}$ WITH $f_x E_s$
dR/dE_s
·8
·7
·6
·5
·4
·3
·2
·15
·1
2
3
4
5
6
7
8
9
10
$f_x E_s$ (MHz)

FIG. 6·8

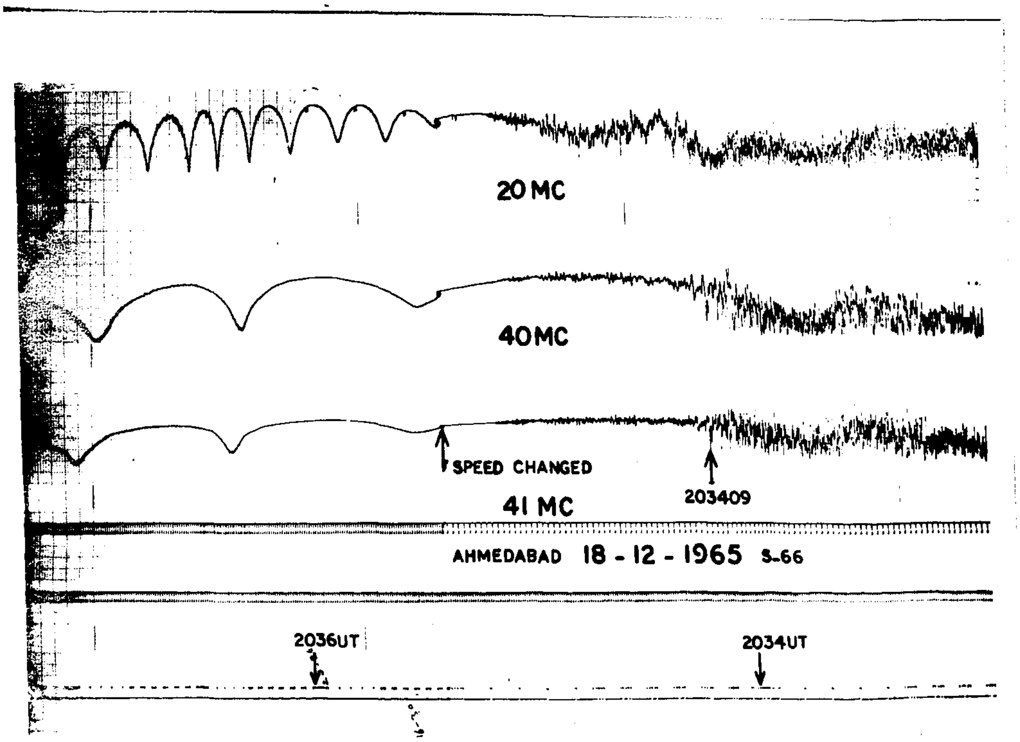

Fig.6.9 An illustration of satellite signal record showing scintillation boundary.

Vancouver, Canada (DeMendonca, 1960); Boston, Mass. (Aarons et al, 1963) and Illinois, U.S.A. (Yeh and Swenson, 1964).

This phenomenon occurs on the northern and southern sides of Ahmedabad. At the time of cessation of scintillation, the sub-ionospheric latitude is calculated. For determining the sub-ionospheric latitude, it has been assumed that the irregularities occurred at a height of 350 Km.

6.5 Dependence of scintillation boundary on magnetic activity

The values of sub-ionospheric latitudes at the time of cessation of scintillation have been plotted in Figs.6.10 and 6.11 separately for winter and summer respectively. In these figures, open circles are drawn for the transits which showed continued scintillations towards the north. Closed circles are drawn for the transits which showed continued scintillation towards the south. The points indicate the sub-ionospheric latitudes at which scintillation stopped or started and the arrows indicate the directions in which scintillations continued. From these figures, it can be seen that the scintillation boundary moves towards the north as the A_p index increases. This movement is more conspicuous in winter than in summer. Yeh and Swenson (1964) have noted that such transitions move to a lower latitude when magnetic activity increases. Such an effect has also been noted by Aarons et al (1963). These results are for the middle latitude stations, Illinois (40°N) and Massachusetts (43°N). If we compare the low latitude and middle latitude results,

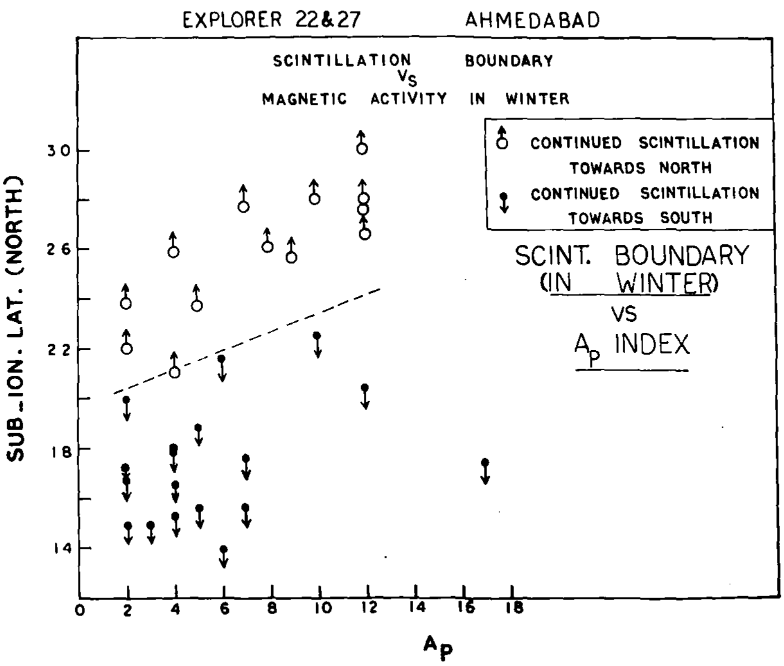
EXPLORER 22&27 AHMEDABAD
SCINTILLATION BOUNDARY
Vs
MAGNETIC ACTIVITY IN WINTER
CONTINUED SCINTILLATION TOWARDS NORTH
CONTINUED SCINTILLATION TOWARDS SOUTH
SCINT. BOUNDARY (IN WINTER)
VS
Ap INDEX
SUB.-ION. LAT. (NORTH)
30
26
22
18
14
0
2
4
6
8
10
12
14
16
18
Ap

FIG. 6·10

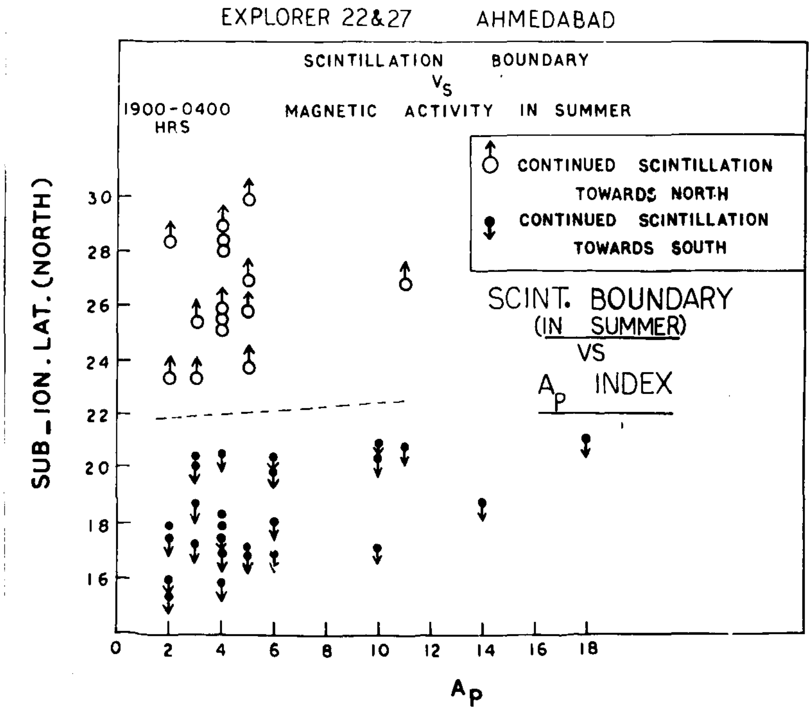
EXPLORER 22&27 AHMEDABAD
SCINTILLATION BOUNDARY
VS
MAGNETIC ACTIVITY IN SUMMER
1900-0400 HRS
CONTINUED SCINTILLATION TOWARDS NORTH
CONTINUED SCINTILLATION TOWARDS SOUTH
SCINT. BOUNDARY
(IN SUMMER)
VS
AP INDEX
SUB_ION. LAT. (NORTH)
30
28
26
24
22
20
18
16
0
2
4
6
8
10
12
14
16
18
AP

FIG. 6·11

it seems that the transition regions shift towards the south at middle latitudes and towards the north at low latitudes with increase in magnetic activity. More results over low latitude stations will be needed to confirm this behaviour.

6.6 Occurrence of scintillation

For studying the occurrence of scintillation, the satellite transits have been divided into two groups; one group with scintillation in any part of the transit and the other group without any scintillation throughout the transit. If scintillation is seen in any part of a transit, that transit is considered as one with scintillation. The percentage occurrence of scintillation has been calculated for each one hour group separately for summer and winter. These values are shown in Figs.6.12 and 6.13. In general, the scintillation activity is found to be predominant in summer. In winter, during 1964-65, there was not a single transit, which gave intense scintillations throughout the transit. In summer, there were many instances at night when intense scintillations could be seen throughout the transit. The day time scintillation was also more evident in summer. Since the scintillations are due to the irregularities in the ionosphere, the percentage occurrence of spread F has also been found during the same period. These values are shown in Fig.6.14. In both the seasons, it can be seen that spread F is mainly a right time phenomenon. It can also be seen that spread F activity is more in summer. It has been already noted

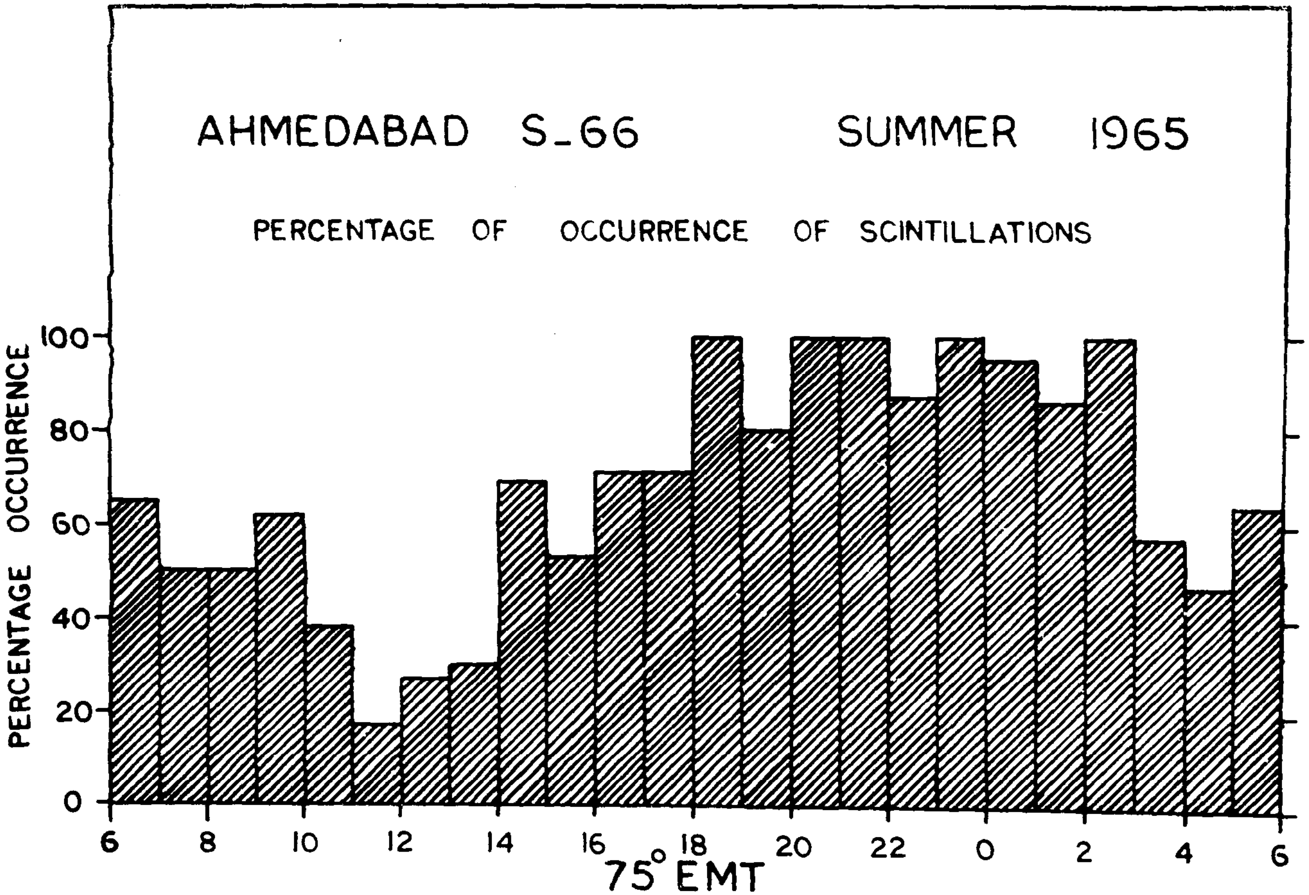
AHMEDABAD S_66 SUMMER 1965
PERCENTAGE OF OCCURRENCE OF SCINTILLATIONS
PERCENTAGE OCCURRENCE
0
20
40
60
80
100
6
8
10
12
14
16
18
20
22
0
2
4
6
75° EMT

FIG. 6·12

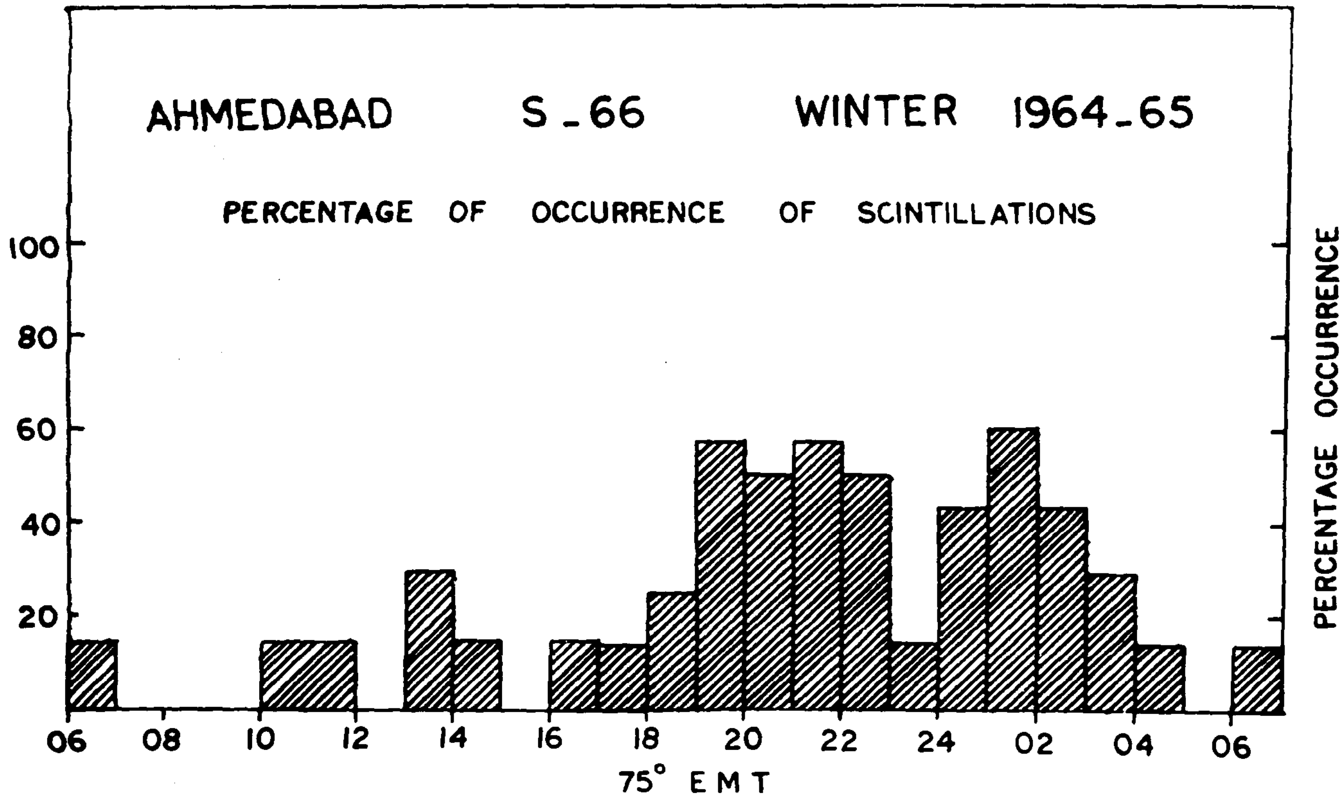
AHMEDABAD S_66 WINTER 1964_65
PERCENTAGE OF OCCURRENCE OF SCINTILLATIONS
100
80
60
40
20
06 08 10 12 14 16 18 20 22 24 02 04 06
75° EMT
PERCENTAGE OCCURRENCE

FIG. 6·13

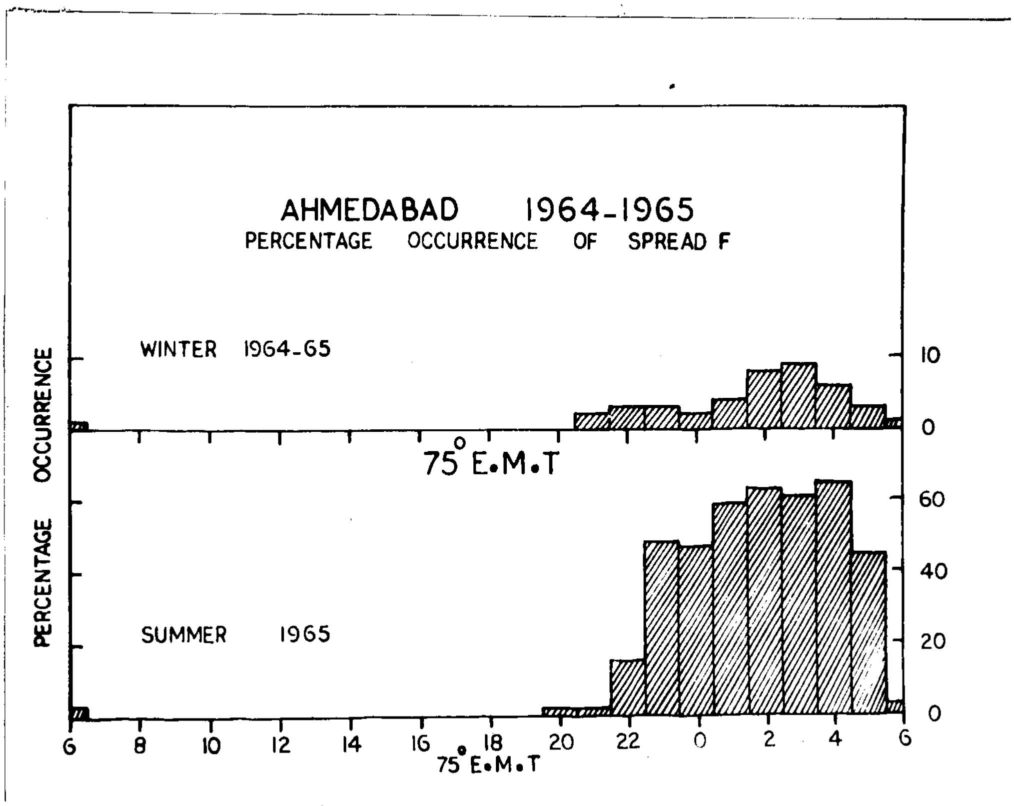
AHMEDABAD 1964-1965
PERCENTAGE OCCURRENCE OF SPREAD F
WINTER 1964-65
SUMMER 1965
PERCENTAGE OCCURRENCE
75° E.M.T
10
0
60
40
20
0
6
8
10
12
14
16
18
20
22
0
2
4
6
75° E.M.T

FIG. 6·14

that both sporadic E and spread F can give rise to satellite scintillations. The occurrence of day-time scintillations in the absence of spread F may be attributed to sporadic E ionisation.

6.7 Dependence of scintillation depth on zenith angle

The zenith angle of a satellite changes continuously within a transit. Still it is not possible to derive a relationship between scintillation depth and zenith angle, because the scintillation depth depends on other factors also. The latitudinal variation of scintillation depth can mask the zenith angle dependence.

In Fig.6.15, the values of scintillation depths have been plotted against sub-satellite latitude. Since our aim is only to see whether there is any latitudinal effect, the sub-ionospheric latitudes have not been determined. The values determined in the presence of spread F and sporadic E and in the presence of sporadic E alone have been plotted separately. From this figure, it can be seen that the latitudinal variation of scintillation depth is negligible when spread F and sporadic E are present simultaneously. When sporadic E alone is present the scintillation depth shows minimum values on the southern side of Ahmedabad.

In Fig.6.16, the values of scintillation depths measured in the presence of spread F and sporadic E have been plotted against zenith angle. The scintillation depth increases with zenith angle. There is no appreciable difference between the

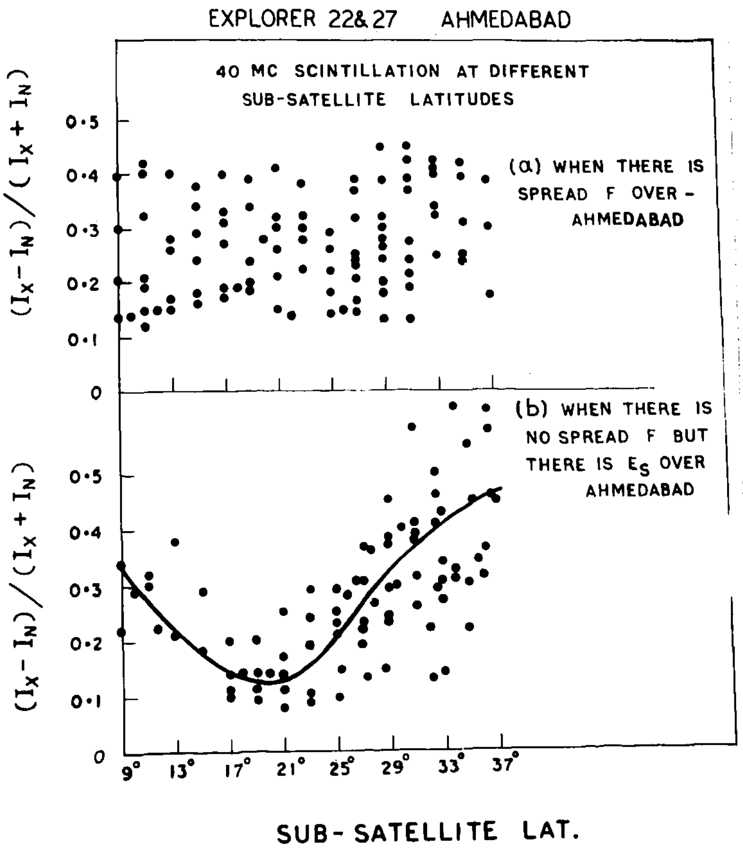
EXPLORER 22& 27 AHMEDABAD
40 MC SCINTILLATION AT DIFFERENT
SUB-SATELLITE LATITUDES
(a) WHEN THERE IS
SPREAD F OVER -
AHMEDABAD
(b) WHEN THERE IS
NO SPREAD F BUT
THERE IS E_S OVER
AHMEDABAD
$(I_X - I_N)/(I_X + I_N)$
0·5
0·4
0·3
0·2
0·1
0
9°
13°
17°
21°
25°
29°
33°
37°
SUB-SATELLITE LAT.

FIG. 6·15

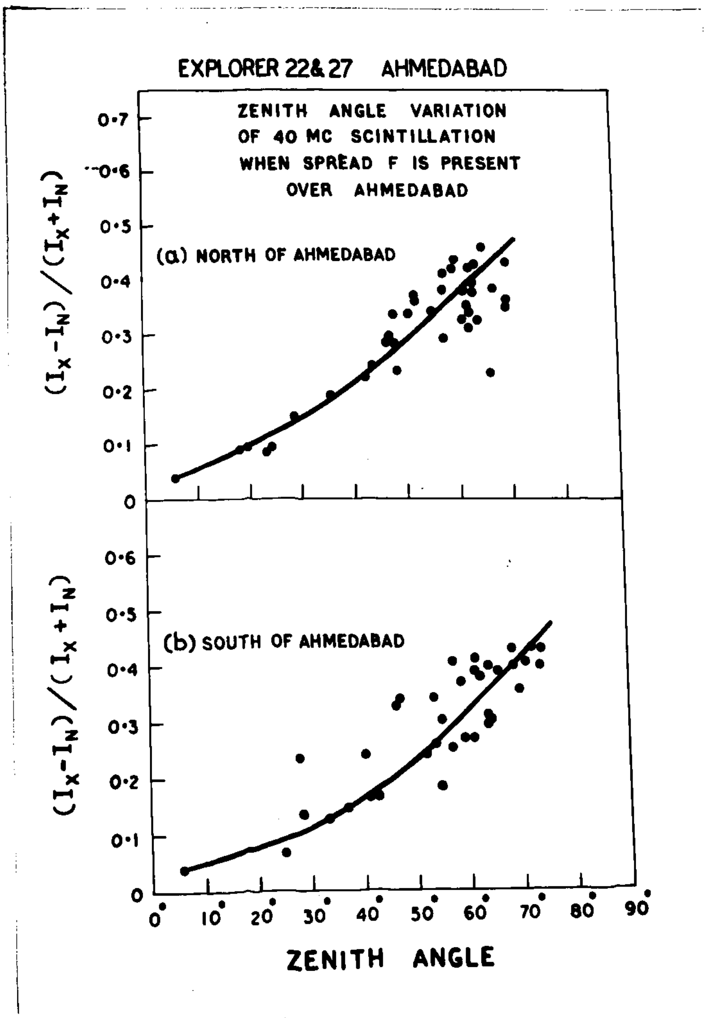
EXPLORER 22& 27 AHMEDABAD
ZENITH ANGLE VARIATION
OF 40 MC SCINTILLATION
WHEN SPREAD F IS PRESENT
OVER AHMEDABAD
(a) NORTH OF AHMEDABAD
(b) SOUTH OF AHMEDABAD
$(I_X - I_N)/(I_X + I_N)$
$(I_X - I_N)/(I_X + I_N)$
0·7
0·6
0·5
0·4
0·3
0·2
0·1
0
0·6
0·5
0·4
0·3
0·2
0·1
0
0° 10° 20° 30° 40° 50° 60° 70° 80° 90°
ZENITH ANGLE

FIG. 6·16

values on the northern and southern sides of Ahmedabad. In Fig.6.17, the values of scintillation depth, measured in the presence of sporadic E alone, have been plotted against zenith angle. In this case, scintillation depth does not seem to change with zenith angle. It is also possible that the latitudinal effect masks the zenith angle effect.

Over Brisbane (27.5°S) Singleton and Lynch (1961a) have also noticed that the little scintillation activity, experienced in the case of transits not involving spread F, does not depend on zenith angle to any great extent. In the case of transits involving spread F, Singleton and Lynch (1962a) have shown that the scintillation activity increases with zenith angle, the effect being negligible below about 50°.

6.8 Dependence of ratio of 20 MHz scintillation depth to 40 MHz scintillation depth on zenith angle

In Fig.6.18, the ratio of 20 MHz scintillation depth to 40 MHz scintillation depth is plotted against the zenith angle. At Ahmedabad spread F and sporadic E are often present simultaneously. On one occasion there was only spread F and sporadic E was not seen on the ionogram. The ratios of scintillation depths calculated during this transit are shown as open circles, in the diagram. The closed circles indicate the values calculated in the presence of spread F and sporadic E. It can be seen that the ratio decreases when the zenith angle increases. The ratio seems to decrease at a faster rate when spread F and sporadic E are present simultaneously.

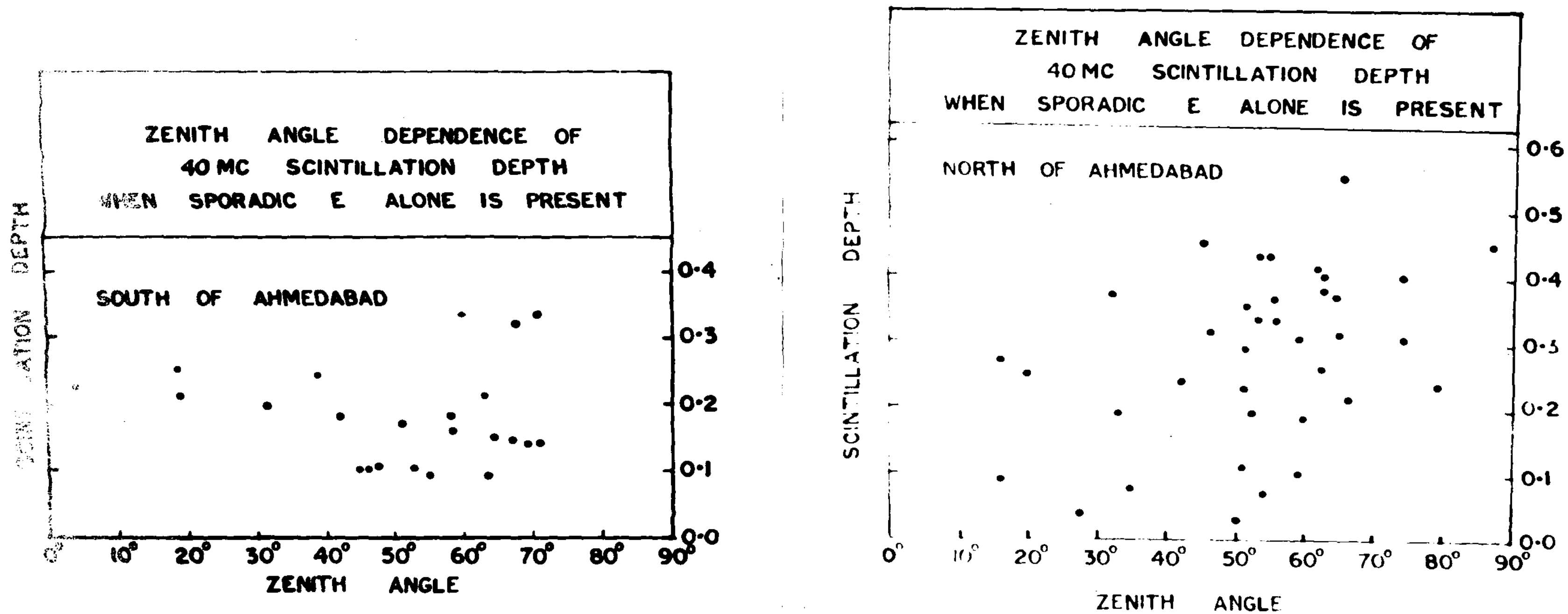
ZENITH ANGLE DEPENDENCE OF
40 MC SCINTILLATION DEPTH
WHEN SPORADIC E ALONE IS PRESENT
SOUTH OF AHMEDABAD
0·4
0·3
0·2
0·1
0·0
10°
20°
30°
40°
50°
60°
70°
80°
90°
ZENITH ANGLE
ZENITH ANGLE DEPENDENCE OF
40 MC SCINTILLATION DEPTH
WHEN SPORADIC E ALONE IS PRESENT
NORTH OF AHMEDABAD
SCINTILLATION DEPTH
0·6
0·5
0·4
0·3
0·2
0·1
0·0
0°
20°
30°
40°
50°
60°
70°
80°
90°
ZENITH ANGLE

FIG. 6·17

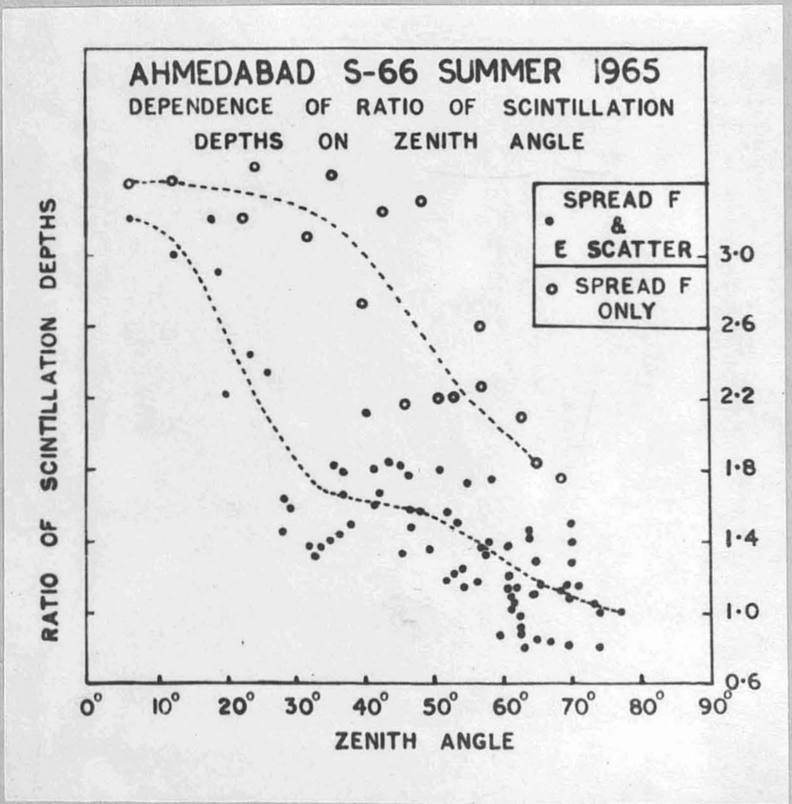
AHMEDABAD S-66 SUMMER 1965
DEPENDENCE OF RATIO OF SCINTILLATION DEPTHS ON ZENITH ANGLE
SPREAD F & E SCATTER
SPREAD F ONLY
RATIO OF SCINTILLATION DEPTHS
3·0
2·6
2·2
1·8
1·4
1·0
0·6
0° 10° 20° 30° 40° 50° 60° 70° 80° 90°
ZENITH ANGLE

FIG. 6·18

6.9 Discussion

The role of sporadic E ionisation in producing satellite signal scintillations has not been investigated till now. From the present results, it can be clearly seen that there is a definite relationship between scintillation depth and the critical frequency of sporadic E. When spread F and sporadic E are present simultaneously, this relationship is not obeyed. Singleton and Lynch (1962) determined the correlation between the mean scintillation index for each pass and the critical frequency of E_s as recorded at Brisbane. They obtained a poor correlation. In the present analysis, the scintillation depth at the time when the satellite reached 23^{o}N latitude, is well correlated with the critical frequency of sporadic E.

The close association between radio star scintillation and spread F is well known (Booker, 1958; Briggs, 1958). Several workers (Kent, 1959; Yeh and Swenson, 1959) have reported a high correlation between satellite scintillation and spread F. The present low latitude results over Ahmedabad also show good correlation with spread F.

From the topside ionograms taken by the Alouette satellite, King et al (1963) have noticed that the boundary of the spread F region is fairly sharp. Such a type of spread F can give rise to the scintillation boundary that is seen in some of the satellite transits recorded at Ahmedabad.

Singleton and Lynch (1962) determined the zenith angle at the time of closest approach of the satellite for studying the dependence of scintillation depth on zenith angle. In the present analysis, the zenith angles have been calculated at different points on the trajectory. The increase of scintillation depth with zenith angle can still be seen clearly.

Briggs and Parkin (1963) have given the theoretical values of ratio of 20 MHz scintillation depth to 40 MHz scintillation depth for various zenith angles. The shape of the experimental curve obtained at Ahmedabad, in the presence of spread F alone, is similar to the theoretical curve given by Briggs and Parkin (1963). When spread F and sporadic E are present simultaneously, the shape of the curve is quite different from the theoretical curve.

CHAPTER VII

CONCLUSIONS

The conclusions derived from the present investigation are listed in this chapter.

I. The diurnal variation of electron content is more on the bottomside of maximum electron density level (h_mF_2) than on the topside.

II. During 1964-65, the electron content and the maximum electron density increased from winter to summer. While n_{max} increased by about 17 %, electron content increased by about 60 %.

III. The night time values of N_a/N_b are larger than the day time values. The values of night time N_a/N_b determined at Ahmedabad are in agreement with the results of Pound and Yeh (1966).

IV. There is good correlation between N_T/n_{max} and h_mF_2 during day time.

V. In summer and equinox, the day time values of N_T over Ahmedabad decrease with magnetic activity. In winter, the effect of magnetic activity on N_T is not clear. This is in agreement with the middle latitude results of Garriott (1960), Yeh and Swenson (1961) and Lyon (1965).

VI. In all the seasons, N_T increases with magnetic activity at night.

VII. In summer, the ratio N_a/N_b decreases with magnetic activity during day time and increases with magnetic activity in the night. In winter, while the daytime values increase with magnetic activity the night time values decrease. In equinox, the dependence of N_a/N_b on magnetic activity is not clear.

VIII. The day time and night time values of N_T increase linearly with 10.7 cm solar flux. In winter, the day time value of N_T increases at a slow rate till the solar flux reaches a value of about 100 units. Beyond, this, it increases at a faster rate. During night time, N_T seems to increase with solar flux at the same rate in all the seasons.

IX. The day time values of N_T/n_{max} increase linearly with 10.7 cm solar flux. The rate of change seems to increase from winter to summer.

X. In the absence of spread F, there is good correlation between satellite signal scintillations and sporadic E at Ahmedabad. The scintillation rate and depth increase with f_xE_s. The empirical relationship between scintillation depth and f_xE_s is given by

$$S_{20} = 0.02\ (f_xE_s)^{1.5}$$

$$S_{40} = 0.006\ (f_xE_s)^{2.0}$$

where S_{20} and S_{40} are the scintillation depths measured at 20 MHz and 40 MHz respectively. The empirical relationship between the ratio of 20 MHz depth to 40 MHz depth and f_xE_s is given by

$$S_{20}/S_{40} = 0.8 + 13.3\ (f_xE_s)^{-1.75}$$

XI. The scintillation boundary, as seen from Ahmedabad, seems to move northward with magnetic activity. The results of middle latitude stations (Aarons et al, 1963; Yeh and Swenson, 1964) indicate a movement in the opposite direction.

XII. In the presence of Spread F, the scintillation depths at 20 MHz and 40 MHz increase with zenith angle. In the presence of sporadic E alone, the zenith angle effect is not noticeable.

XIII. The scintillation activity is found to be more in summer than in winter. During the period of observation, the same feature is seen in the case of spread F occurrence also.

REFERENCES

Aarons, J., J.Mullen and Basu Sunanda	1963	J.Geophys.Res., <u>68</u>, 3159.
Appleton, E.V.	1932	J.Inst.Elect.Engrs., <u>71</u>, 642.
Argence, E. and K.Rawer	1962	Space Research, <u>III</u>,
Basler, R.P. and R.N.Dewitt	1962	J.Geophys.Res., <u>67</u>, 587.
Bhonsle, R.V., Aldo V.da Rosa, and O.K.Garriott	1965	Radio Science, <u>69D</u>, 929.
Blumle, L.J.	1962	J.Geophys.Res., <u>67</u>, 4601.
Booker, H.G.	1958	Proc.I.R.E., <u>46</u>, 298.
Bolton, J.G., O.B.Slee and G.J.Stanley	1953	Austr.J.Phys., <u>A6</u>, 434.
Bowhill, S.A.	1958	J.Atmos.& Terres.Phys., <u>13</u>, 175.
Blackband, W.T.	1959	Nature, <u>183</u>, 1172.
Briggs, B.H.	1958	J.Atmos.& Terres.Phys., <u>12</u>, 34.
Briggs, B.H. and J.A.Parkin	1963	J.Atmos.& Terres.Phys., <u>25</u>, 339.
Calvert, W., T.E.VanZandt, R.W.Knecht and G.B.Goe	1963	Proc.of the International Conference on the Ionosphere in London, p.324.
Dueno, B.	1955	Cornell University School of Elect.Eng. Tech.Rep., 27.
Evans, J.V.	1956	Proc.Phys.Soc., London, <u>69B</u>, 953.
Evans, J.V. and G.N.Taylor	1961	Proc.Roy.Soc., <u>A-263</u>, 189.
Garriott, O.K.	1960a	J.Geophys.Res., <u>65</u>, 1139.

Garriott, O.K.	1960b	Space Research, I, 340.
Garriott, O.K. and de Mendonca F.	1963	J.Geophys.Res., 68, 4917.
Helliwell, R.A., J.H.Crary, J.H.Pope and R.L.Smith	1956	J.Geophys.Res., 61, 139.
Hey, J.S., S.J.Parsons and J.W.Phillips	1946	Nature, 158, 234.
Hibberd, F.H.	1959	J.Geophys.Res., 64, 945.
Hibberd, F.H.	1964	Scientific Report 213, The Pennsylvania State Univerisity.
Hibberd, F.H. and W.J.Ross	1966	J.Geophys.Res., 71, 2243.
Hunt, D.C. and T.E.vanZandt	1961	J.Geophys.Res., 66, 1673.
Kazantsev, A.N.	1959	Planet Sp.Sc., 1, 130.
Kent, G.S.	1959	J.Atmos.& Terres.Phys., 16, 10.
King, J.W., D.Eccles, P.A.Smith, P.Dannahy, A.Legg, E.O.Olatunji, K.Rice, G.Webb and M.Williams	1963	R.R.S./I.M.112 Radio Research Station, Slough, Report.
Kraus, J.D. and J.S.Albus	1958	Proc.I.R.E., 46, 610.
Lawrence, R.S., Jane Posakony, O.K.Garriott and S.C.Hall	1963	J.Geophys.Res., 68, 1889.
Little, C.G.		Unpublished.
Little, C.G. and R.S.Lawrence	1960	Space Research, I, 371.
Little, C.G. and B.Lovell	1950	Nature, 165, 423.

Lyon, G.F.	1965	Canad.J.of Phys., 43, 1059.
Mass, J.	1962	Proc.Inst.Rad.Engrs., 50, 466.
Mendonca F.de, Villard, Jr.and O.K.Garriott	1960	Proc.I.R.E., 48, 2028.
Mendonca F.de	1962	J.Geophys.Res., 67, 2315.
Munro, G.H.	1962	J.Geophys.Res., 67, 147.
Nicolet, M.	1963	J.Geophys.Res., 68, 6121.
Parthasarathy, R. and G.C.Reid	1959	Proc.I.R.E., 47, 78.
Peterson, A.M., O.G.Villard, R.L.Leadabrand and P.B.Gallagher	1955	J.Geophys.Res., 60, 497.
Pound, T.R. and K.C.Yeh	1966	University of Illinois, Report December 1966.
Ramakrishnan, S.	1966	Space Research, VII, 1371.
Ross, W.J.	1960	J.Geophys.Res., 65, 2607.
Ross, W.J.	1965	J.Geophys.Res., 70, 597.
Shirke, J.S. and S.Ramakrishnan	1966	Proc.Ind.Acad.Sc., LXIII, 338.
Singleton, D.G. and G.J.E.Lynch	1962	J.Atmos.& Terres.Phys., 24, 353.
Slee, O.B.	1958	Nature, 181, 1610.
Smith, F.G.	1950	Nature, 165, 422.
Somayajulu, Y.V., Thhi Ram Tyagi and V.P.Bhatnagar	1963	Space Research, IV, 498.
Somayajulu Y.V.and Tuhi Ram Tyagi	1966	National Physical Laboratory, India Scientific Report No.26.
Swenson, G.W. and K.C.Yeh	1961	University of Illinois, Report, August 1961.
Swenson, G.W.	1963	Cospar Information Bulletin, No.15, 20.

Taylor, G.N.	1966	Electron density Profiles in the Ionosphere and Exosphere, ed.Frihagen.
Thomson, J.H.	1958	Phil.Mag., 3, 912.
Titheridge, J.E.	1961	J.Geophys.Res., 66, 3103.
Titheridge, J.E.	1964	J.Atmos.& Terres.Phys., 26, 177.
Vassy, E.	1961	J.Atmos.& Terres.Phys., 23, 85.
Willmore, A.C., R.L.F.Boyd and S.J.Bowen	1962	Proc.International Conference on the Ionosphere, London, 517.
Wright, J.W.	1960	J.Geophys.Res., 65, 185.
Yeh, K.C.	1960	J.Geophys.Res., 65, 2548.
Yeh, K.C. and G.W.Swenson	1961	J.Geophys.Res., 66, 1061.
Yeh, K.C. and B.J.Flaherty	1966	J.Geophys.Res., 71, 4557.